Smart Polymer Electromechanical Actuators for Soft Microrobotic Applications

Reza Montazami

Dissertation submitted to the faculty of the
Virginia Polytechnic Institute and State University
in partial fulfillment of the requirements for the degree of

Doctor of Philosophy

In

Materials Science and Engineering

James R. Heflin, Chair
Donald J. Leo
Abby R. Whittington
Sean G. Corcoran

June 3, 2011

Blacksburg Virginia

Keywords: Smart Materials, Ionic Electroactive Polymer Actuators, Electromechanical Actuator, Soft Microrobotics

Smart Polymer Electromechanical Actuators for Soft Microrobotic Applications

Reza Montazami

ABSTRACT

Ionic electroactive polymer (IEAP) actuators are a class of electroactive polymer devices that exhibit electromechanical coupling through ion transport in the device. They consist of an ionomeric membrane coated with conductive network composites (CNCs) and conductive electrodes on both sides. A series of experiments on IEAP actuators with various types of CNCs has demonstrated the existence of a direct correlation between the performance of actuators and physical and structural properties of the CNCs. Nanostructure of CNC is especially important in hosting electrolyte and boosting ion mobility.

This dissertation presents a series of systematic experiments and studies on IEAP actuators with two primary focuses: 1) CNC nanostructure, and 2) ionic interactions.

A novel approach for fabrication of CNC thin-films enabled us to control physical and structural properties of the CNC thin-films. We, for the first time, facilitated use of layer-by-layer ionic self-assembly technique in fabrication of porous and conductive CNCs based on polymer and metal nanoparticles. Results were porous-conductive CNCs. We have studied the performance dependence of IEAP actuators on nano-composition and structure of CNCs by systematically varying the thickness, nanoparticle size and nanoparticle concentration of CNCs. We have also studied influence of the waveform frequency, free-ions and counterions of the ionomeric membrane on the performance and behavior of IEAP actuators.

Using the LbL technique, we systematically changed the thickness of CNC layers consisting of gold nanoparticles (AuNPs) and poly(allylamine hydrochloride). It was observed that actuators consisting of thicker CNCs exhibit larger actuation curvature, which is evidently due to uptake of larger volume of electrolyte. Actuation response-time exhibited a direct correlation to the sheet-resistance of CNC, which was controlled by varying the AuNP concentration. It was observed that size and type of free-ions and counterion of ionomeric membrane are also influential on the actuation behavior or IEAP actuators and that the counterion of ionomeric membrane participates in the actuation process.

This dissertation is dedicated to my wife, Nastaran Hashemi, and my parents Behrouz Montazami and Simin Shahbaz.

Acknowledgements

My highest appreciation and gratitude go to my wonderful academic advisor and mentor, Professor James R. Heflin. I cannot put in words my deepest appreciation for his help, support, guidance, patience and encouragement. I have learned a lot from his astounding knowledge in Physics and Materials Science. Professor Heflin gladly offered his knowledge and experience when needed. His trust in me and the freedom he provided me, helped me to adopt scientific and critical thinking.

I would also like to thank Professor Donald Leo for his excellent guidance and advice. I learned a lot from Professor Leo, and am very thankful that I had the opportunity to benefit from his knowledge. I would also like to express my special gratitude to Professor Abby Whittington for her generous help, advice, and support. I would also like to thank Professor Sean Corcoran for his advice, insights and valuable recommendations.

In addition to my committee members, I would also like to thank Professor Karen DePauw, the Dean of the Graduate School, who changed the way I see to world, and helped me to be a better person. I am very appreciative of Professor David Clark, the Head of the MSE department for giving me the opportunity to join this wonderful department.

Special thanks go to my family, specially my beloved soul mate and better half, Nastaran Hashemi. Thank you for being there with me during all the hard times in my academic life and personal life; I sincerely appreciate all your support. And special thanks to my parents, Behrouz Montazami and Simin Shahbaz, and my parents-in-law, Ghodratollah Hashemi and Nayereh Rajabi, for their unconditional love and support. I also like to specially thank my uncle, Ali Shahbaz for always being there for me. I would also like to thank my brother Ali and my sister-in-law Niloofar. I also like to specially mention Misha as she made Nastaran and me happier and brought a lot of fun into our lives.

Thanks also go to my colleagues and collaborators Dong Wang, Dr. Vaibhav Jain, Dr. Jason Ridley, Manpreet Kaur, Jonathan Metzman, Jeong-Ah Lee, Matt Green, Dr. Andy Sarles and Dr. Minjae Lee from Virginia Tech; and Yang Liu and Dr. Sheng Liu from Penn State University, for insightful discussions and productive collaborations, as well as all IEAD MURI members.

I would like to specially thank Professor Timothy Long, Professor Harry Gibson, Professor Richey Davis, Professor Leo Piilonen and Professor Barbar Akle for all their help, support and insightful dissuasions.

I would also like to thank Dr. Banahalli Ratna, the Director of the Center for Bio/Molecular Science and Engineering at the Naval Research Laboratory, for giving me the opportunity and the privilege of working with her group during the summer of 2009. Also special thanks to Dr. Christopher Spillmann at the Naval Research Laboratory for allowing me the privilege to work with him during my visit to the Naval Research Laboratory; and Dr. Jawad Naciri for all his help and guidance.

I also would like to thank my friends who helped me go through some of the most stressful times; in no particular order, Rodi Movassagh, Sanaz Fesharaki, Mohammad Kianinia, Parisa and Dr. Babak Bazrgari, Dr. Bita and Dr. Majid Manteghi, Parastoo Mokri, Parhum Delgoshaei, Omid Shoghli, Dr. Jennifer Cover, Nasrin Afzal, Dr. Vaibhav Jain, Dong Wang, Nicole Fahrenfeld, Dr. Ali Yeilaghi, Dr. Jason Ridley, Mehri Shams, Dr. Najma Yousefi, Matt Green, Dr. Alireza Farjoud and Moataz Bellah Abdel Salam.

I would also like to sincerely thank the U.S. Army Research Office for providing financial support for this work under Grant No. W911NF-07-1-0452 Ionic Liquids in Electro-Active Devices (ILEAD) MURI

Table of Contents

List of Figures

Chapter One

Chapter Two

Chapter Three

Chapter Four

Chapter Five

Chapter Six

Chapter Seven

Chapter Eight

Chapter Nine

Chapter Ten

List of Tables

Chapter 1
Introduction

Materials science and Engineering is a multidisciplinary field, focusing mainly on the physical properties of materials and investigating relations between the properties of materials and their physical structures at molecular and/or atomic scales. The *Science* aspect of the field very often employs multidisciplinary skills and elements from *chemistry*, *physics* and more recently *nanotechnology*. Materials science is very similar to chemistry as both fields are concerned about the relation between the structure of the species and their properties. However, unlike chemistry that is mainly focused on the molecular structure of species, materials science is more involved with the bulk of materials. On the other word, atoms are the main building blocks of chemistry whereas molecules and their arrangements are at the center of attention in materials science. The *Engineering* aspect of the field is tightly related to *mechanical engineering*, *aerospace engineering*, *chemical engineering* and other fields of study in which there are needs for materials with specific properties. A good example is the *Thermal Protection System* of space shuttles that consists of about 27000 ceramic tiles that can withstand temperatures as high as 1700°C. Another good example is use of carbon fibers in the newly designed Boeing 787 Dreamliner, which significantly decreases the weight and thus fuel consumption of the aircraft. These are only two out of thousands of examples in which materials engineering has helped other engineering fields by proving new means and materials for better designs. Of course, there is still much more to accomplish in Materials Science and Engineering. As we are reaching our limitations with the current technologies, it is materials science that can provide new materials needed for breakthroughs in science and engineering.

1.1 Smart Materials

Smart materials are defined as materials that exhibit a *fast*, *repeatable*, *reversible* and *significant* change in at least one of their physical properties in response to an external stimulus. It is important to emphasize on *repeatable* and *significant*, otherwise all materials can fall under the category of smart materials. For instance, all materials have thermal expansion tendencies, yet

the change is too small and usually too slow. Thus thermal expansion, although repeatable and reversible, is not a characteristic of smart materials.

Smart materials can be found in form of solid solution, compound or composite. No pure material, i.e. element, has smart material characteristics. Smart materials should not be confused with smart structures. Smart structures may contain parts consisting of pure materials. For example bimetallic strips, used in thermostats, consist of two strips of steel and copper, physically bonded at two ends. The strips are two separate, distinguishable pieces. Thus although bimetallic strips exhibit reversible significant sideway displacements, they are smart structures and not smart materials. Similar to solid-state materials, smart materials can also be divided into three main categories: metals, ceramics/crystals and polymers, of course with the "smart" prefix.

1.1.1 Shape Memory Alloys

One of the most common form of smart metals is a shape memory alloy (SMA). SMAs maintain memory of their initial, cold-forged shape and can return to that pre-deformation shape when exposed to higher temperature. The mechanism of actuation in SMAs is very similar to a phase change in any material. For instance, as materials transform from solid to liquid, they change shape. This is what happens in SMAs, except in this phase change molecules remain close to each other and are closely packed thus the structure remains solid; also atomic bonds remain in place so upon heating the structure transforms to its original (cold) conformation.[1,2] Discovery of SMAs dates back to early 1930. In 1932, A Ölander observed, for the first time, pseudoelastic behavior in a gold-cadmium alloy. Later, in 1938, Greninger and Mooradian discovered temperature dependence of the martensitic phase in copper-zinc alloy. In most cases the motion of SMAs is repeatable but it is not reversible (one-way memory effect); that is, just like biological muscle that only contracts, SMAs respond to thermal stimulus only when they are deformed. As a result, at least two sets of SMA devices are needed to arrange a reversible motion. A less common class of SMAs have two shape memories, one at high temperature and one at low temperature (two-way memory effect) and can alter between the two phases without application of an external force. Although most two-way SMAs are unstable and impractical for applications as they cannot conduct work in the cooling cycle, there are a few examples of two-way SMAs that have shown significant mechanical properties in both heating and cooling cycles.[3,4] SMAs are widely used in aerospace, robotics and medical applications.

1.1.2 Smart Ceramics

Smart ceramics/crystals very often have piezoelectric properties. Piezoceramic, also known as electroactive ceramics (EACs) are electromechanical transducers that can work both as sensors (mechanical force to electrical signal) and actuators (electrical signal to mechanical force). Among the three aforementioned categories of smart materials, smart ceramics are by far the most commercialized one, with numerous applications in military, medicine, research and day to day life. French scientist, Paul Langevin, developed the first practical application of piezoceramics, SONAR, in 1917 during the World War I. Since then, piezoceramics have been used in many devices such as digital wrist watches and piezoelectric igniters that are used on a daily basis. In addition, piezoceramics are also used in sophisticated scientific instruments such as scanning electron microscopy (SEM) and atomic force microscopy (AFM) to precisely control the position of the platforms.

1.1.3 Smart Polymers

According to Dr. Yoseph Bar-Cohen, one of the pioneers in the field of smart polymers, the first documented experiment with smart polymers is attributed to German physicist Wilhelm Rontgen. In 1880, Rontgen designed an experiment in which he tested the effect of an electric field on a rubber-band with a fixed end and a mass attached to other end. Rontgen observed length change in the rubber-band when it was subjected to an electric field. Smart polymers are more diverse compared to smart metals and smart ceramics, both in variety of stimulus and variety of response. Different classes of smart polymers (electromechanical, electrochromic, ferromagnetic, pH sensitive, thermomechanical, etc.) respond to a wide variety of stimuli (electric field, pH, temperature, magnetic field, etc.). Another significant difference between smart polymers and other categories of smart materials is the physical properties of smart polymers. Unlike smart metals and smart ceramics that are rigid and fragile, smart polymers are soft and flexible with significantly lower density.

Among different classes of smart polymers, electroactive polymers are by far the most common. Although generally the term *polymer* brings to mind plastics and primarily insulators, there is a class of polymers that are semiconductive/conductive. One may ask why we should even bother with conductive polymers when there is already a large class of well-known conductive materials, metals. Metals are certainly the most conductive materials; however, polymers have

certain mechanical, thermal and even electrical properties that cannot be found in metals. Polymers are flexible, and can be formed into thin-films while maintaining their mechanical properties. From a materials engineering point of view, materials can exhibit two fracture modes: ductile and brittle. This classification is mainly based on materials deformation characteristics. Most metals are brittle, as they cannot experience plastic deformation. On the other hand, most polymers are ductile. One other characteristic of polymers is the possibility of ion conduction. While metals only conduct electrons, there are classes of electron conducting and ion conducting polymers (ionic polymers). In addition, polymers can exhibit interesting reversible changes in their chemical structures whereas metals usually do not have such characteristics. For instance, electrochromic polymers, once subjected to an electric field, can undergo reversible redox states and exhibit changes in their optical properties. [5]

Generally, polymers that exhibit any form of response to an external electric field are called electroactive polymers. Electrochromic polymers are good examples of electroactive polymers. Application of an external electric field causes the polymeric network to reduce or oxidize, which results in a change in the optical transmittance. Changing the polarity of the electric field reverses the redox reaction and takes the polymer to its initial state or to a different redox state. Presented in **Figure 1.1** is an electrochromic device in its reduced (dark blue) and oxidized (pale yellow) states, built with two electrochromic polymers: polyaniline and poly(aniline sulfonic acid).

Another good example of electroactive polymers is electromechanical polymers. Electromechanical polymers exhibit a mechanical deformation when subjected to an external electric field. The mechanical deformation can be the result of electrostatic force between the electrodes[6] (dielectric electroactive polymers), electrical polarization in crystalline polar polymers[7,8] (ferroelectric electroactive polymers and liquid crystal polymers), ion diffusion[9] (conductive polymers), or mobility of ions within the polymeric network[10] (ionic electroactive polymers). Liquid crystal polymers behave similar to ferroelectric electroactive polymers; the only difference is in building blocks of the polymeric network. Liquid crystal polymers consist of mesogens whereas ferroelectric polymers consist of crystalline polar units. Thermomechanical liquid crystal elastomers (discussed in chapter 9) exhibit similar behavior in response to variations in temperature. [11,12]

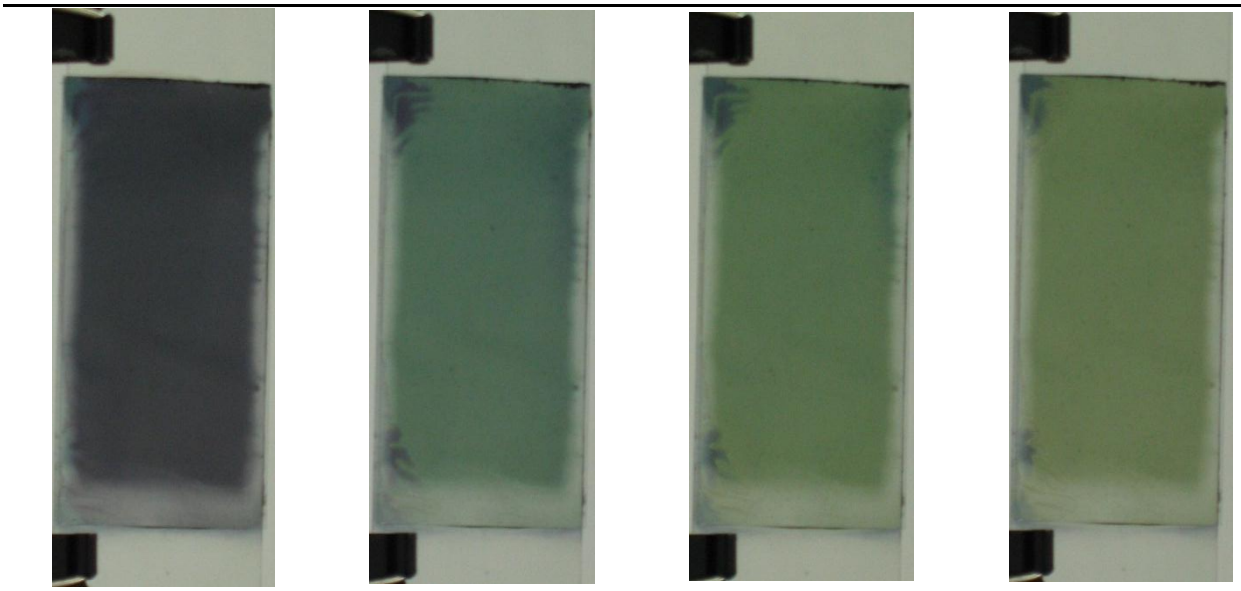

Figure 1.1. Electrochromic device based on two electrochromic polymers in transition from reduced state (left) to oxidized state (right)

This work is focused on design, fabrication and characterization of bending ionic electroactive polymer actuators, hereafter IEAP actuators. IEAP actuators are five layer bimorph structures consist of two electrolyte rich conductive network composite (CNC) thin-film structures fabricated on the surfaces of the ionomeric membrane forming ionic polymer-metal composite (IPMC), and two metal electrodes on the surfaces of IPMC. This work emphasizes on two main objectives to improve the performance of IEAP actuators. One is to study the influence of physical properties of CNCs on the performance of IEAP actuators, and second is to understand ionic interactions within the IPMC. Functionality of IEAP actuators is based on mobility of ions within IPMC. We have designed and fabricated porous conductive thin-film structures based on metal nanoparticles to simultaneously improve porosity and electrical conductivity of CNCs to enhance mobility of ions in IPMC. We have studied the influence of physical structure of CNC on the performance of IEAP actuators by varying the nanoparticles type, thickness and volume density of CNCs and have shown that all these factors are strongly influential on the performance of IEAP actuators. In an effort to understand ionic interaction within IPMC, we have modified chemical structure of the ionomeric membrane, and have also used different ions in IPMC. The results suggest that both counterion of the ionomeric membrane and type of free

ions in IPMC are significantly influential on actuation direction and performance of IEAP actuators.

1.2 Document Organization

An overview of electromechanical polymers, also known as electroactive polymer actuators, is presented in **chapter 2**. Background and brief history of electroactive polymers, including dielectric, ferroelectric, liquid crystal, conductive polymers, electroactive gels and ionic electroactive polymers are mentioned. An in-depth overview of ionic electroactive polymer actuators is discussed with emphasis on ionomeric membrane, conductive network composite, outer electrodes and electrolytes. Next, overview of the history and assembly concept of layer-by-layer ionic self-assembly technique is discussed to emphasize the value of this technique in fabrication of thin-film nanostructures. Finally layer-by layer ionic self-assembly of spherical nanoparticles is discussed along with background information.

Chapter 3 contains the details of materials and methods used in this research. First, materials, equipment and method used in fabrication of IPMCs are discussed in detail, along with equipment and techniques used to characterize IPMCs. Next materials, equipment and methods used in assembly of IEAP actuators are discussed in detail along with equipment and methods for characterization of IEAP actuators. In addition, blueprints and details of an in-house made probe station is presented.

Chapter 4 presents a brief summary of our preliminary work, including experiments with different metal nanoparticles which lead to choosing the optimum materials for CNCs, and proof-of-concept experiments to show porous-conductive CNCs are advantageous.

Chapter 5 contains our study on the influence of the thickness of CNC on the performance of IEAP actuators. Actuators consisting of different CNC thicknesses were fabricated and tested for their mechanical performance. The growth rate of CNC as a function of number of bilayers is presented along with the curvature dependence on the thickness of CNC. Next, techniques for deducing intrinsic strain, net intrinsic strain, and net strain of the actuators are presented along with the results. Finally, limiting factors in actuation speed are reported and discussed.

Chapter 6 details fabrication of CNCs with different nanoparticle volume fractions as a mean to alter conductivity of CNCs. The influence of nanoparticle volume fraction on charging/discharging times and current flow in through the actuator are discussed. Mechanical performance of actuators based on mobility of each type of ion is also characterized. Finally, frequency dependence of motion of cations is studied and described.

Chapter 7 is dedicated to studies on ion transport in IEAP actuators. Mechanical response of IEAP actuators is characterized as a function of waveform frequency. Motion of ions in response to fast and slow frequencies are discussed. Equivalent electric circuit for the actuator is presented, and turnover frequency of each ion is calculated for the presented case-study. Lastly, it is shown how mobility of ions can be manipulated by frequency to eliminate secondary bending due to motion of slower ions.

Chapter 8 presents alternative ways to influence actuation performance of IEAP actuators. The counterion of ionomeric membrane is changed from proton through ion exchange, and it is shown that the performance of actuators depends on the counterion. It is also suggested that counterion of ionomeric membrane actually participates in the actuation process. Next, different ionic liquids are used as the ion source and their influence on actuation is discussed. Finally, a report on the influence of ions in IPMC on the actuation process is presented.

Chapter 9 details study of nematic liquid crystal elastomer thermomechanical actuator. It is described how embedment of gold nanoparticles in the polymeric network is used to increase thermal conductivity of the actuators. Response of the actuator to slow and fast heating rates are studied and discussed. Moreover, protocol for incorporation of nanoparticles in the polymeric network, with minimal effect on elasticity, is presented. Finally, mechanical and thermal properties of the actuators are discussed.

The dissertation ends with a summary of all the presented topics in this research, along with recommendations to further improve performance of IEAP actuators, and suggestions on possible applications of IPMCs and IEAP actuators.

References

1 Kazuhiro Otsuka and Xiaobing Ren, "Recent developments in the research of shape memory alloys," Intermetallics **7** (5), 511-528 (1999).

2 L. McDonald Schetky, *Shape-Memory Alloys*. (John Wiley & Sons, Inc., 2000).

3 Jeff Perkins and R. Sponholz, "Stress-Induced Martensitic Transformation Cycling and Two-Way Shape Memory Training in Cu-Zn-Al Alloys," Metallurgical and Materials Transactions A **15** (2), 313-321 (1984).

4 R. Stalmans, J. Van Humbeeck, and L. Delaey, "The two way memory effect in copper-based shape memory alloys -- thermodynamics and mechanisms," Acta Metallurgica et Materialia **40** (11), 2921-2931 (1992).

5 R Montazami, V Jain, and JR Heflin, "High Contrast Asymmetric Solid State Electrochromic Devices Based on Layer-by-Layer Deposition of Polyaniline and Poly (aniline sulfonic acid)," Eelectrochimica Acta **56** (2), 5 (2010).

6 R Pelrine, R Kornbluh, Q Pei, and J Joseph, "High-speed electrically actuated elastomers with strain greater than 100%," SCIENCE **287** (5454), 836 (2000).

7 QM Zhang, V Bharti, and X Zhao, "Giant electrostriction and relaxor ferroelectric behavior in electron-irradiated poly(vinylidene fluoride-trifluoroethylene) copolymer," Science **280** (5372), 2101-2104 (1998).

8 W. Lehmann, H. Skupin, C. Tolksdorf, E. Gebhard, R. Zentel, P. Kruger, M. Losche, and F. Kremer, "Giant lateral electrostriction in ferroelectric liquid-crystalline elastomers," Nature **410** (6827), 447-450 (2001).

9 MR GANDHI, P MURRAY, GM SPINKS, and GG WALLACE, "MECHANISM OF ELECTROMECHANICAL ACTUATION IN POLYPYRROLE," Synthetic Metals **73** (3), 247-256 (1995).

10 Mohsen Shahinpoor and Kwang J. Kim, "Solid-state soft actuator exhibiting large electromechanical effect," Applied Physics Letters **80** (18), 3445-3447 (2002).

11 EM Terentjev, "Liquid-crystalline elastomers," Journal of Physics Condensed Matter **11**, 239-258 (1999).

12 CM Spillmann, JH Konnert, JR Deschamps, J Naciri, and BR Ratna, "Molecular Packing in Electroclinic Liquid Crystal Elastomer Films," Chemistry of Materials **20** (19), 6130-6139 (2008).

Chapter 2

Literature Review and Background

2.1 Electroactive Polymer Actuators

In the recent years (since the late 1990s), there has been increasing interest in electromechanical polymer actuators, which is a subcategory of electroactive smart polymers. Electromechanical polymer actuators are transducers capable of converting electric current into mechanical force (actuators) and vice versa (in some cases) (sensors). This capability along with unique mechanical properties have made this class of electroactive polymers interesting for several applications including in the military, medical, aerospace and automotive industries. There are several types of electroactive polymer actuators that I will explain in the following paragraphs.

2.1.1 Dielectric polymers

In dielectric polymers, the electrostatic force between the electrodes squeezes the polymer and as a result mechanical deformation occurs. Dielectric actuators generate large strain (10-35%), but a relatively strong external electric field (hundreds to thousands of volts depending on the geometry) is required to actuate dielectric polymers.[1] Dielectric polymer actuators consist of a passive elastomer layer which is sandwiched between two plate electrodes. Application of voltage across the two plates, and thus across the thickness of the elastomer, results in generation of an electrostatic pressure from the Coulomb force acting between the electrodes. The pressure on the elastomer causes mechanical deformation of the elastomer. Silicone and acrylic elastomers are common dielectric polymers. Generally, polymers with high dielectric constant, high electrical breakdown and low elastic modulus are suitable dielectric polymer actuators. One great advantage of dielectric polymer actuators is that they can be cast in different shapes and can also be used in the form of stacks.

2.1.2 Ferroelectric polymers

Ferroelectric polymers are crystalline polar polymers that maintain permanent electric polarization. The electric polarization can be altered by an external electric field. The external electric field causes the polar components (crystalline units) to rotate and align with the electric

field, which results in slight (angstrom-scale) change in the length of each structural unit of polymer. Given the large number of structural units, the accumulated change is considerable and results in mechanical deformation of the polymer. As a result the entire polymeric network is deformed and mechanical deformation occurs.[2,3] Ferroelectric polymers can be used as both sensors and actuators, and are considered as inexpensive actuators. Polyvinylidene fluoride (PVDF) is one of the most common ferroelectric polymers.

2.1.3 Liquid crystal polymers

The mechanism of actuation in liquid crystals is exactly the same as that in ferroelectric polymers, except that the crystalline units are replaced by mesogens, which are the fundamental units of liquid crystals.

2.1.4 Conductive polymers

Functionality of conductive polymers is based on the reversible counterion insertion and expulsion. This process (insertion and expulsion of ions) in fact drives the polymer between different redox states. Once a counterion is inserted into the polymeric structure, depending on the charge of the ion, the polymer undergoes reduction or oxidation. The reverse happens once the ion is exported from the polymeric network. Presence or absence of ions in the polymeric network results in expansion or contraction of the network, which in turn causes actuation. Conductive polymer actuators usually consist of three layers, an electrolyte layer sandwiched between two conductive polymer electrodes (for instance polypyrrole and polyaniline). Upon application of voltage, the cathode undergoes oxidation and simultaneously the anode undergoes reduction. That is, protons travel from the anode toward the cathode to balance the electric charge, and as a result disturb the balance of the system and cause mechanical deformation. The process can be reversed by changing the polarity of the applied voltage.

2.1.5 Electroactive gels

The actuation mechanism in electroactive gels is usually a chemical reaction, changing the material from acidic to alkaline, which results in the material become denser or swollen, respectively. The chemical reaction can be initiated electrically, by application of a voltage across two electrodes surrounding the electroactive gel. Upon application of the voltage, the cathode side becomes more alkaline, while simultaneously the anode side becomes more acidic.

As a result, the actuator bends toward the anode. The actuation process in electroactive gels is relatively slow, on the scale of tens of minutes, due to the time required for ions to diffuse, and depends on the geometry of the actuator. One other issue with such actuators is significantly short lifespan. Since the actuation is relatively large, the electrodes usually are damaged and fail after a couple of actuation cycles. Polyacrylonitrile is an example of an electroactive gel.

2.1.6 Ionic electroactive polymers

Functionality of ionic electroactive polymers is based on mobility of ions within the polymeric network. This class of electromechanical polymers differs from conductive polymers (mentioned above) as the redox state of ionic electroactive polymers does not change during the actuation process. As an electric potential is applied across the polymer, ions move within the polymeric network toward the oppositely charged electrodes and cause mechanical deformation. The voltage required for actuation of IEAP actuators ($\leq$4V) is significantly smaller than that required for actuation of other types of actuators. The work presented in this dissertation mainly concerns ionic electroactive polymer actuators. In the next section, I will go through a more in-depth review of ionic electroactive polymer actuators and their potential applications.

2.2 Ionic Electroactive Polymers Actuators

Ionic electroactive polymer (IEAP) actuators are a class of electromechanical devices that function based on transport of ions through the device, in the presence of an electric field, and their accumulation at oppositely charged electrodes. The backbone structure of IEAP actuators is an ionomeric membrane (also known as ion-exchange membrane) which is permeable to either or both cations and anions, depending on its chemical structure and physical properties. Nafion® is the single most widely used ionomeric membrane in IEAP actuators. Since the functionality of IEAP actuators is based on mobility of ions, it would be logical to presume that increasing the density of ions in the device and facilitating their mobility would improve the performance of actuators. The IEAP actuators with the largest actuation performance typically consist of two conductive network composite (CNC) layers formed on the surfaces of the ionomeric membrane containing an electrolyte. Depending on their physical and chemical properties, CNC layers may influence the electrolyte intake capacity, electrical conductivity, mobility of ions, mechanical properties, and electrical capacitance of the device. They also provide a conductive network that uniformly distributes electric charge across the ionomeric membrane interface. To further

improve electrical conductivity and uniform charge distribution across the device and also to protect the device from the ambient conditions, ultra-thin leafs of precious metal electrodes (very often gold or platinum) are used to encapsulate the device. Schematic of an IEAP actuator is presented in **Figure 2.1**.

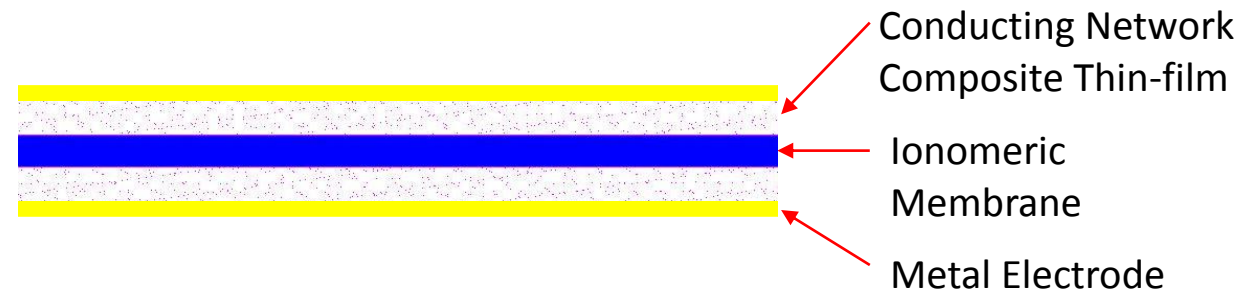

Figure 2.1. A not-to-scale schematic of a five layer IEAP bending actuator. Ionomeric membrane at the center is coated with CNCs and outer electrodes

Motion of ions of different size and charge through the ionomeric membrane and CNCs and their accumulation at the oppositely-charged electrodes generates stress, which in turn causes mechanical strain, **Figure 2.2**. Motion of ions toward or away from each electrode is due to attractive or repulsive forces between the electrically charged electrode and the ions and can be reversed upon switching the polarity of the electric field.

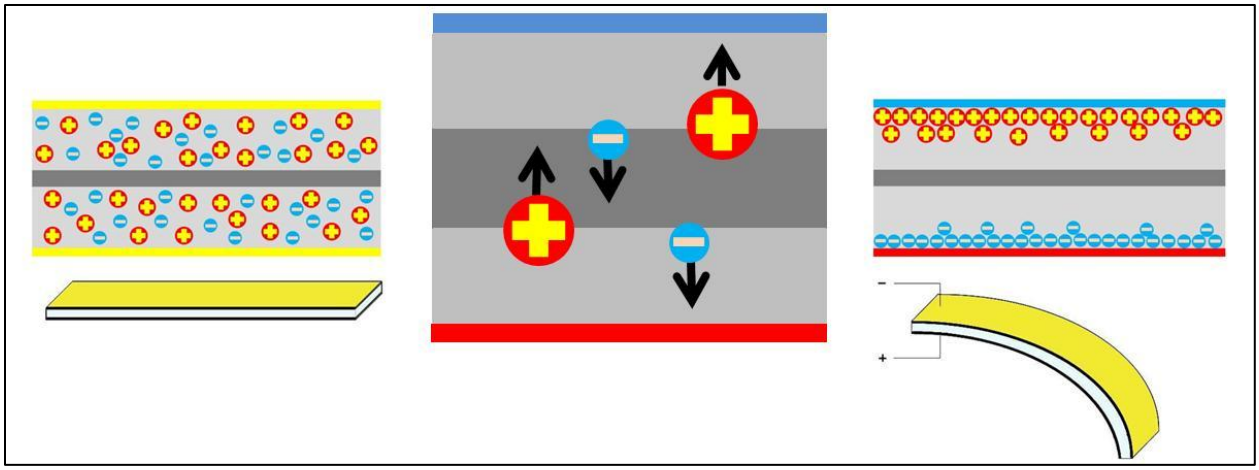

Figure 2.2. Accumulation of different size ions at oppositely-charged electrodes generates stress, sufficient enough to mechanically bend the actuator

In the following subsections, I will talk in detail about each component of a five layer IEAP actuator.

2.2.1 Ionomeric Membrane

The ionomeric membrane is the backbone of the IEAP actuator structure, thus its chemical and physical properties are of significant importance to the performance of IEAP actuators. Low Young's modulus, thermal and mechanical stability, water insolubility and ion exchange capability are among the most important characteristics of ionomeric membranes for IEAP actuators. There are several ionomeric membranes that have these characteristics yet only two of them are studied in significant detail for IEAP actuator applications, Nafion and Flemion®. Among these two ionomeric membranes, Nafion is by far the most studied one.

Nafion

Nafion is an ionomeric membrane developed in the late 1960s by Walter Grot of DuPont®. Nafion has some unique properties that make it very suitable for IEAP actuators. Some of Nafion's properties are high thermal stability (up to 190°C), good mechanical properties (can be casted or extruded into mechanically stable thin-films) and high chemical stability (at normal temperature, only alkali metals can degrade Nafion). Nafion has a large tetrafluoroethylene (Teflon) backbone, **Figure 2.3**. The aforementioned properties of Nafion are

due to the presence of perfluorovinyl ether short side-chains in the backbone structure and its ionic properties are the result of sulfonate (SO_3^-) ionic groups.[4,5] The sulfonate ionic groups in Nafion are located, but not fixed, at the ends of the side-chains of perfluorinated alkenes, therefore they can position in such way to form hydrophilic nano-channels of approximately 2.5nm diameter, also known as cluster networks that allow transport of small ions. This model, proposed by Schmidt-Rohr *et al*[6], is among the most accepted models. This type of behavior is not seen in other types of ionic polymer groups such as styrene/divinylbenzene-based polymers. Under neutral conditions, Nafion is considered a proton exchange membrane; that is the membrane is only permeable to cations. However, in cases in which external factors are present such as electric field in the case of actuators, anions can also drift through the nano-channels of Nafion due to attractive and repulsive forces generated by the electric field.

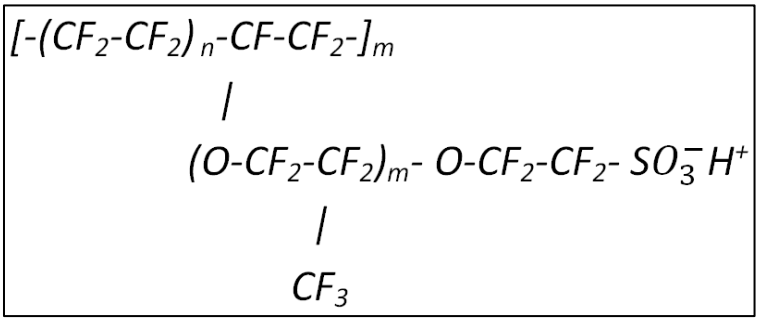

Figure 2.3. Chemical structure of Nafion

Flemion

Flemion was developed by Asahi Glass® in the mid-1970s. In contrast to Nafion, Flemion has carboxylate (COO^-) ionic groups, **Figure 2.4**. Several research groups have study Flemion as the ion exchange membrane in IEAP actuators and have reported promising results. Wang *et al*[7] have reported improvement of the overall performance of IEAP actuators when Nafion was replaced by Flemion. Nemat-Nasser *et al*[8] also compared Nafion-based IEAP actuators with Flemion-based IEAP actuators and have reported Flemion as the preferred ionomeric membrane for bending actuators. They reported that Flemion-based IEAP actuators have higher ion-exchange capacity, better surface conductivity, higher hydration capacity, higher longitudinal

stiffness, and exhibited greater bending actuation without reverse relaxation under a sustained DC voltage, which is typical of Nafion-based IEAP actuators.

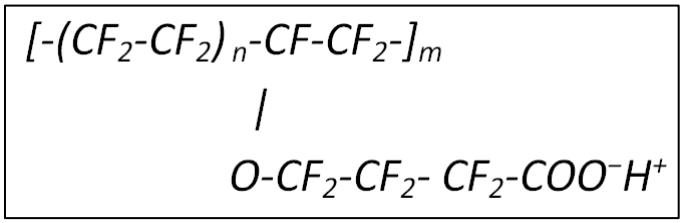

Figure 2.4. Chemical structure of Flemion

Aquivion

Aquivion also known as Hyflon® is another ionomeric membrane used in IEAP actuators. Hyflon was first developed by Dow Chemicals® in the early 1980s, and now is produced as Aquivion by Solvay Solexis®.[9-12] Nafion, Flemion and Aquivion have identical backbone structures of tetrafluoroethylene and are perfluorinated ionomeric polymers, **Figure 2.5**. However, unlike Flemion which has carboxylate ionic groups, Nafion and Aquivion have sulfonate ionic groups. Identical backbone and end-groups structures make Nafion and Aquivion very similar to each other. The main difference between these two ionomeric polymers is that Nafion has long side-chains whereas Aquivion has short side-chains, which results in different properties. The short flexible side-chains of Aquivion result in a better coupling between the ions and the ionomeric membrane and improves the electromechanical properties of actuators in the form of larger bending, compared to Nafion based samples, yet it does not affect the actuation speed.[13]

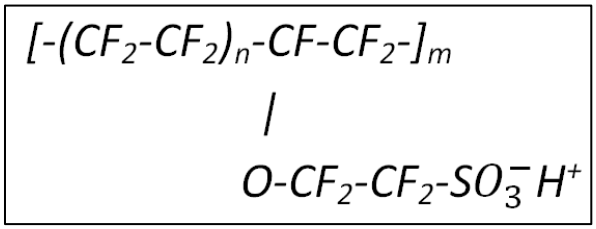

Figure 2.5. Chemical structure of Aquivion

2.2.2 Conductive Network Composite (CNC)

Several studies have demonstrated that the actuation behavior of IEAP actuators depends on the properties of the CNC layers.[14-18] CNCs are designed to act as reservoirs for electrolyte (aqueous or ionic liquid) solution. The mobility of ions through the CNC layer, in the presence of an electric field, depends on several factors such as size, length, conformation and number of nano/micro-channels, as well as the interaction of ions with the nano/micro-channels and of course the strength of the electric field. The mobility of the ions defines attributes of CNC layers and can ultimately define the characteristics of IEAP actuators. Most of these attributes can be tuned and optimized by variation of the composite materials, fabrication technique, and the physical and chemical properties of the CNC layers. One other highly important factor in performance of IEAP actuators is the ratio between the size of the ions and the diameter of the nano/micro-channels in the CNC layers. This ratio is very influential on the mobility of ions and in addition to tuning physical properties of CNC it can also be tuned by choice of proper electrolyte.[19] Several research groups have modified the properties of different components of IEAP actuators in order to enhance their performance and/or to better understand the mechanism of actuation and mobility of ions. For instance, Akle *et al.* formed CNCs from composites of RuO_2 particles and gold flakes at different ratios and studied the effects of porosity and conductivity on the performance of actuators.[14] The most significant factor here was that the porosity of CNC layers was controlled separately from their conductivity. Porosity was controlled by the spherical RuO_2 nanoparticles which are not electrically conductive, and conductivity was controlled by the gold flakes (approximately two dimensional) which do not contribute to the three dimensional structure of CNC. As a result, CNCs with higher RuO_2 concentration were more porous and less conductive, and ones with higher gold flakes concentration were more conductive and less porous. It was shown that porosity of the CNC layer is more influential on increasing the mechanical performance of actuators compared to conductivity of the CNC layer. In their set of experiments the sample with 100% RuO_2 and no gold flakes exhibited the largest mechanical strain, as shown in **Figure 2.6**.

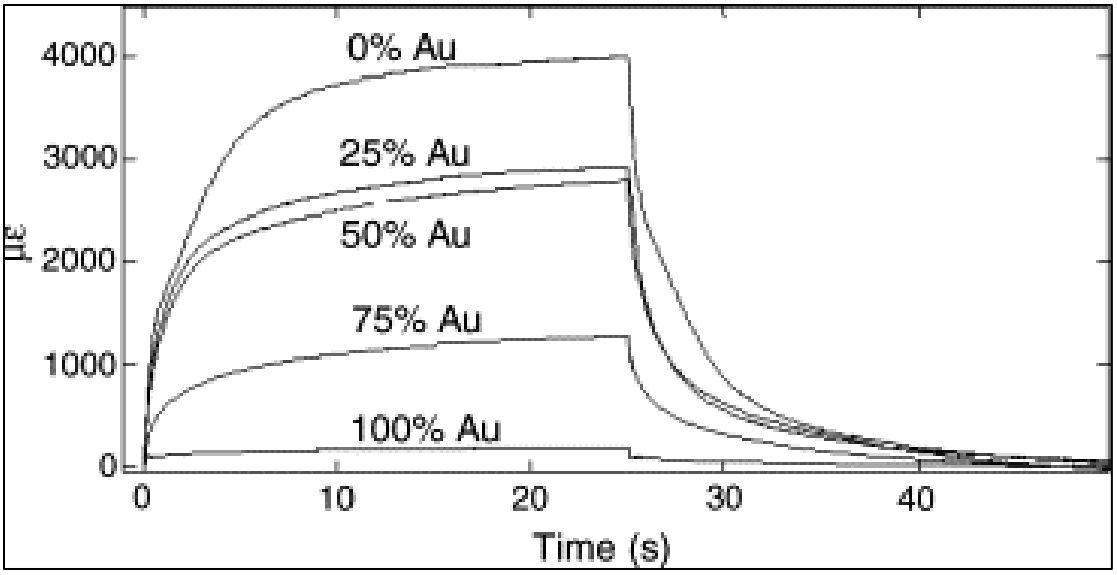

Figure 2.6. Strain output to the application of square wave potentials of ±2 V[14]

In a different study, Kim *et al.* studied the mechanical behavior of IEAP actuators consisting of ionomeric membranes with different thicknesses.[20] In this study, tip displacement and tip force were characterized as a function of ionomeric membrane (Nafion) thickness and applied voltage. A set of samples with thicknesses ranging from approximately 0.5mm to 1.1mm were tested. This range of thickness is on the higher limit as most other actuators are in the 20-200 micron range. As presented in **Figures 2.7** and **2.8**, they showed that in comparison with actuators with thinner ionomeric membranes, actuators with thicker ionomeric membranes generate larger force for a constant voltage; however the tip displacement is smaller for an actuator with thicker ionomeric membrane.

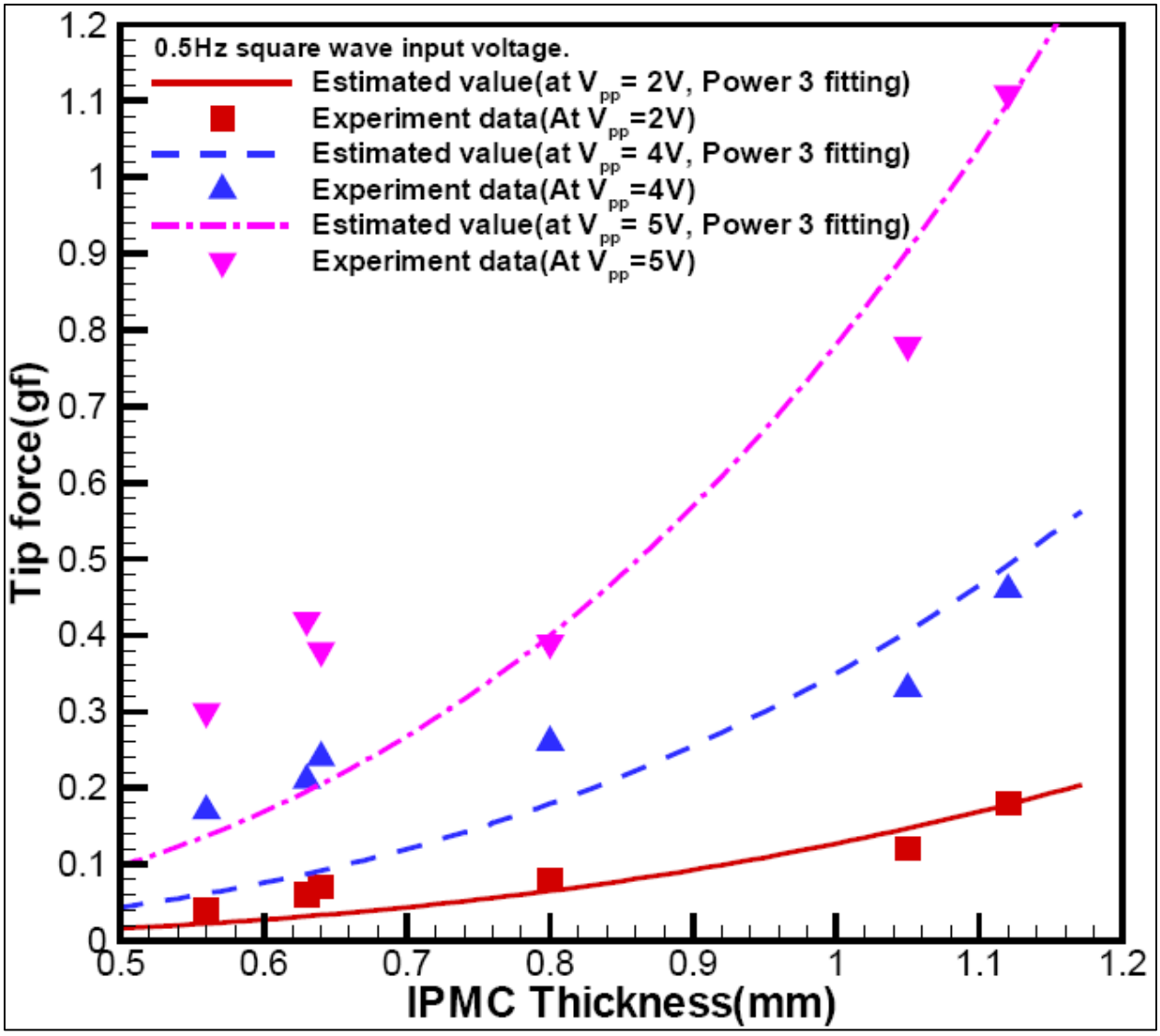

Figure 2.7. Tip force of IPMC strip according to variation of film thickness[20]

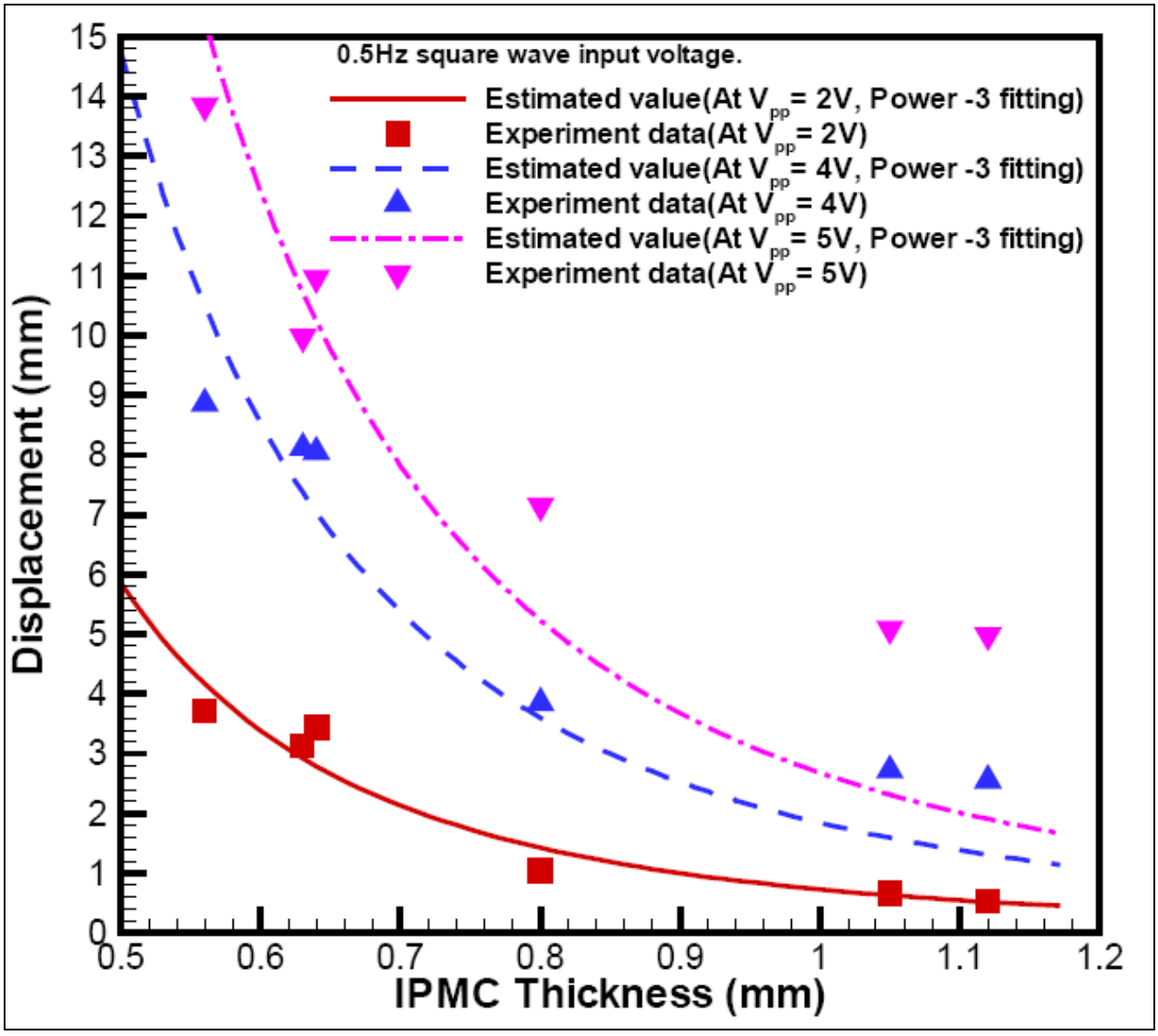

Figure 2.8. Displacement of IPMC strip according to variation of film thickness[20]

In a study to examine the influence of different metal fractions in the CNC on performance of IEAP actuators, Bennet *et al.* employed a new plating method based on an impregnation/reduction process to simultaneously plate multiple metals as electrodes onto Nafion. [21] They embedded different ratios of precious and non-precious metals onto Nafion and showed that both categories of metals can be used in forming CNC layers; however, increasing ratio of precious metals in the alloy improves the stability and lifespan of the actuators, **Figure 2.9**. Also precious metals, primarily gold or platinum, are advantageous as they eliminate the

oxidation problem and do not require further processing steps such as a co-reduction process or deposition of an ultra-thin protective layer.

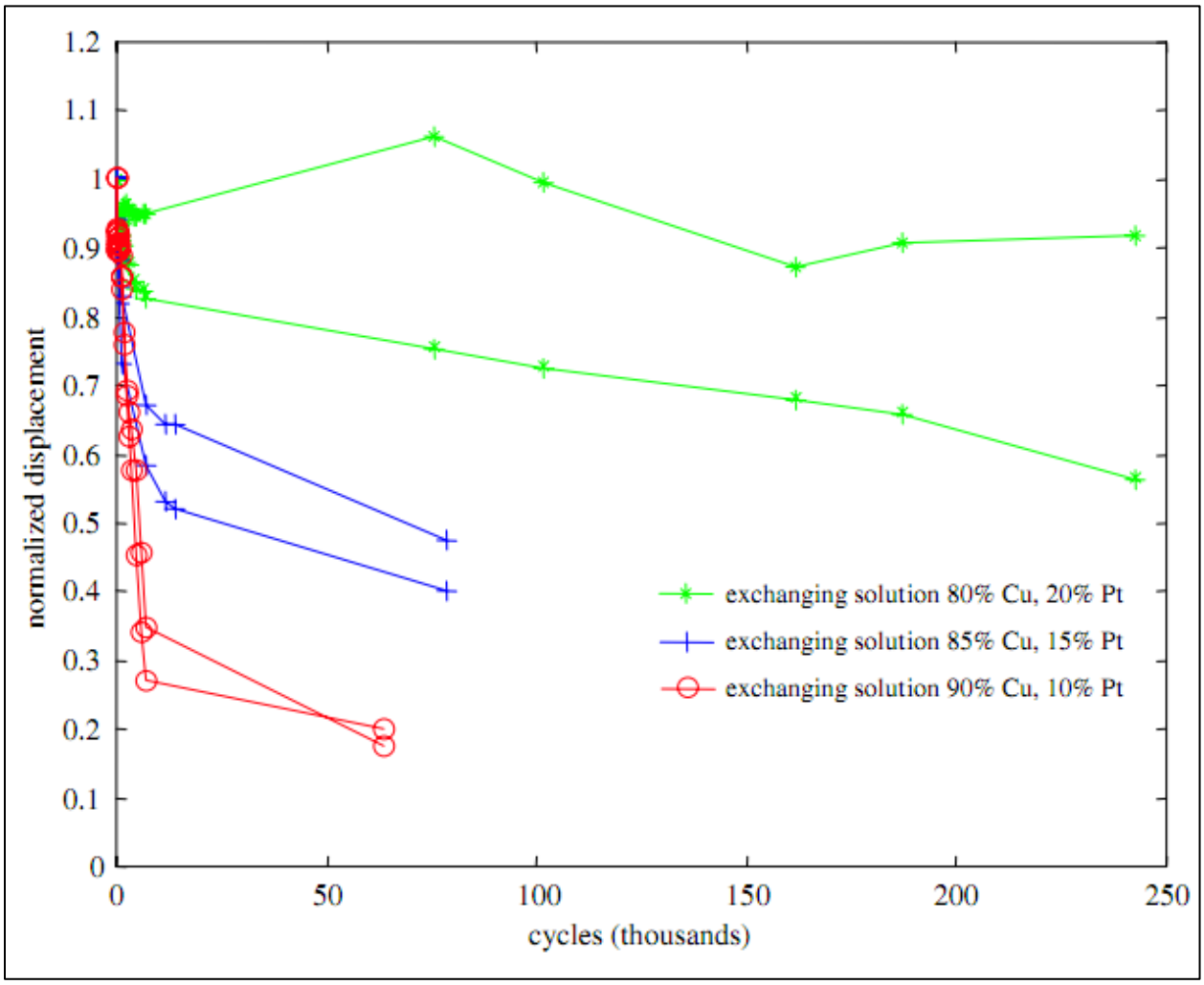

Figure 2.9. Normalized tip displacement versus the number of actuation cycles for three sets of two samples each plated with a copper/platinum alloy electrode using different ion-exchange solutions. The input was a 1.25 V, 1.0 Hz sine wave.[21]

The fabrication method of the CNC is clearly influential on the properties of the actuator. Several methods have been used to form CNC layers on ionomeric membranes to fabricate IEAP actuators. Plating is a traditional method and has been employed by several research groups to form CNC layers on Nafion.[8,22-25] In this method, metal penetrates into the membrane and forms a polymer-metal interfacial area, which is responsible for high electrical capacitance of these

composites. The high density of such composites limits the electrolyte uptake, which generally results in smaller and slower strain response. Painting and spin coating are alternative methods for directly forming the CNC on the membrane. Akle *et al.*[26,27] developed a highly effective method for fabricating electrodes with large polymer-metal interfacial area. In this method, a mixture of metal and Nafion polymer are painted directly onto the Nafion membrane and then hot-pressed into the surface, **Figures 2.10** and **2.11**.

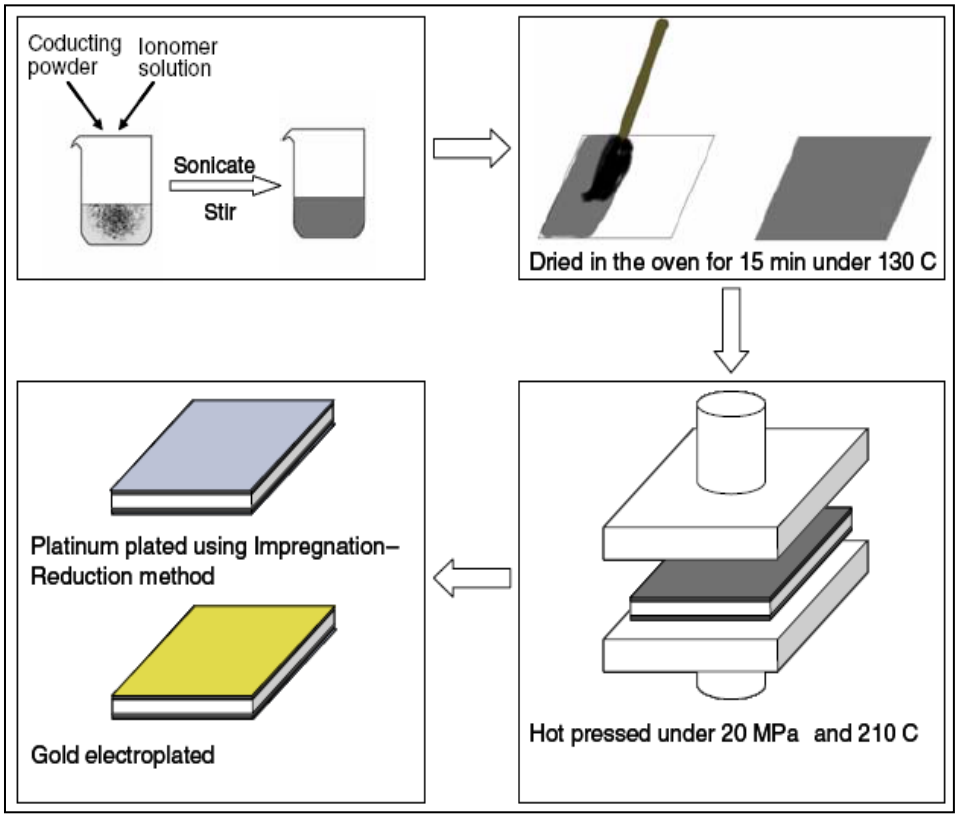

Figure 2.10. Schematic showing the four steps Direct Assembly Process (DAP) for building dry transducers[27]

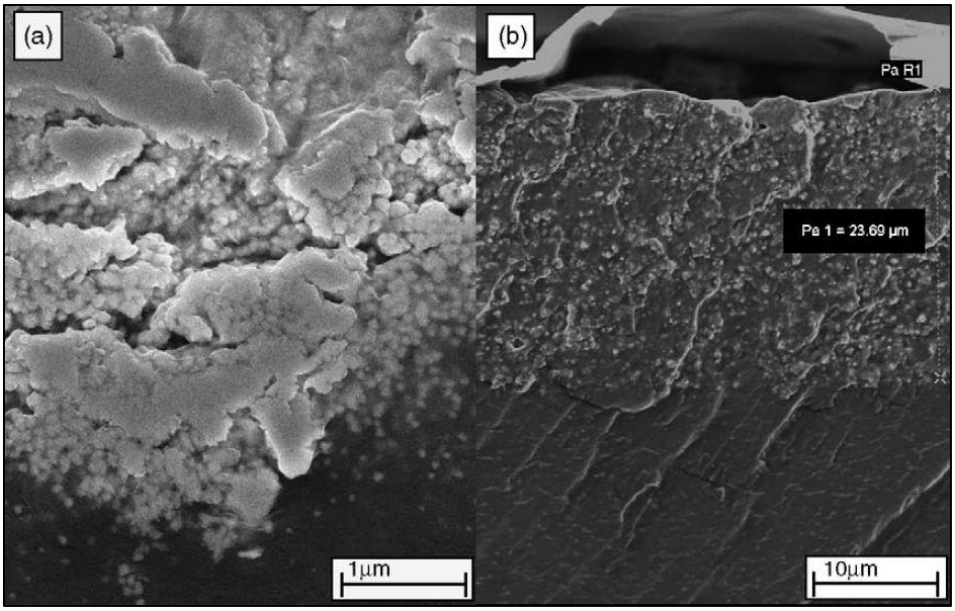

Figure 2.11. SEM images of (a) electrode built using the traditional impregnation/reduction method and (b) electrodes built using the direct assembly process[14]

2.2.3 Outer Electrodes

The outer electrodes have two primary purposes. First is provide means for uniform distribution of electric charge across the actuator, thus actuation is simultaneous and uniform across the device. And second, the outer electrodes encapsulate the actuator and act as protective shields, blocking moisture from penetrating into the system and preventing electrolyte from getting out. The outer electrodes are ultra-thin films of precious metals to minimize blockage force caused by the electrode and also prevent chemical reactions with the surroundings such as oxidation. Gold, platinum and silver are among the most used materials for the outer electrodes. The outer electrodes can be in the form of leafs and be pressed on both sides of the device or can be deposited by electroplating, or other direct deposit methods.

2.2.4 Electrolyte

Technically, any substance with free ions, either in the form of solution or compound, can be used as the ion source of IEAP actuators. For the purpose of IEAP actuators, electrolytes can be divided into two main categories: aqueous and ionic liquids.

Aqueous Electrolytes

Aqueous electrolytes are water-based acid, base, or salt solutions. Use of aqueous electrolytes in IEAP actuators causes many fundamental problems; most important is that it limits the operating voltage of actuators to values below the voltage of water hydrolysis. Bennett *et al.* have shown that use of ionic liquids can eliminate this issue.[28,29] Another issue with using aqueous electrolytes is the decreased lifespan of actuators due to evaporation of the electrolyte.[30-32] In addition, slow switching speed, low ionic conductivity and low environmental stability are other problems associated with aqueous electrolytes.[33]

Ionic Liquids

Ionic liquids are salts that are in their liquid phase at low temperatures. There is not an exact definition for "*low temperature"* in this case, yet generally ionic liquids are expected to exist in their liquid state in room temperature, though less than 100°C is also sometimes considered valid. Ionic liquids consist of near 100% ions with minimal impurity. Ionic liquids have high electric conductivity, very high environmental stability, large electrochemical window and low volatility. They are non-flammable, thermally stable, and have near zero vapor pressure. The concept of ionic liquids is not new. Yet there are disputes on the discovery and discoverer of the first ionic liquid. Ethanolammonium nitrate (melting point 52–55 °C) was first reported in 1888 by S. Gabriel and J. Weiner.[34] One of the first ionic liquid with melting point below room temperature was ethylammonium nitrate (melting point 12 °C), synthesized in 1914 by Paul Walden.[35] In the 1970s and 1980s, several ionic liquids based on alkyl-substituted imidazolium were developed as electrolytes in batteries.[36,37]

After several proof-of-concept IEAP actuators constructed based on aqueous electrolytes as the ion source[25,30,38-43], ionic liquids are now used by many research groups for construction of IEAP actuators. Several improvements and developments are reported on the electromechanical properties and performance of IEAP actuators by these groups. For examples, Bennett *et al*[44] have shown that hydration dependence can be eliminated by use of ionic liquids instead of aqueous electrolytes. They studied the interaction of water miscible EMI-Tf and hydrophobic EMI-Im ionic liquids with the ionomeric membrane and found that interaction between the aforementioned ionic liquids and ionomeric membrane is similar to that between aqueous electrolytes an ionomeric membrane; however the hydration dependence was eliminated in cases

with ionic liquids. Lu *et al*[33] have shown that with ionic liquids, ionomeric polymers can undergo a large number of electrochemical cycles (up to 1 million cycles at 10Hz) before degradation. Kim *et al*[45] have shown that replacing aqueous electrolytes with ionic liquids in IEAP actuators significantly increases the lifetime of the actuators. Akle *et al*[16], Bennett *et al*[28,44], Watanabe *et al*[46,47] and us[48] have shown that using ionic liquids leads to increasing actuation speed and allows higher applied potential.

2.3 Layer-by-Layer Ionic Self-assembly Technique

Fabrication of functional thin films can be achieved via several deposition techniques including physical or chemical vapor deposition, electroplating, spin assisted or spray coating, layer-by-layer (LbL) deposition, and several other techniques. Among all the techniques mentioned above, LbL has several significant advantages that make this technique very useful for fabrication of functional thin films. One key feature of the LbL technique is that any species with multiple ionic charges can be used as one of the components of the LbL assembled thin films[49]. This aspect, along with the fact that charged species can be deposited from aqueous solutions, make a wide range of materials available to be used with this technique such as ionic polymers,[50-52] nano-particles,[53-55] dendrimers,[56-58] quantum dots,[59-61] proteins,[62,63] and DNA.[64,65]

The LbL ionic self-assembly technique was first developed and introduced in 1966 by Iler[66] at Dupont. As a method for depositing charged colloids the technique did not receive much credit nor attention from the scientific community until it was reintroduced in 1991 by Decher *et al* [67]as a process for deposition of charged polymers. Since its redevelopment in 1991, the LbL ionic self-assembly technique has become one of the most preferred techniques for fabrication of thin films and has been practiced by numerous research groups worldwide.

2.3.1 Assembly Concept

The LbL ionic self-assembly technique is based on sequential deposition of oppositely-charged species on a charged substrate.[66,68-70] Although different types of bonds may be involved in formation of the multilayer thin films,[71,72] the most common form of LbL deposition is based on ionic bonds between ionic species[49,70]. **Figure 2.12** shows a schematic of formation of two bilayers via ionic attraction between two ionic polymers.

Exposure of the charged substrate to a dilute aqueous ionic solution of opposite charge forms an ultra-thin layer of the charged molecules on the surface of the substrate. The substrate is then rinsed with deionized (DI) water to wash the loosely bound molecules and immersed in the other dilute aqueous ionic solution with a charge opposite to the charge of the first ionic solution to form another ultra-thin film on the top of the first film. This step is also followed by rinsing with DI water. The two-layer system forms one bilayer. Repetition of these steps results in formation of thin films consisting of several bilayers. A schematic of the LbL ionic self-assembly process is shown in **Figure 2.13**.

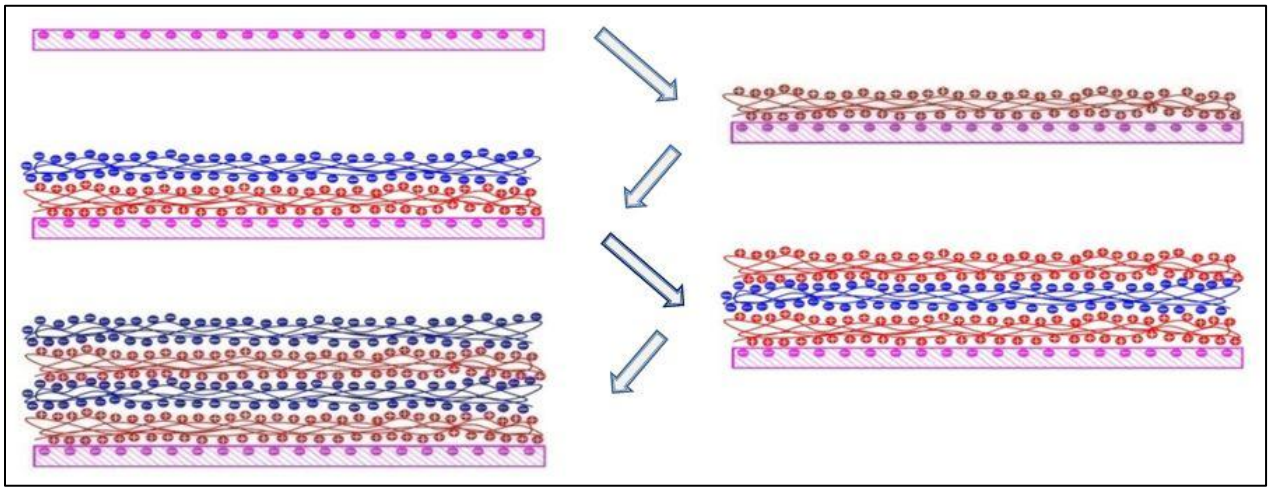

Figure 2.12. Schematic of formation of two bilayers through ionic attraction

Although a wide range of charged materials can be used in the LbL ionic self-assembly technique, as mentioned in section 1.2, only ionic polymers (polycations and polyanions) and charged nanoparticles are used for fabrication of all thin films investigated in this thesis.

2.3.2 Controlled Assembly

Control over the thickness and morphology of each bilayer, and the thin film as a whole, is extremely important in characterization and performance of the functional thin films. The LbL ionic self-assembly technique can be adopted to fabricate thin films of a variety of properties. The morphology and properties of the bilayers can be determined by conditions of the deposition process and characteristics of the ionic species. Deposition conditions such as dipping duration

and number of bilayers, along with solution characteristics such as pH,[73,74] ion concentration,[75] ion type[76], ion strength,[77] and molecular weight[76] can influence the composition of the thin films. Adjusting and optimizing these factors can manipulate the thin films to have desired properties. The dipping duration can vary from 1 to approximately 30 minutes. After a certain amount of time, depending on the conditions and materials, the deposition rate approaches zero due to charge balance between the existing and depositing layers and repulsion of the outer layer towards the polymers in solution. The degree of charge of the materials also effects the deposition quality significantly[78-80].

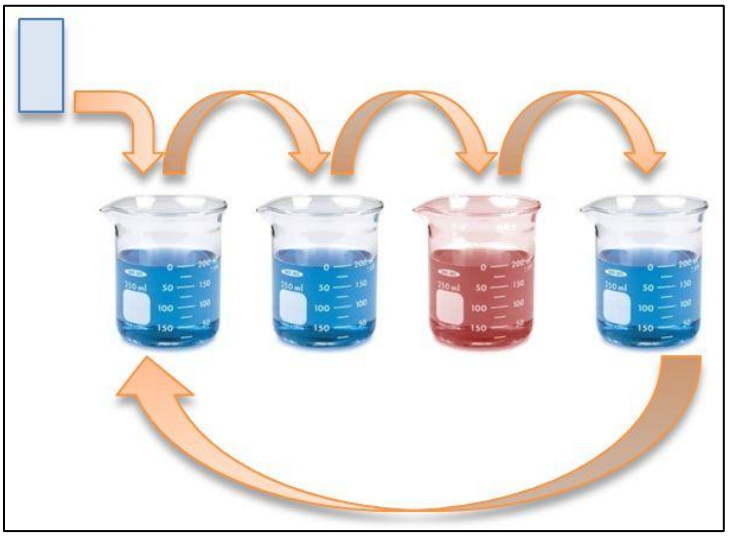

Figure 2.13. Schematic of layer-by-layer ionic self-assembly process

In the case of ionic polymers, varying the charge density of the polymer backbone chains also influence the morphology and the thickness of the thin films. Normally, the polymer molecules are in the form of long chains and the ionic charge is homogeneously distributed among them. Addition of counter-ions, usually through addition of salt, neutralizes some fraction of the charges and reduces the repulsion force along the polymer chain. As a result of the reduced electrostatic repulsion the polymer chains curl and form cluster conformations[81-83]. As shown in **Figure 2.14**, layers deposited from such solutions are generally thicker due to the globular arrangement of the polymer molecules.

Another way to manipulate the charge on the polymer backbone is to adjust the pH of the solution[75,84-86]. This method is especially useful for cases in which the electrolyte is weak, which means that it can be neutralized near neutral pH. Increasing or decreasing the pH increases the charge of carboxyl or amine groups respectively[87-90]. Polyanions are fully charged at high pH and polycations are fully charged at low pH.

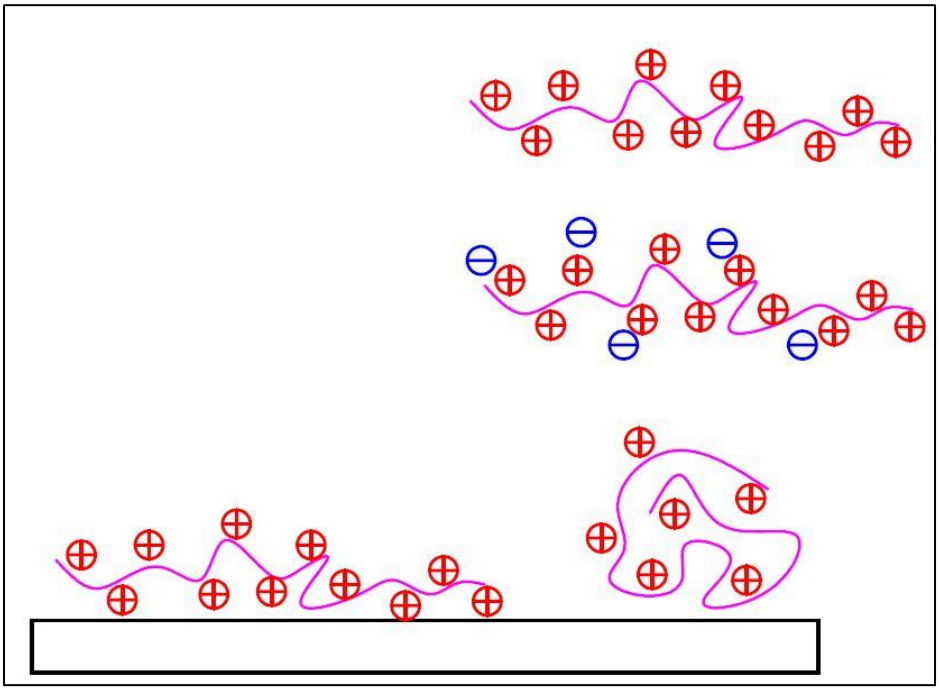

Figure 2.14. Schematic of globular conformation of a polymer chain with low charge density (right) is shown in comparison with a polymer chain with high charge density (left). Polymer chains with lower charge density form globular conformations and so thicker layers.

2.3.3 Incorporation of Nanoparticle

Metallic nanoparticles can be used in fabrication of highly active nanostructures. Presented in **Figure 2.15** is the schematic of formation of two bilayers of nanoparticle-polymer thin-film. Metals like gold, platinum, and palladium are among the most common metals for synthesis of nanoparticles. Metallic nanoparticles are usually synthesized via reduction reaction in aqueous solutions of corresponding chloro-metal anions.[91-93] Other methods such as electrochemical deposition on inert bases[94-96] and metal vapor[97,98] have also been used.

Formation of thin-film structures from metallic nanoparticles on the surface of solid substrates by the LbL ionic self-assembly technique has provided the means for construction of advanced materials.[53,99,100] Kotov *et al.* have shown evidence for ionic self-assembly of ordered nanostructured films composed of poly(diallylmethylammonium chloride) (PDMA-C) and negatively functionalized semiconductor nanoparticles.[53] Titanium dioxide (TiO_2), lead sulfide (PbS) and cadmium sulfide (CdS) were functionalized with thiol and sodium hexametaphosphate and were prepared as aqueous colloid dispersions. It was shown that PDMA-C can be directly self-assemble on a wide variety substrates (eg. quarts, platinum or gold electrodes, ITO coated glass, and Teflon sheet) to form a positively charged foundation for self-assembly of negatively charged nanoparticles. They also showed that the process can be repeated for several cycles to construct thin-films consisting of several bilayers of one or more types of nanoparticles. It was observed that the optical absorbance increase linearly for added number of bilayers, indicating the linear growth of the thin-film.

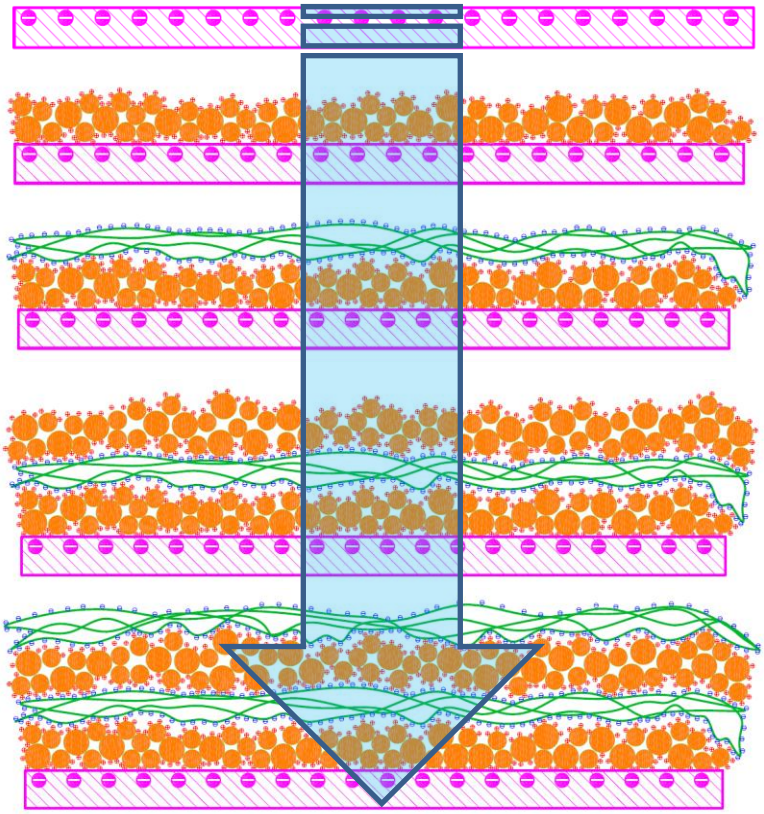

Figure 2.15. Schematic of formation of two bilayers of nanoparticle-polymer thin-film through ionic attraction

Ostrander *et al.* have investigated the structure of LbL ionic self-assembly thin-films of yttrium ion garnet (YIG) nanoparticles functionalized with organic groups.[101] Their study was focused on the control of the nanoparticle density in the thin-film structure. They observed linear dependence of optical density on the growth of the thin-film structure. They compared thin-films of functionalized YIG formed via LbL ionic self-assembly with the thin-films of YIG (not functionalized) formed via in-plane growth of isolated particle domains (lateral expansion mode) and observed that thin-films from functionalized YIG exhibit densely packed nanoparticle layers with greatly reduced number of defects.

Hicks *et al.* have shown that growth rate of polymer-nanoparticle thin-films depends on the pH of the polymer solution along with other details of solution exposure.[102] They have studied two sets of composites, one based on polycation and negatively charged nanoparticles, and the other

based on polyanion and positively charged nanoparticles. In case of negatively charged nanoparticles, higher pH of polycation solution resulted in an increased thin-film thickness. The contrary occurred in case of positively charged nanoparticle and polyanion. It was also observed that nanoparticles with diameters more comparable to polymer repeat unit (~1.6 nm) combine better with counterionic polymers in LbL ionic self-assembly.

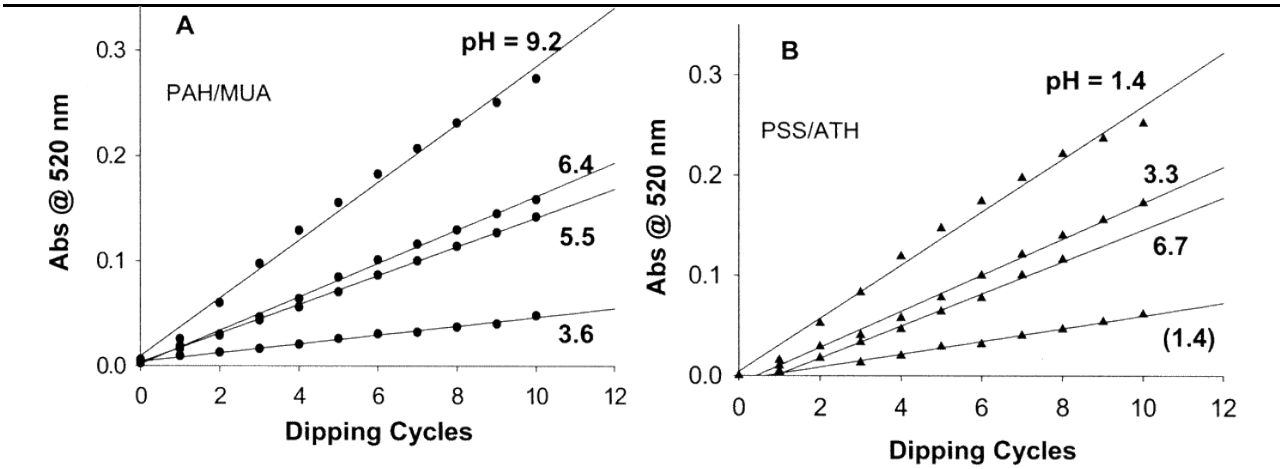

Figure 2.16. Plot of 520-nm absorbance of a LbL ionic self-assembly multilayer film grown on a glass slide as a function of the pH of the polymer solution. (A) Negatively charged nanoparticles system, pH as shown in the figure. (B) Positively charged nanoparticles system, pH as shown in the figure, except for lowest curve (1.4) obtained with a four-step dipping procedure.[102]

Krasteva *et al.* have shown that AuNP-dendrimer thin-films can be fabricated via LbL ionic self-assembly technique.[103] While the AuNPs were utilized to provide electrical conductivity, the dendrimers were served to cross-link the AuNPs and to provide sites for analyte molecules. It was observed that most thin-films physical properties such as thickness and roughness depend on the properties of dendrimers, when electrical properties only depend on AuNPs.

Malikova *et al.* have used LbL ionic self-assembly to achieve structural control over optical properties of AuNP based nanostructures for thin-film sensors with a transduction mechanism based on the variations between AuNP layers. They have demonstrated that LbL ionic self-assembly technique can be utilized for the gradual control over interparticle interactions. LbL ionic self-assembly can be used to control the strength of NP-NP coupling in the layered

composition. Also it was observed that thickness of each layer is comparable with the characteristic length of the interactions.

On another study, Yu *et al.* have shown that AuNPs can be used to form densely packed thin-film structures. AuNP were functionalized with 4-(dimethylamino)pyridine and used along with poly(sodium 4-styrene sulfonate) and poly(allylamine hydrochloride) as counterionic solutions. It was observed that the adsorption matrix resulted in the formation of dense nanoparticle thin-films, and that presence of AuNPs greatly improves the electric conductivity of the thin-film.

Tian *et al.* have shown that polyaniline (PANI) polycation and mercaptosuccinic-acid-capped AuNPs can be used to form stable multilayers via LbL ionic self-assembly technique. Presence of capped AuNPs in the thin-film structure can effectively dope PANI and shift its electroactivity to neutral pH, which is good electroactivity in neutral pH environment. This shift in electroactivity behavior makes the thin-film feasible for bio-assays, such as electrocatalyzation of the oxidation of NADH dehydrogenase and detection of DNA hybridization.

References

1 R Pelrine, R Kornbluh, Q Pei, and J Joseph, "High-speed electrically actuated elastomers with strain greater than 100%," SCIENCE **287** (5454), 836 (2000).

2 QM Zhang, V Bharti, and X Zhao, "Giant electrostriction and relaxor ferroelectric behavior in electron-irradiated poly(vinylidene fluoride-trifluoroethylene) copolymer," Science **280** (5372), 2101-2104 (1998).

3 W. Lehmann, H. Skupin, C. Tolksdorf, E. Gebhard, R. Zentel, P. Kruger, M. Losche, and F. Kremer, "Giant lateral electrostriction in ferroelectric liquid-crystalline elastomers," Nature **410** (6827), 447-450 (2001).

4 Carla Heitner-Wirguin, "Recent advances in perfluorinated ionomer membranes: structure, properties and applications," JOURNAL OF MEMBRANE SCIENCE **120** (1), 1-33 (1996).

5 Kenneth A. Mauritz and Robert B. Moore, "State of Understanding of Nafion," Chemical Reviews **104** (10), 4535-4586 (2004).

6 Klaus Schmidt-Rohr and Qiang Chen, "Parallel cylindrical water nanochannels in Nafion fuel-cell membranes," Nat Mater **7** (1), 75-83 (2008).

7 J Wang, CY Xu, M Taya, and Y Kuga, "A Flemion-based actuator with ionic liquid as solvent," Smart Materials & Structures **16** (2), S214-S219 (2007).

8 Sia Nemat-Nasser and Yongxian Wu, "Comparative experimental study of ionic polymer--metal composites with different backbone ionomers and in various cation forms," Journal of Applied Physics **93** (9), 5255-5267 (2003).

9 A. Ghielmi, P. Vaccarono, C. Troglia, and V. Arcella, "Proton exchange membranes based on the short-side-chain perfluorinated ionomer," Journal of Power Sources **145** (2), 108-115 (2005).

10 Nikhil H. Jalani and Ravindra Datta, "The effect of equivalent weight, temperature, cationic forms, sorbates, and nanoinorganic additives on the sorption behavior of Nafion®," JOURNAL OF MEMBRANE SCIENCE **264** (1-2), 167-175 (2005).

11 J. Halim, F. N. Büchi, O. Haas, M. Stamm, and G. G. Scherer, "Characterization of perfluorosulfonic acid membranes by conductivity measurements and small-angle x-ray scattering," ELECTROCHIMICA ACTA **39** (8-9), 1303-1307 (1994).

12 K. D. Kreuer, M. Schuster, B. Obliers, O. Diat, U. Traub, A. Fuchs, U. Klock, S. J. Paddison, and J. Maier, "Short-side-chain proton conducting perfluorosulfonic acid ionomers: Why they perform better in PEM fuel cells," Journal of Power Sources **178** (2), 499-509 (2008).

13 J. Lin, Y. Liu, and QM Zhang, "Charge dynamics and bending actuation in Aquivion membrane swelled with ionic liquids," POLYMER (2010).

14 BJ Akle, MD Bennett, and DJ Leo, "High-strain ionomeric-ionic liquid electroactive actuators," Sensors and Actuators A: Physical **126** (1), 173-181 (2006).

15 M Shahinpoor and KJ Kim, "Novel ionic polymer-metal composites equipped with physically loaded particulate electrodes as biomimetic sensors, actuators and artificial muscles," Sensors and Actuators A: Physical **96** (2-3), 125-132 (2002).

16 BJ Akle, DJ Leo, MA Hickner, and JE McGrath, "Correlation of capacitance and actuation in ionomeric polymer transducers," J. Mater. Sci. **40** (14), 3715-3724 (2005).

17 R. Tiwari and K.J. Kim, "Effect of metal diffusion on mechanoelectric property of ionic polymer-metal composite," APPLIED PHYSICS LETTERS **97**, 244104 (2010).

18 M. Porfiri, "Charge dynamics in ionic polymer metal composites," JOURNAL OF APPLIED PHYSICS **104** (10), 104915-104915-104910 (2008).

19 Tatsuhiro Okada, Gang Xie, Oddvar Gorseth, Signe Kjelstrup, Norito Nakamura, and Tomoaki Arimura, "Ion and water transport characteristics of Nafion membranes as electrolytes," ELECTROCHIMICA ACTA **43** (24), 3741-3747 (1998).

20 B Kim, M B Kim, J Ryu, I-H Oh, S-K Lee, S-E Cha, and J Pak, "Analysis of mechanical characteristics of the ionic polymer metal composite (IPMC) actuator using cast ion-exchange film," Proc. SPIE Smart Materials and Structure **5051**, 9 (2003).

21 MD Bennett and DJ Leo, "Manufacture and characterization of ionic polymer transducers employing non-precious metal electrodes," Smart Materials & Structures **12** (3), 424-436 (2003).

22 P Millet, R Durand, E Dartyge, G Tourillon, and A Fontaine, "Precipitation of metallic platinum into Nafion ionomer membranes," Journal of the Electrochemical Society **140**, 1373 (1993).

23 Tariq Rashid and Mohsen Shahinpoor, presented at the Proc. SPIE Smart Materials and Structure, Newport Beach, CA, USA, 1999 (unpublished).

24 K Oguro, Y Kawami, and H Takenaka, "Bending of an ion-conducting polymer film-electrode composite by an electric stimulus at low voltage," Journal of Micromachine Society **5** (1), 27-30 (1992).

25 M Shahinpoor, Y Bar-Cohen, JO Simpson, and J Smith, "Ionic polymer-metal composites (IPMCs) as biomimetic sensors, actuators and artificial muscles - a review," Smart Materials & Structures **7** (6), R15-R30 (1998).

26 BJ Akle, K Wiles, DJ Leo, and J McGrath, presented at the Proc. SPIE Smart Materials and Structure, 2004 (unpublished).

27 BJ Akle, MD Bennett, DJ Leo, KB Wiles, and JE McGrath, "Direct assembly process: a novel fabrication technique for large strain ionic polymer transducers," J. Mater. Sci. **42** (16), 7031-7041 (2007).

28 MD Bennett and DJ Leo, "Ionic liquids as stable solvents for ionic polymer transducers," Sensors & Actuators: A. Physical **115** (1), 79-90 (2004).

29 MD Bennett and DJ Leo, San Diego, CA, USA, 2004 (unpublished).

30 M Shahinpoor and KJ Kim, "Ionic polymer-metal composites: I. Fundamentals," Smart Materials & Structures **10** (4), 819-833 (2001).

31 M Shahinpoor, "Ionic polymer-conductor composites as biomimetic sensors, robotic actuators and artificial muscles - a review," Electrochemica Acta **48** (14-16), 2343-2353 (2003).

32 M Shahinpoor and KJ Kim, "Mass transfer induced hydraulic actuation in ionic polymer-metal composites," Journal of Intelligent Material Systems and Structures **13** (6), 369-376 (2002).

33 W Lu, AG Fadeev, BH Qi, E Smela, BR Mattes, J Ding, GM Spinks, J Mazurkiewicz, DZ Zhou, GG Wallace, DR MacFarlane, SA Forsyth, and M Forsyth, "Use of ionic liquids for pi-conjugated polymer electrochemical devices," Science **297** (5583), 983-987 (2002).

34 S. Gabriel and J. Weiner, "Ueber einige Abkömmlinge des Propylamins," Berichte der deutschen chemischen Gesellschaft **21** (2), 2669-2679 (1888).

35 P. Walden, Bull. Acad. Imper. Sci. (St. Petersburg), 1800, 405-422 (1914).

36 Helena L. Chum, V. R. Koch, L. L. Miller, and R. A. Osteryoung, "Electrochemical scrutiny of organometallic iron complexes and hexamethylbenzene in a room temperature

molten salt," JOURNAL OF THE AMERICAN CHEMICAL SOCIETY **97** (11), 3264-3265 (1975).

37 John S. Wilkes, Joseph A. Levisky, Robert A. Wilson, and Charles L. Hussey, "Dialkylimidazolium chloroaluminate melts: a new class of room-temperature ionic liquids for electrochemistry, spectroscopy and synthesis," Inorganic Chemistry **21** (3), 1263-1264 (1982).

38 Mohsen Shahinpoor and Kwang J. Kim, presented at the Smart Structures and Materials 2001: Electroactive Polymer Actuators and Devices, Newport Beach, CA, USA, 2001 (unpublished).

39 Mohsen Shahinpoor and Kwang J. Kim, "Solid-state soft actuator exhibiting large electromechanical effect," Applied Physics Letters **80** (18), 3445-3447 (2002).

40 M Shahinpoor, KJ Kim, and DJ Leo, "Ionic polymer-metal composites as multifunctional materials," Polymer Composites **24** (1), 24-33 (2003).

41 M Shahinpoor and KJ Kim, "Ionic polymer-metal composites: III. Modeling and simulation as biomimetic sensors, actuators, transducers, and artificial muscles," Smart Materials & Structures **13** (6), 1362-1388 (2004).

42 M Shahinpoor and KJ Kim, "Ionic polymer-metal composites: IV. Industrial and medical applications," Smart Materials & Structures **14** (1), 197-214 (2005).

43 M Shahinpoor and KJ Kim, "Solid-state soft actuator exhibiting large electromechanical effect," Applied Physics Letters **80** (18), 3445-3447 (2002).

44 M.D. Bennett, D.J. Leo, G.L. Wilkes, F.L. Beyer, and T.W. Pechar, "A model of charge transport and electromechanical transduction in ionic liquid-swollen Nafion membranes," POLYMER **47** (19), 6782-6796 (2006).

45 D. Kim, K. J. Kim, and Y. Tak, "Self-oscillating electroactive polymer actuator," APPLIED PHYSICS LETTERS **90** (18) (2007).

46 Masashi Watanabe, Hirofusa Shirai, and Toshihiro Hirai, "Ionic polarization in bending-electrostrictive response of polyurethane films," JOURNAL OF APPLIED PHYSICS **90** (12), 6316-6320 (2001).

47 Masashi Watanabe, Hirofusa Shirai, and Toshihiro Hirai, "Wrinkled polypyrrole electrode for electroactive polymer actuators," JOURNAL OF APPLIED PHYSICS **92** (8), 4631-4637 (2002).

48 S Liu, R Montazami, Y Liu, V Jain, M Lin, JR Heflin, and QM Zhang, "Layer-by-layer self-assembled conductor network composites in ionic polymer metal composite actuators with high strain response," Applied Physics Letters **95** (2), 3 (2009).

49 JL Lutkenhaus and PT Hammond, "Electrochemically enabled polyelectrolyte multilayer devices: from fuel cells to sensors," Soft Matter **3** (7), 804-816 (2007).

50 P Stroeve, V Vasquez, MAN Coelho, and JF Rabolt, "Gas transfer in supported films made by molecular self-assembly of ionic polymers," THIN SOLID FILMS **284**, 708-712 (1996).

51 V. Jain, H. Yochum, H. Wang, R. Montazami, M. A. V. Hurtado, A. Mendoza-Galvan, H. W. Gibson, and J. R. Heflin, "Solid-state electrochromic devices via ionic self-assembled multilayers (ISAM) of a polyviologen," Macromolecular Chemistry and Physics **209** (2), 150-157 (2008).

52 Vaibhav Jain, Rabindra Sahoo, Joerg R. Jinschek, Reza Montazami, Hank M. Yochum, Fredrick L. Beyer, Anil Kumar, and James R. Heflin, "High contrast solid state electrochromic devices based on Ruthenium Purple nanocomposites fabricated by layer-by-layer assembly," Chemical Communications (31), 3663-3665 (2008).

53 Nicholas A. Kotov, Imre Dekany, and Janos H. Fendler, "Layer-by-Layer Self-Assembly of Polyelectrolyte-Semiconductor Nanoparticle Composite Films," The Journal of Physical Chemistry **99** (35), 13065-13069 (1995).

54 N Malikova, I Pastoriza-Santos, M Schierhorn, NA Kotov, and LM Liz-Marzan, "Layer-by-layer assembled mixed spherical and planar gold nanoparticles: control of interparticle interactions," Langmuir **18** (9), 3694-3697 (2002).

55 AA Mamedov and NA Kotov, "Free-standing layer-by-layer assembled films of magnetite nanoparticles," Langmuir **16** (13), 5530-5533 (2000).

56 J Anzai, Y Kobayashi, N Nakamura, M Nishimura, and T Hoshi, "Layer-by-layer construction of multilayer thin films composed of avidin and biotin-labeled poly (amine) s," Langmuir **15** (1), 221-226 (1999).

57 RF Aroca, PJG Goulet, DS DOS SANTOS, RA Alvarez-Puebla, and ON OLIVEIRA, "Silver nanowire layer-by-layer films as substrates for surface-enhanced Raman scattering," Analytical chemistry(Washington, DC) **77** (2), 378-382 (2005).

58 FN Crespilho, F Huguenin, V Zucolotto, P Olivi, FC Nart, and ON Oliveira, "Dendrimers as nanoreactors to produce platinum nanoparticles embedded in layer-by-layer films for methanol-tolerant cathodes," ELECTROCHEMISTRY COMMUNICATIONS **8** (2), 348-352 (2006).

59 S Jaffar, KT Nam, A Khademhosseini, J Xing, RS Langer, and AM Belcher, "Layer-by-layer surface modification and patterned electrostatic deposition of quantum dots," Nano Letters **4** (8), 1421-1426 (2004).

60 CA Constantine, KM Gattas-Asfura, SV Mello, G Crespo, V Rastogi, TC Cheng, JJ DeFrank, and RM Leblanc, "Layer-by-layer films of chitosan, organophosphorus hydrolase and thioglycolic acid-capped CdSe quantum dots for the detection of paraoxon," J. Phys. Chem. B **107** (50), 13762-13764 (2003).

61 KV Sarathy, PJ Thomas, GU Kulkarni, and CNR Rao, "Superlattices of Metal and Metal-Semiconductor Quantum Dots Obtained by Layer-by-Layer Deposition of Nanoparticle Arrays," J. Phys. Chem. B **103** (3), 399-401 (1999).

62 JD Hong, K Lowack, J Schmidt, and G Decher, "Layer-by-layer deposited multilayer assemblies of polyelectrolytes and proteins: from ultrathin films to protein arrays," PROGRESS IN COLLOID AND POLYMER SCIENCE **93**, 98-98 (1993).

63 T Cassier, K Lowack, and G Decher, "Layer-by-layer assembled protein/polymer hybrid films: nanoconstruction via specific recognition," Supramolecular Science **5** (3-4), 309-315 (1998).

64 J Lang and M Liu, "Layer-by-layer assembly of DNA films and their interactions with dyes," J. Phys. Chem. B **103** (51), 11393-11397 (1999).

65 LP Lu, SQ Wang, and XQ Lin, "Fabrication of layer-by-layer deposited multilayer films containing DNA and gold nanoparticle for norepinephrine biosensor," Analytica chimica acta **519** (2), 161-166 (2004).

66 R. K. Iller, "Multilayers of colloidal particles," Journal of Colloid and Interface Science **21**, 569-594 (1966).

67 G.; Hong Decher, J.D., "Buildup of ultrathin multilayer films by a self-assembly process 1. Consecutive adsorption of anionic and cationic bipolar amphiphiles on charged surfaces," Macromol. Chem., Macromol. Symp **46**, 231 (1991).

68 G Decher, M Eckle, J Schmitt, and B Struth, "Layer-by-layer assembled multicomposite films," Current Opinion in Colloid & Interface Science **3**, 32-39 (1998).

69 Gero Decher, "Fuzzy Nanoassemblies: Toward Layered Polymeric Multicomposites," Science **277** (5330), 1232-1237 (1997).

70 G. Decher, J. D. Hong, and J. Schmitt, "Buildup of ultrathin multilayer films by a self-assembly process: III. Consecutively alternating adsorption of anionic and cationic polyelectrolytes on charged surfaces," THIN SOLID FILMS **210-211** (Part 2), 831-835 (1992).

71 W. B. Stockton and M. F. Rubner, "Molecular-Level Processing of Conjugated Polymers. 4. Layer-by-Layer Manipulation of Polyaniline via Hydrogen-Bonding Interactions," Macromolecules **30** (9), 2717-2725 (1997).

72 Svetlana A. Sukhishvili and Steve Granick, "Layered, Erasable, Ultrathin Polymer Films," Journal of the American Chemical Society **122** (39), 9550-9551 (2000).

73 MF Rubner, "pH-Controlled fabrication of polyelectrolyte multilayers: Assembly and applications," Multilayer thin films: sequential assembly of nanocomposite materials, 133 (2003).

74 SS Shiratori and MF Rubner, "pH-dependent thickness behavior of sequentially adsorbed layers of weak polyelectrolytes," Macromolecules **33** (11), 4213-4219 (2000).

75 HG Bungenberg de Jong, "Crystallisation-coacervation-flocculation," Colloid Science **2**, 232-255 (1949).

76 Sarah L. Clark, Martha Montague, and Paula T. Hammond, "Selective deposition in multilayer assembly: SAMs as molecular templates," Supramolecular Science **4** (1-2), 141-146 (1997).

77 SL Clark, M Montague, and PT Hammond, "Templating of Layer-by-Layer Thin Films: Use of Surface Functionality to Direct Polyion Deposition," POLYMERIC MATERIALS SCIENCE AND ENGINEERING-WASHINGTON- **77**, 620-621 (1997).

78 Y Lvov, G Decher, and H Moehwald, "Assembly, structural characterization, and thermal behavior of layer-by-layer deposited ultrathin films of poly (vinyl sulfate) and poly (allylamine)," Langmuir **9** (2), 481-486 (1993).

79 A Krozer, SA Nordin, and B Kasemo, "Layer by Layer Deposition of 5–50-nm Colloidal Silica Particles Studied by Quartz Microbalance," Journal of Colloid and Interface Science **176** (2), 479-484 (1995).

80 AF Xie and S Granick, "Local electrostatics within a polyelectrolyte multilayer with embedded weak polyelectrolyte," Macromolecules **35**, 1805-1813 (2002).

81 HGM Van de Steeg, MA Cohen Stuart, A De Keizer, and BH Bijsterbosch, "Polyelectrolyte adsorption: a subtle balance of forces," Langmuir **8** (10), 2538-2546 (1992).

82 B. C. Bonekamp, H. A. Vanderschee, and J Lyklema, Journal of Croatica Chemica Acta **56**, 695-704 (1983).

83 M.A.C. Stuart and H Tamai, "Dynamics of adsorbed polymers. 2. Thickness relaxation of poly (ethylene oxide) on glass as a function of segmental binding energy," Langmuir **4** (5), 1184-1188 (1988).

84 D Yoo, SS Shiratori, and MF Rubner, "Controlling bilayer composition and surface wettability of sequentially adsorbed multilayers of weak polyelectrolytes," Macromolecules **31** (13), 4309-4318 (1998).

85 S. S. Shiratori and M. F. Rubner, "pH-Dependent Thickness Behavior of Sequentially Adsorbed Layers of Weak Polyelectrolytes," Macromolecules **33** (11), 4213-4219 (2000).

86 ST Dubas and JB Schlenoff, "Polyelectrolyte multilayers containing a weak polyacid: construction and deconstruction," Macromolecules **34** (11), 3736-3740 (2001).

87 MR Bohmer, OA Evers, and JMHM Scheutjens, "Weak polyelectrolytes between two surfaces: adsorption and stabilization," Macromolecules **23** (8), 2288-2301 (1990).

88 J Blaakmeer, MR Bohmer, MA Stuart, and GJ Fleer, "Adsorption of weak polyelectrolytes on highly charged surfaces. Poly (acrylic acid) on polystyrene latex with strong cationic groups," Macromolecules **23**, 2301-2309 (1990).

89 MR Böhmer, Y El Attar Sofi, and A Foissy, "Calorimetry of Poly-(Acrylic Acid) Adsorption on TiO~ 2," Journal of Colloid and Interface Science **164**, 126-135 (1994).

90 L Dupont and A Foissy, "Evaluation of the adsorption trends of a low molecular-weight polyelectrolyte with a site-binding model," Colloids and Surfaces A: Physicochemical and Engineering Aspects **110** (3), 235-248 (1996).

91 Li-Ping Lu, Shu-Qing Wang, and Xiang-Qin Lin, "Fabrication of layer-by-layer deposited multilayer films containing DNA and gold nanoparticle for norepinephrine biosensor," Analytica chimica acta **519** (2), 161-166 (2004).

92 Chia-Cheng Chen, Chieh-ming J. Chang, and Po-wen Yang, "Vapor-liquid equilibria of carbon dioxide with linoleic acid, [alpha]-tocopherol and triolein at elevated pressures," Fluid Phase Equilibria **175** (1-2), 107-115 (2000).

93 W. Chen, W. P. Cai, Z. X. Chen, and L. D. Zhang, "Structural change of mesoporous silica with sonochemically prepared gold nanoparticles in its pores," Ultrasonics Sonochemistry **8** (4), 335-339 (2001).

94 Michael O. Finot, George D. Braybrook, and Mark T. McDermott, "Characterization of electrochemically deposited gold nanocrystals on glassy carbon electrodes," Journal of Electroanalytical Chemistry **466** (2), 234-241 (1999).

95 Michael O. Finot and Mark T. McDermott, "Characterization of n-alkanethiolate monolayers adsorbed to electrochemically deposited gold nanocrystals on glassy carbon electrodes," Journal of Electroanalytical Chemistry **488** (2), 125-132 (2000).

96 Samuel Guerin and George S. Attard, "Electrochemical behaviour of electrodeposited nanostructured palladium+platinum films in 2 M H2SO4," ELECTROCHEMISTRY COMMUNICATIONS **3** (10), 544-548 (2001).

97 Martin H. Magnusson, Knut Deppert, Jan-Olle Malm, Jan-Olov Bovin, and Lars Samuelson, "Size-selected gold nanoparticles by aerosol technology," Nanostructured Materials **12** (1-4), 45-48 (1999).

98 Paul J. Collier, Jonathan A. Iggo, and Robin Whyman, "Preparation and characterisation of solvent-stabilised nanoparticulate platinum and palladium and their catalytic behaviour towards the enantioselective hydrogenation of ethyl pyruvate," Journal of Molecular Catalysis A: Chemical **146** (1-2), 149-157 (1999).

99 Janos H. Fendler and Fiona C. Meldrum, "The Colloid Chemical Approach to Nanostructured Materials**," Advanced Materials **7** (7), 607-632 (1995).

100 F. C. Meldrum, N. A. Kotov, and J. H. Fendler, "Utilization of Surfactant-Stabilized Colloidal Silver Nanocrystallites in the Construction of Mono- and Multiparticulate Langmuir-Blodgett Films," LANGMUIR **10** (7), 2035-2040 (1994).

101 John W. Ostrander, Arif A. Mamedov, and Nicholas A. Kotov, "Two Modes of Linear Layer-by-Layer Growth of Nanoparticle−Polylectrolyte Multilayers and Different Interactions in the Layer-by-layer Deposition," JOURNAL OF THE AMERICAN CHEMICAL SOCIETY **123** (6), 1101-1110 (2001).

102 Jocelyn F. Hicks, Young Seok-Shon, and Royce W. Murray, "Layer-by-Layer Growth of Polymer/Nanoparticle Films Containing Monolayer-Protected Gold Clusters," LANGMUIR **18** (6), 2288-2294 (2002).

103 Nadejda Krasteva, Isabelle Besnard, Berit Guse, Roland E. Bauer, Klaus Müllen, Akio Yasuda, and Tobias Vossmeyer, "Self-Assembled Gold Nanoparticle/Dendrimer Composite Films for Vapor Sensing Applications," NANO LETTERS **2** (5), 551-555 (2002).

Chapter 3
Experimental Details

This chapter is provides information on the instruments, materials, techniques and protocols used to conduct the research reported in this dissertation. All the instruments and materials used in this research, with few exceptions, are commercially available. **Section 3.1** contains information on the equipment, materials and protocols for fabrication and characterization of ionic polymer-metal composites. In **Section 3.2** the details of ion exchange process are described along with the materials used for this purpose. **Section 3.3** is devoted to instruments, materials and protocols for final assembly and characterization of IEAP actuators. Blueprints of the in-house fabricated probe station are also provided in this section along with some detail required for maintenance of the instrument.

3.1 Ionic Polymer-Metal Composite

3.1.1 Fabrication Equipment

Automated Dipper

A *StratoSequence 6* (nanoStrata, Inc.) was used to deposit the LbL multilayer thin-films that serve as CNCs on the ion exchange membranes, **Figure 3.1**. This unit contains a platform, capable of holding up to eight beakers (Corning 1000, 150ml) and a sample holder capable of holding four glass slide size sample simultaneously. In our sets of experiments, we used two of the eight beakers for charged solutions and the other six for rinsing steps. The two beakers containing charged solutions were placed at opposite locations on the rotational platform of the instrument with three beakers of deionized water in between them, so deposition of each single layer is followed by three consecutive rinses. The position of the platform (raised or lowered) is controlled by gas pressure provided from a gas cylinder. Each time the platform is lowered, it mechanically engages with a structure that causes it to rotate 45° to the position of next beaker. The samples are secured to the sample holder by small screws. The sample holder itself is attached to an electrical motor, enabling it to spin samples during the deposition process. The speed of the spinning can be reduced or increased relatively, but there is no calibration as there is

no unit presented on the spin speed control dial. The time the samples are in each beaker (dipping time) and the number of multilayers can be set from the controlling software. The spinning can be turned ON or OFF from the controlling software. Deionized water in the rinsing beakers can be replaced after each use to prevent contamination. The contaminated water is sucked out by a pump and clean water, supplied from an external source, is then pumped in.

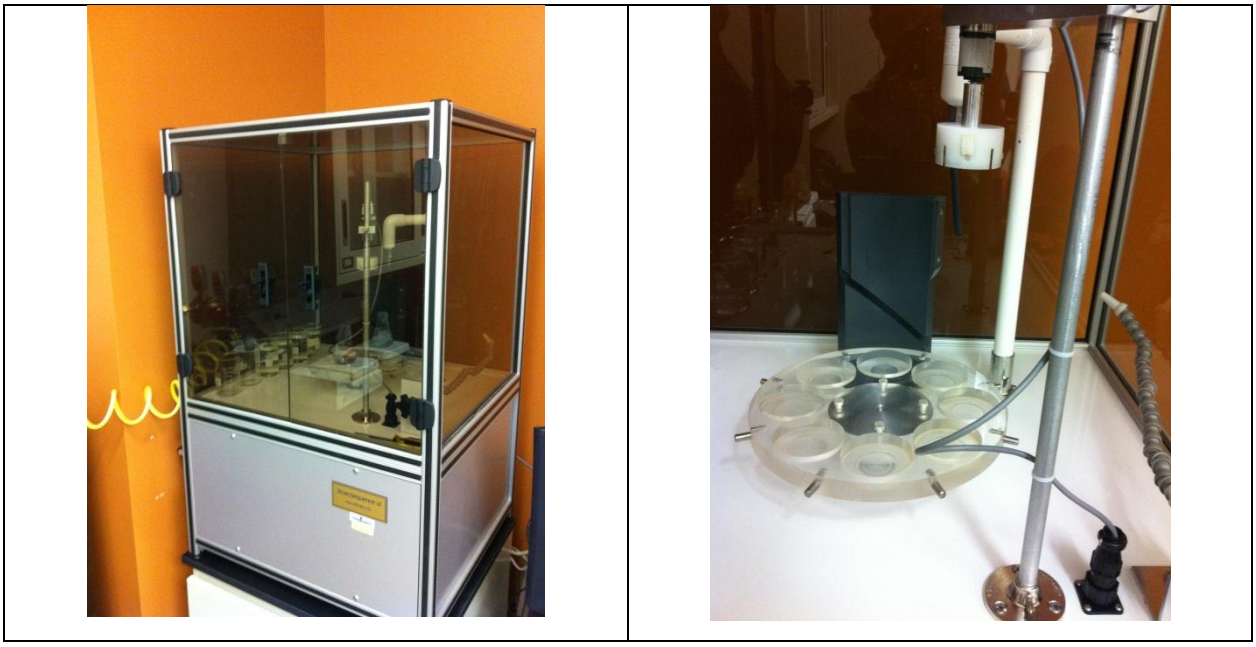

Figure 3.1. (Left) Automated dipper unit is shown along with the solution platform and sample holder (right)

Glass Frames

Glass frames were used to support the ionomeric membrane in the solutions during the CNC deposition process. The glass frames are made from ordinary, 1”×3” microscope glass slides. As shown in **Figure 3.2**, a rectangle of approximately ¾”×2-½” was removed from the glass slide to allow exposure of both sides of ionomeric membrane to solutions. Approximately ½” from the top and a total of ¼” from the sides were left to support the ionomeric membrane.

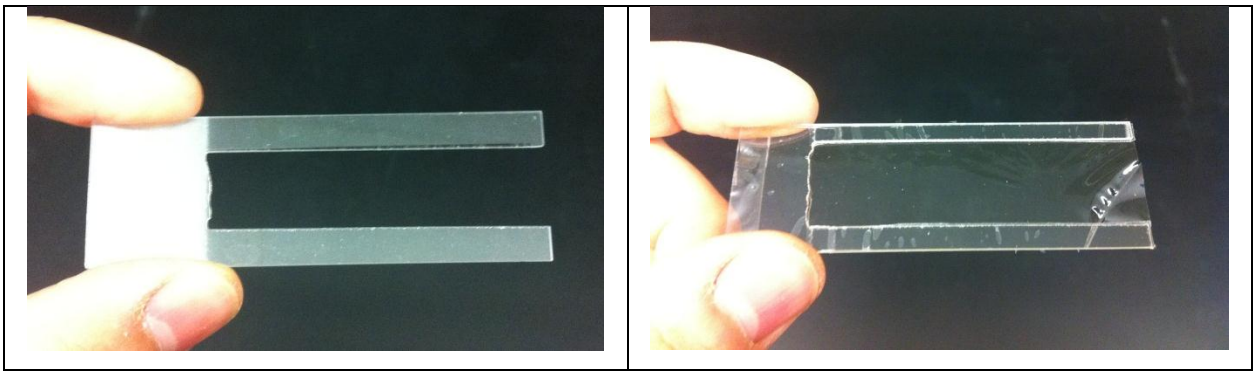

Figure 3.2. (Left) glass frame used to hold the membrane during LbL ionic self-assembly process. (Right) 25 µm thick Nafion membrane attached to a glass frame

3.1.2 Materials

PAH

Poly(allylamine hydrochloride) (PAH) (CAS No. 71550-12-4, Average M_W ~56000) (Sigma Aldrich) was used as the cationic polyelectrolyte solution for layer-by-layer thin-film fabrication. Chemical structure of PAH is shown in **Figure 3.3**. PAH was prepared at a concentration of 10mM at pH 4 in deionized water. PAH is generally prepared by the polymerization of allylamine, and it is available in different average molecular weights, all under the same CAS number. Due to its positive charge, it is to be used in combination with an anionic solution to form layer-by-layer thin-films.

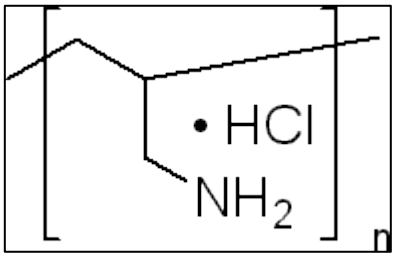

Figure 3.3. Chemical structure of Poly(allylamine hydrochloride), a cationic polyelectrolyte used in formation of LbL thin-films

Nanoparticles (type, charge and size)

Nanoparticles were purchased from Purest Colloids, Inc. For most of the work presented in this dissertation, gold nanoparticles were used. Other nanoparticles (platinum, palladium and copper) were used for preliminary studies. False color TEM image of 30 nm diameter AuNP is shown in **Figure 3.4**. The gold nanoparticles were dispersed in aqueous solution and had an average particle diameter of 3 nm. They were functionalized on the surface with charge groups that yielded a surface potential of -40 mV as determined by zeta potential measurements. The size

and charge of the particles were measured using dynamic light scattering technique and zeta potential measurements, respectively. Gold nanoparticles of larger sizes were purchased from Ted Pella, Inc. but preliminary tests did not exhibit uniform thin-film formation. Other nanoparticles (PtNPs 35-40 nm, -50 mV), (PdNPs 20-25 nm, -40mV) and (CuNPs 200-250 nm) formed relatively good thin-films, yet performance of the actuators were not as good as actuators based on AuNPs, with the exception of CuNPs. Yet to prevent chemical reactions within the system and between the system and atmosphere (oxidation of CuNPs), AuNPs of 3 nm diameter were chosen as the primary nanoparticles for this work. The concentration of 3 nm AuNPs is 20 ppm. Presented in **Figure 3.5** is the scaled schematic of CuNP, PtNP, PdNP and AuNP.

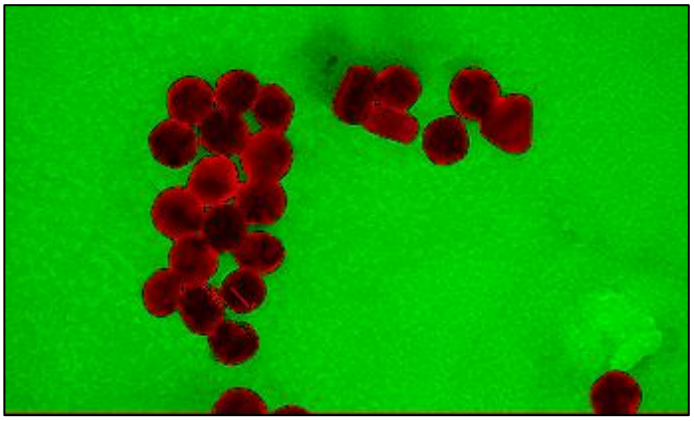

Figure 3.4. False colored, TEM image of 30nm AuNPs from Ted Pella confirming the spherical geometry of the nanoparticles.

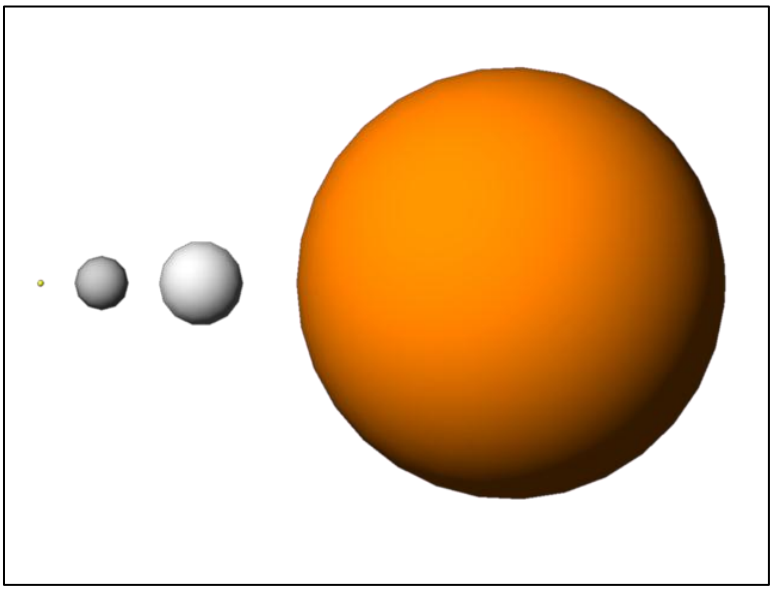

Figure 3.5. Scaled schematic of AuNP (3 nm), PdNP (25 nm) PtNP (40 nm) and CuNP (200)

Nafion

Extruded sheets of 25 µm and 90 µm thick Nafion were purchased from Ion Power, Inc. In preliminary studies, casted Nafion was also used, however it did not exhibit acceptable results compared to extruded Nafion samples. Also, Nafion films of different thicknesses were tested and were shown that for fabrication of fast actuators, 25 µm Nafion is the most suitable candidate. 90 µm Nafion was used in samples made for studying the mobility of ions, where longer travel path is desired to better observe the time difference between motion of cations and anions. All Nafion films used in this work were in acidic form. The chemical structure of Nafion is shown in **Figure 3.6**.

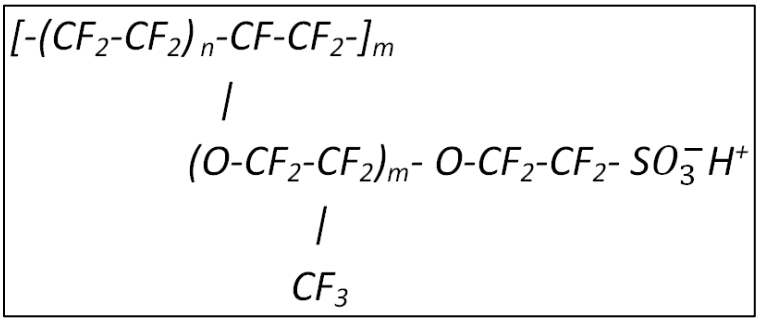

Figure 3.6. Chemical structure of Nafion in its acid form (proton counterion)

3.1.3 Protocols

Glass frames were cleaned with Piranha solution for one hour to remove possible organic residue from the surface of the frame. The frames were then washed and rinsed with deionized water. To secure the ionomeric membrane, double-sided tape (3M Scotch Permanent Double Sided Tape) was applied to the glass frame and the excess was cut and removed using a blade. The frame with double-sided tape was then placed on a sheet of ionomeric membrane, taped-side facing the membrane, and carefully pushed to adhere the ionomeric membrane. A blade was then used to cut ionomeric membrane on the outer edges of the glass frame. The samples were then handled carefully as the frames are extremely fragile. Prior to the thin-film fabrication process, the samples (frames with ionomeric membrane on them) were placed in deionized water for approximately 10 minutes. This step preswells the membranes so that more uniform deposition can be achieved. The samples were then secured to the sample holder of the automated dipper. The PAH solution was placed on the dipper's platform as the first solution and the nanoparticle solution was placed at the opposite position, position five. Positions 2-4 and 6-8 were occupied with beakers for rinsing. The beaker at position 2 was filled with deionized water for the first cycle as its initial position is after the position of water replacing system. The immersion times

for PAH and nanoparticles were set to 5 minutes each and the time for each the rinsing was set to 1 minute each. Rinsing water was replaced after each use. The sample holder was set to spin at the lowest possible speed. After completion of the deposition process, samples were left on the holder to dry in ambient conditions. Ionomeric membranes with CNC layers on both sides (IPMCs) were then cut out of the frame using a blade.

3.1.4 Characterization Equipment

The size and charge of nanoparticles were measured by dynamic light scattering (DLS) and Zeta potential measurement techniques, using a Zetasizer Nano-ZS (Malvern Instruments). DLS measurements were carried out in 12 mm polystyrene cuvettes (DTS 0012) at λ=633nm, and Zeta potential measurements were carried out in disposable capillary cells (DTS 1061), both from Malvern. Malvern DTS software was used to operate the instrument, collect and analyze the data.

Thickness of CNC nanocomposites was measured using a DekTak 150 Stylus Profiler (Veeco). A stylus with 2.5 μm tip radius was used with 3mg force for all the measurements. Measurements were taken on films deposited on glass substrates, rather than ionomeric membrane, with the assumption that the CNC thickness is approximately the same on glass and the ionomeric membrane. The reason for measuring the thickness of the CNC on glass was that 1) softness of ionomeric membrane would interfere with the measurement and 2) it was almost impossible to remove the CNC from part of ionomeric membrane to provide a step height change without damaging the membrane. To take measurements on glass, plastic tweezers were used to make scratches on the surface and remove the CNC. The stylus tip was then probed over the scratched area; starting from a coated area and ending at a coated area, with the scratch in between. The average step height was then calculated by subtracting the average height at the scratched area from that of fully coated area.

The sheet resistance of the CNC thin-films were measured using a Jandel Multi Height Probe equipped with a cylindrical 4-point resistivity probe head (needle radius 500 μm, spacing 1 mm and adjustable load of 10-30g) and controlled by a Jandel RM3-AR test unit. The test unit was used as a combined constant current source and digital voltmeter. The test unit is specially designed for use in making resistivity measurements in combination with four-point probe

equipment. Measurements were taken under low current between 10-100 nA (unless otherwise noted in experimental details) to compensate for the high resistance of the samples. Following on the instructions provided by Jandel, only resistance readings corresponding to 10 – 100 mV potentials were recorded as valid values. The sheet resistance in this system is calculated from **equation 3.1**

$$\boldsymbol{R_s}(\Omega/\square) = \mathbf{4.5324} \times \frac{\boldsymbol{V}\ (\boldsymbol{V})}{\boldsymbol{I}\ (\boldsymbol{A})} \qquad \textbf{3.1}$$

where R_s is sheet resistance and has the unit of ohms/square ($\Omega/\square$)

3.2 Ion Exchanged Nafion

3.2.1 Materials

In most of this work, Nafion was used as received with an H^+ counterion (acid form). In some cases presented in **chapter 8**, the hydrogen was replaced with EMI cationic molecule. EMI-Cl (CAS # 65039-09-0) was used as 0.5 M aqueous electrolyte to exchange the hydrogen counterion of Nafion through an ion exchange process.

3.2.2 Protocol

Salt solutions were prepared at 0.5 M concentration by dissolving the proper amount of the EMI-Cl in deionized water. The solution was then stirred overnight.

Ionic membranes of the desired size (0.5" × 4.5") were cut out of a sheet of 90 micron thick Nafion (Ion Power Inc.) and boiled in diluted sulfuric acid solution (~ 1M, 9:1 water : acid ratio) at ~ 100°C for 120 minutes. Water was added frequently to keep the volume of the mixture constant and to compensate for the evaporated water. The samples were then boiled in deionized water at 100°C for 120 minutes. The samples were then dried using a wipe and cut into smaller pieces.

Samples were then placed in salt solution container with tightened caps, and heated to 80°C for two days. The temperature was then reduced to 60°C for another eight days.

Samples were then placed under vacuum (-29 mm Hg) and heated to 115°C for three days. Then the samples were cut into smaller pieces, weighed and soaked in ionic liquids to uptake ~ 40 wt% of their dry weight.

The samples were then made into actuators (see next section).

3.3 Ionic Electroactive Polymer Actuators

3.3.1 Assembly Equipment

Hot-Press

A PHI hot-press unit, **Figure 3.7**, equipped with a PHI 5000 controller/programmer was used to attach gold leaf outer electrodes on both sides of IPMCs. The hot-press unit has two heating plates; the temperature of each can be controlled separately.

Figure 3.7. The PHI hot-press unit, heating plates are at the top-left of the image

3.3.2 Materials

Gold Leaf

Gold leaves were purchased from L.A. GOLD LEAF. Leaves are 3-1/8" squares of 24K gold, and are "transfer" type (versus loose). The gold leaves are placed on wax paper and the thickness is 50 nm. Transfer type gold leaf is placed on wax paper and it is easier to handle, whereas the loose type which does not have the wax paper and may tear during the process, or get attached to the wrong surface (for example to the Teflon

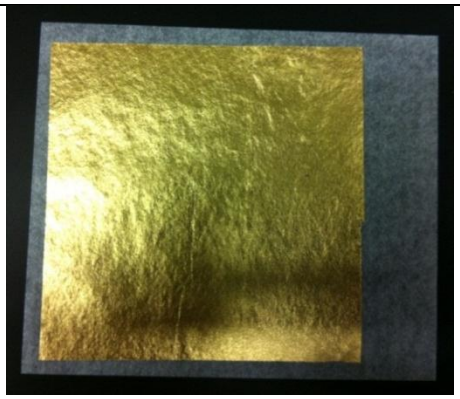

Figure 3.8. 50 nm thick gold leaf on a wax paper

film instead of IPMC). These leaves are also available in Silver (pure) and white gold (12K), yet the pure gold (24K) is the most suitable for IEAP actuators because of its minimum interaction with the environment. A gold leaf on wax paper is shown in **Figure 3.8**.

Ionic Liquids

Three types of ionic liquids were used in this work. 1-Ethyl-3-methylimidazolium trifluoromethanesulfonate (EMI-Tf) (molecular formula: $C_7H_{11}F_3N_2O_3S$) is the most common ionic liquid used in IEAP actuators. Triethylsulfonium bis(trifluoromethylsulfonyl)imide (TES-TFSI) (molecular formula: $C_8H_{15}F_6NO_4S_3$) and 1-Butyl-1-methylpyrrolidinium bis(trifluoromethylsulfonyl)imide (BMP-TFSI) (molecular formula: $C_{11}H_{20}F_6N_2O_4S_2$) were used for the experiments presented in Chapter 7.

Presented in **Figures 3.9** and **3.10** are the chemical structures and three-dimensional chemical structures of three ionic liquids used in this work.

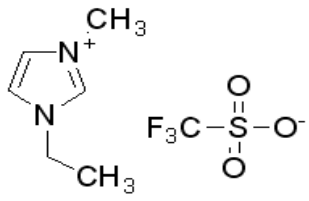	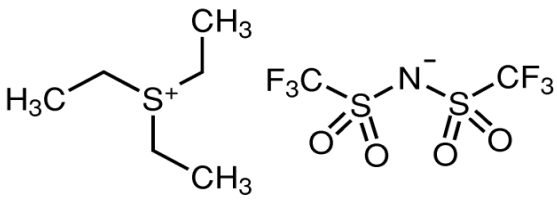	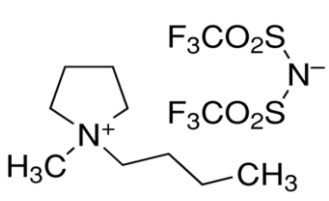
EMI-TF	TES-TFSI	BMP-TFSI

Figure 3.9. Chemical structure of the three ionic liquids used in this research

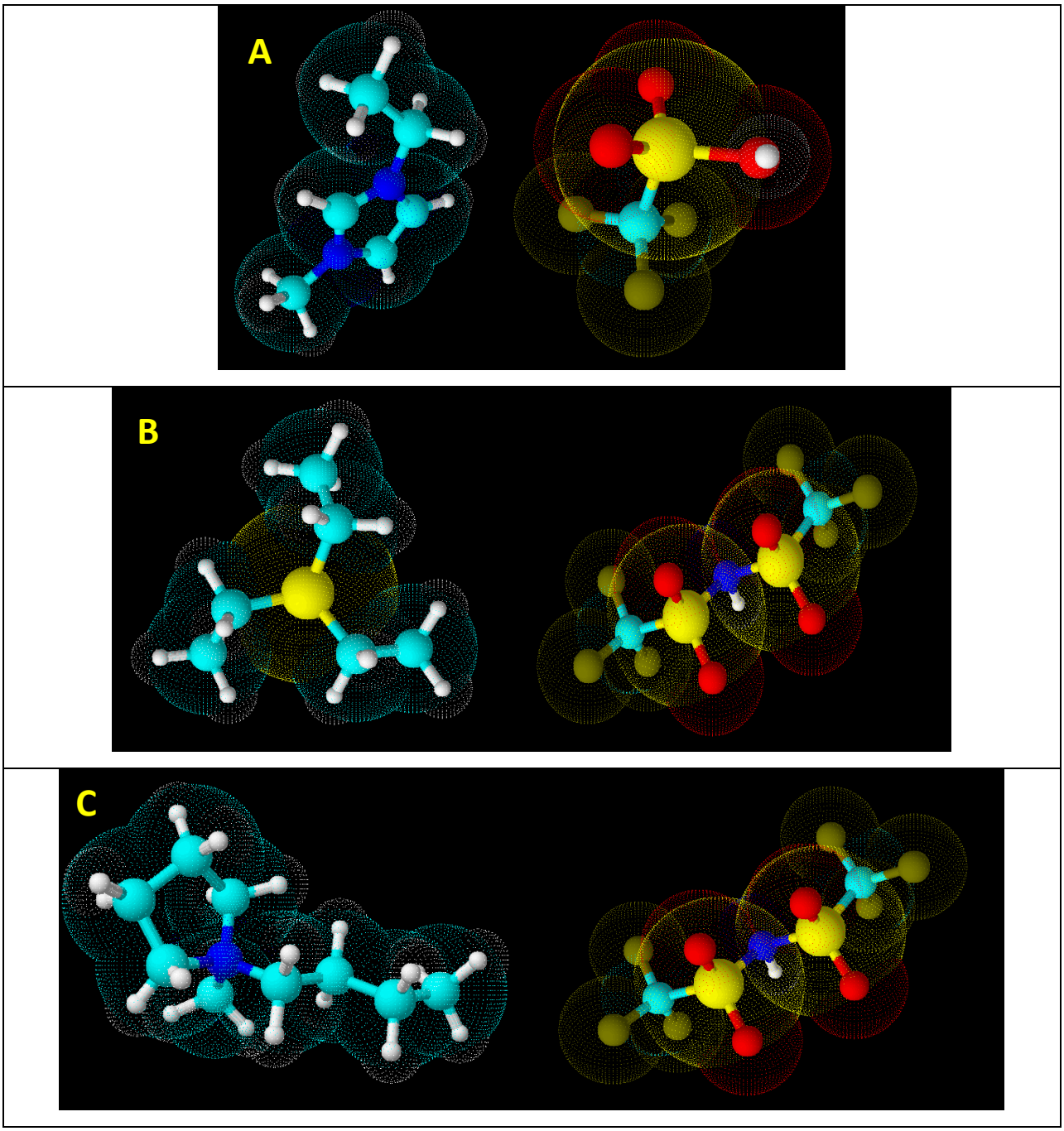

Figure 3.10. A) 1-Ethyl-3-methylimidazolium trifluoromethanesulfonate (EMI-Tf) (molecular formula: $C_7H_{11}F_3N_2O_3S$), B) Triethylsulfonium bis(trifluoromethylsulfonyl)imide (TES-TFSI) (molecular formula: $C_8H_{15}F_6NO_4S_3$), C) 1-Butyl-1-methylpyrrolidinium bis(trifluoromethylsulfonyl)imide (BMP-TFSI) (molecular formula: $C_{11}H_{20}F_6N_2O_4S_2$)

3.3.3 Protocol

To soak the IPMC with ionic liquid, the ionic liquid was first mixed with ethanol (1:1) and heated to about 90°C. The IPMC was weighed with a high-precision microbalance (0.1 mg) and weight was recorded as "dry weight". The target weight with an increase of 40 wt% was calculated from

$$\boldsymbol{w_t = w_d \times 1.4} \qquad \textbf{3.2}$$

where w_t and w_d are *target* and *dry* weights respectively. The IPMC was then placed in the heated ionic liquid-ethanol solution for about 15 minutes. The IPMC was then removed from the solution, dried with a piece of filter paper (by pushing and not wiping) and placed in a vacuum oven at 110°C for 15 minutes to evaporate the ethanol. The weight of the sample was then measured. If the weight was less that the target value, the sample was soaked in the ionic liquid-ethanol solution again, and the above steps would be repeated until the desired weight was achieved. Extra care should be taken not to over soak the sample as it is extremely hard to remove ionic liquid from the IPMC.

After reaching the target ionic liquid intake, gold leaves should be pressed to both sides of the IPMC to make it into an IEAP actuator. It is recommended to do this immediately following the ionic liquid intake to prevent moisture from getting into the system. Gold leaf electrodes isolate the IPMC and prevent moisture from entering the device. To prepare the hot-press unit, the temperature of each plate was set to 95°C, the plates were then pushed together to expedite heating process, which is a time consuming process. To prepare the samples for hot-press, a piece of Teflon film was placed on an aluminum plate, and a sheet of gold leaf was placed on the Teflon film, face up. The sample(s) was then placed on the gold leaf very carefully, as moving the sample while on the leaf would destroy the leaf and sample. Another sheet of gold leaf was placed on the sample carefully, face down. A piece of Teflon film was placed on the top and another aluminum plate was placed on the top of the pile. Extra care must be taken to minimize any unwanted movement of films or plates. Any movement in the horizontal plane may cause the sample to move over the gold leaves, which makes the sample and gold leaves unusable. Once the plates of the hot-press reached the desired temperature, the plates were opened and the sample stack was placed on the lower plate. The plates were then closed and a pressure of

approximately 1000 lb_f (pound-force) was applied for 25 seconds. The plates were then opened and stack was removed. After removing the upper aluminum plate and the Teflon film, upper gold leaf sheet was slowly removed. Samples were then removed using plastic tweezers.

The IEAP actuators were then placed between filter papers and in zip-lock bags to isolate them from the ambient moisture, as well as from possible scratch and tear. At the time of use, a small stripe (~ 1×6 mm^2) was cut from the main piece, using a blade. It is also recommended to push the blade on the main piece rather than moving the blade across the sample.

3.3.4 Characterization Equipment

Probe station

An actuator probe station was designed and constructed to assist operation, force measurements, electroanalytical measurements, charging and discharging studies and imaging of IEAP actuators. Presented in **Figure 3.11** is the in-house made probe station. In this section the design and construction steps are described. Blueprints of the designed parts are also provided for maintenance and reproduction of the parts. All the designed parts are made of ¾" thick polyoxymethylene (POM) also known as Delrin.

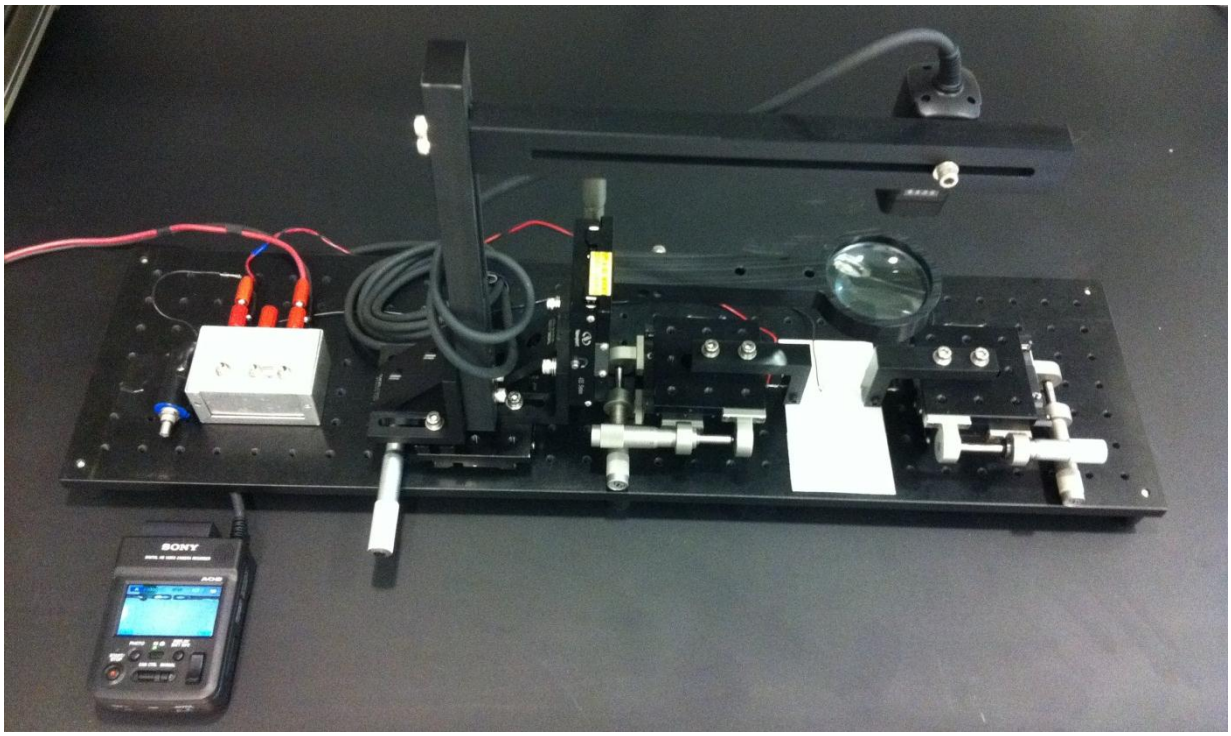

Figure 3.11. In-house fabricated probe station

The probe station consists of three main platforms, two of which are x-y micropositioners with cathode and anode electrodes that will hold and connect to the IEAP actuator, and one is the camera tower which holds and positions the camera and magnifying lens. The control box is a separate unit connected to the electrodes. The camera is controlled by a separate control unit, provided by the camera manufacturer.

Some of the key features of the probe station are:

- Low cost compared to commercially available probe stations
- Large camera travel range in the x-y-z directions
- Upgradeable with new camera, lens, and micro-positioners based on need
- Compatible with potentiostat and data logger
- Multi-meter output

Micropositioners

The two micropositioners are mirror symmetry relative to each other, with an exception of an LED added to one to indicate anode. Each micropositioner consists of two linear micropositioners (one degree of freedom) at 90° rotation on x-y plane. This provides two degrees of freedom for each unit, 20 mm in the x direction and 30 mm in the y direction. An "L" shape extension was designed to attach to the top of each micropositioner to hold the metal electrodes. The extensions are extended 31.75 mm (1-¼") out from the top micropositioner to keep the micropositioners out of the range of camera, when zoomed in. Metal electrodes are attached to the "L" shape extensions and secured by screws. The micropositioners are base-mounted to maximize accuracy and minimize hand-induced vibrations, **Figure 3.12 (top)**.

The camera tower is placed on a micropositioner that allows 40 mm movement in the y direction. The camera tower consists of two pieces perpendicular to each other, one is the main tower which holds the camera shaft in the z direction and one is the camera shaft that holds the camera above the micropositioners and in the x direction. The camera tower allows 140 mm displacement of the camera shaft. The camera shaft allows 254 mm displacement of the camera. The camera shaft has features to prevent the camera from tilting, **Figure 3.12 (bottom)**.

Figure 3.12. Top: Micropositioner is shown. The "L" shape extension can be seen at the top. Bottom: The camera mounted to the camera shaft.

As shown in **Figure 3.13**, a magnifying lens is used to improve the limited zoom and focus features of the camera. The lens is secured to a holder, which is extended to be centered with the camera. The holder is attached to a micropositioner, allowing 35 mm displacement in the z direction, which is to be used for fine focusing. There are two open slots on the micropositioner, thus the position of the holder can be adjusted by ± 25.4 mm, in case lenses with different focal lengths are to be used. The slots can also be used to add other lenses to the instrument.

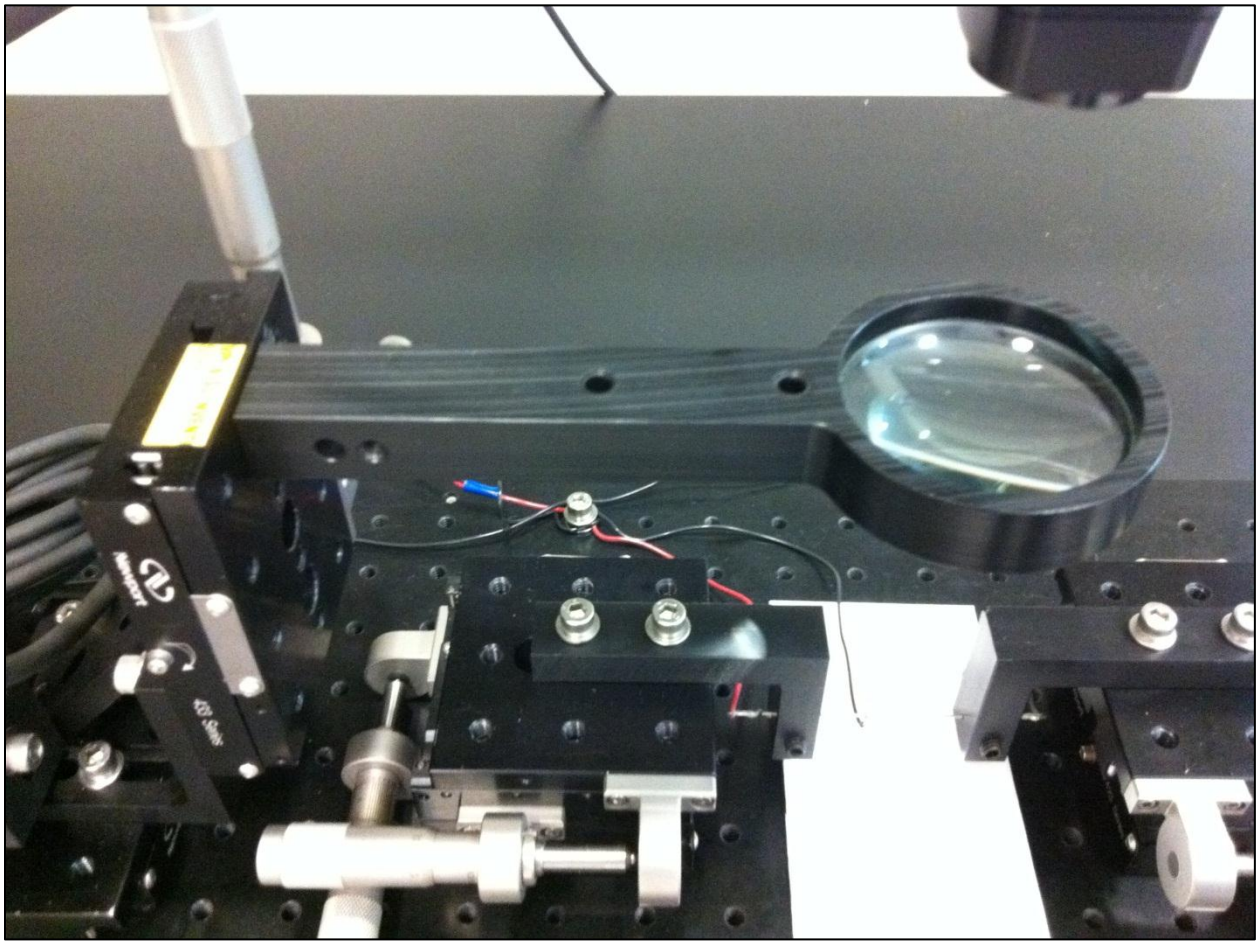

Figure 3.13. Magnifying lens and fine focus micropositioner

The control box consists of six banana jacks and three 2-way smooth slide switches (double pole, double throw (DPDT)). Two of the jacks are for input power, two are for multimeter output and two are output to electrodes on the micropositioners. One of the DPDT switches is to turn on/off the power of the control box, one is for changing the polarity of the input power, and one is to

turn on/off the power to electrodes. Single pole. single throw (SPST) switches could be used for turning the power on/off on the control box and electrodes, yet DPDT switches were used as SPST switches.

The instrument is mounted to a ½" polyoxymethylene base with rubber legs to minimize vibration and also to allow portability of the instrument.

Blue prints of the camera shaft, camera tower, lens holder and sample holders are presented in **Figure 3.14** through **3.18** in the next five pages.

Figure 3.14. Blue print of the camera shaft

Figure 3.15. Blue print of the camera tower

Figure 3.16. Blue print of the lens holder (top view)

Figure 3.17. Blue print of the lens holder (side views)

Figure 3.18. Blue print of the sample holders

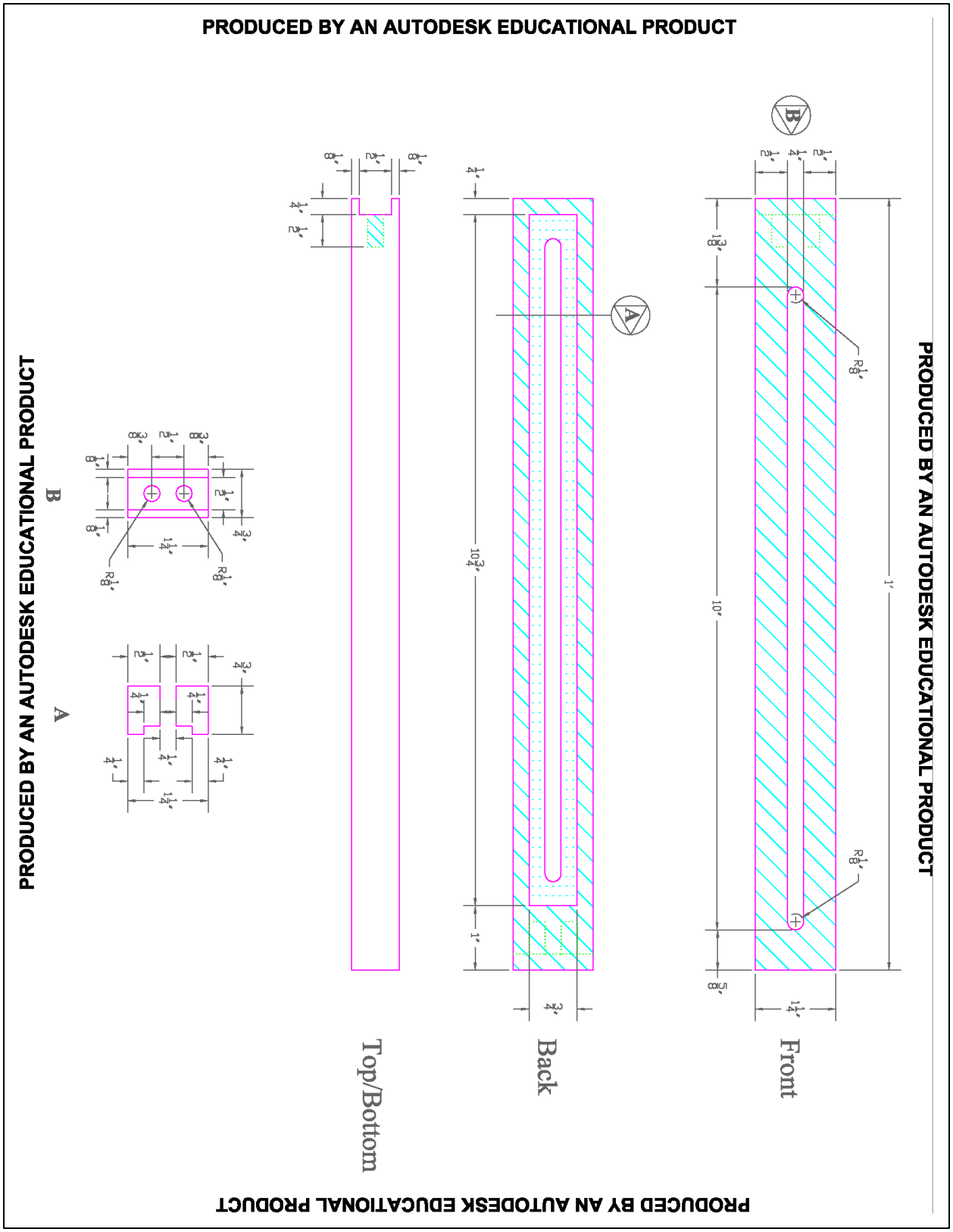
PRODUCED BY AN AUTODESK EDUCATIONAL PRODUCT
PRODUCED BY AN AUTODESK EDUCATIONAL PRODUCT
PRODUCED BY AN AUTODESK EDUCATIONAL PRODUCT
PRODUCED BY AN AUTODESK EDUCATIONAL PRODUCT
Front
Back
Top/Bottom
A
B

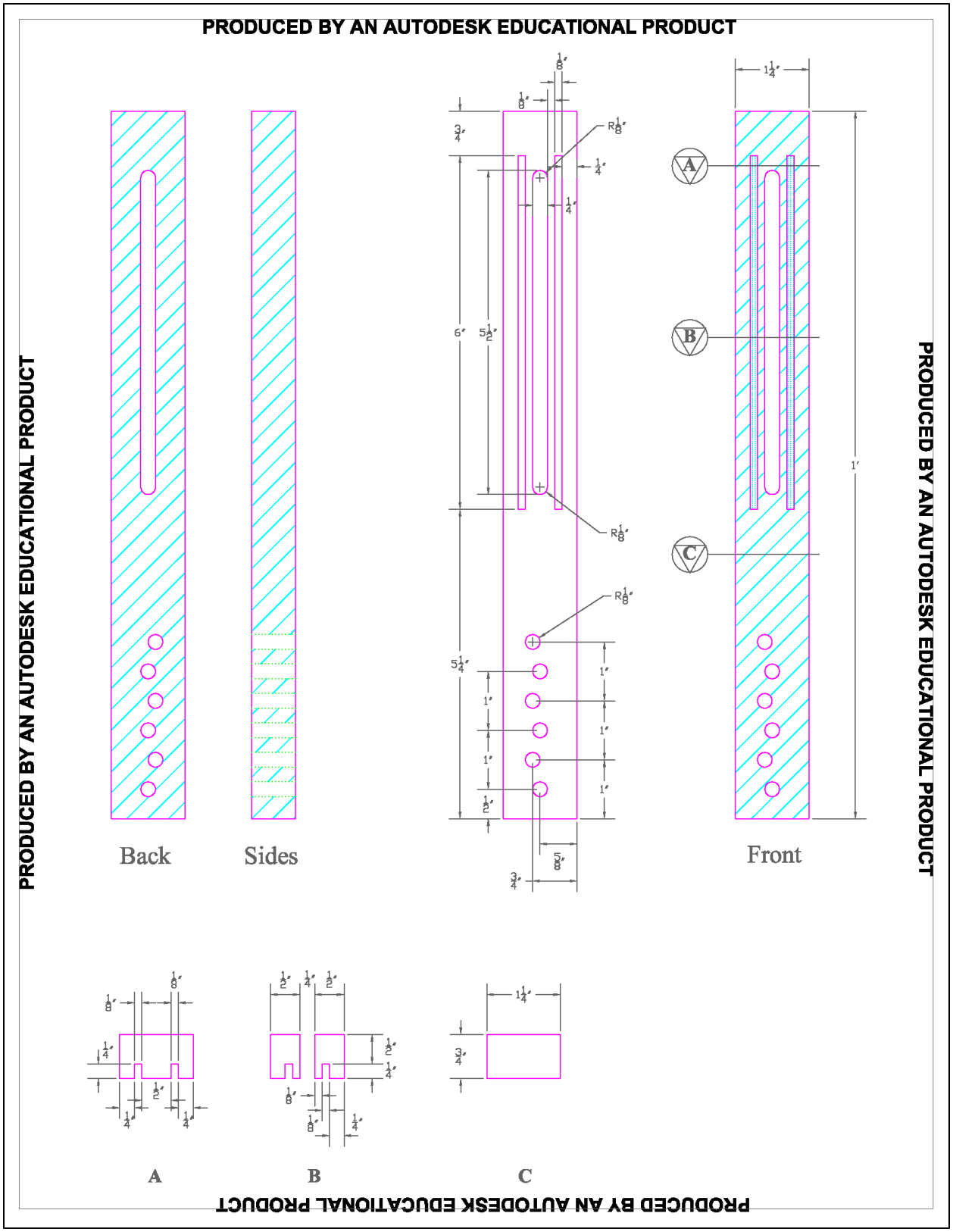
PRODUCED BY AN AUTODESK EDUCATIONAL PRODUCT
PRODUCED BY AN AUTODESK EDUCATIONAL PRODUCT
PRODUCED BY AN AUTODESK EDUCATIONAL PRODUCT
Back
Sides
Front
A
B
C
A
B
C
PRODUCED BY AN AUTODESK EDUCATIONAL PRODUCT

Lens Holder

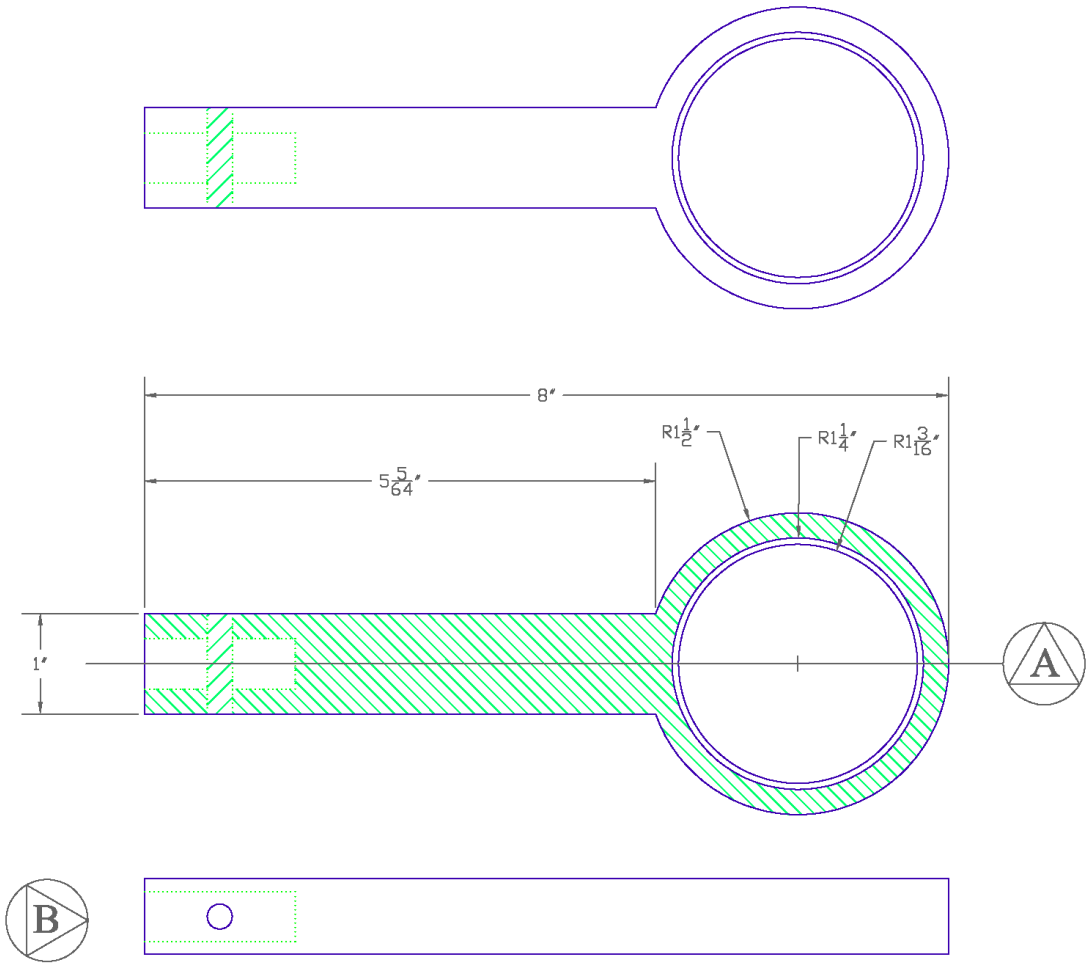

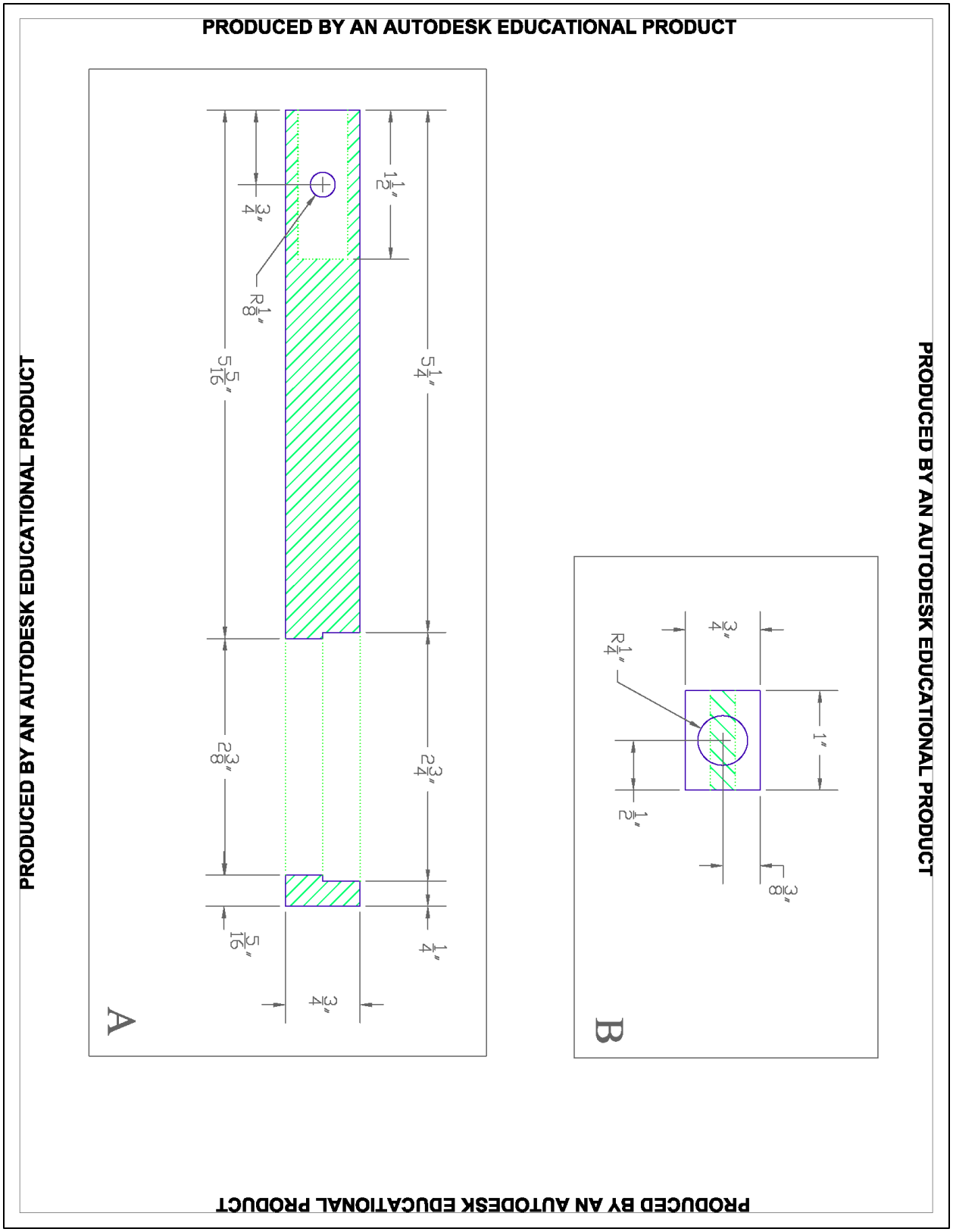
PRODUCED BY AN AUTODESK EDUCATIONAL PRODUCT
PRODUCED BY AN AUTODESK EDUCATIONAL PRODUCT
PRODUCED BY AN AUTODESK EDUCATIONAL PRODUCT
PRODUCED BY AN AUTODESK EDUCATIONAL PRODUCT
A
B
1 1/2"
3/4"
R 1/8"
5 5/16"
5 1/4"
2 3/8"
2 3/4"
5/16"
1/4"
3/4"
3/4"
R 1/4"
1"
1/2"
3/8"

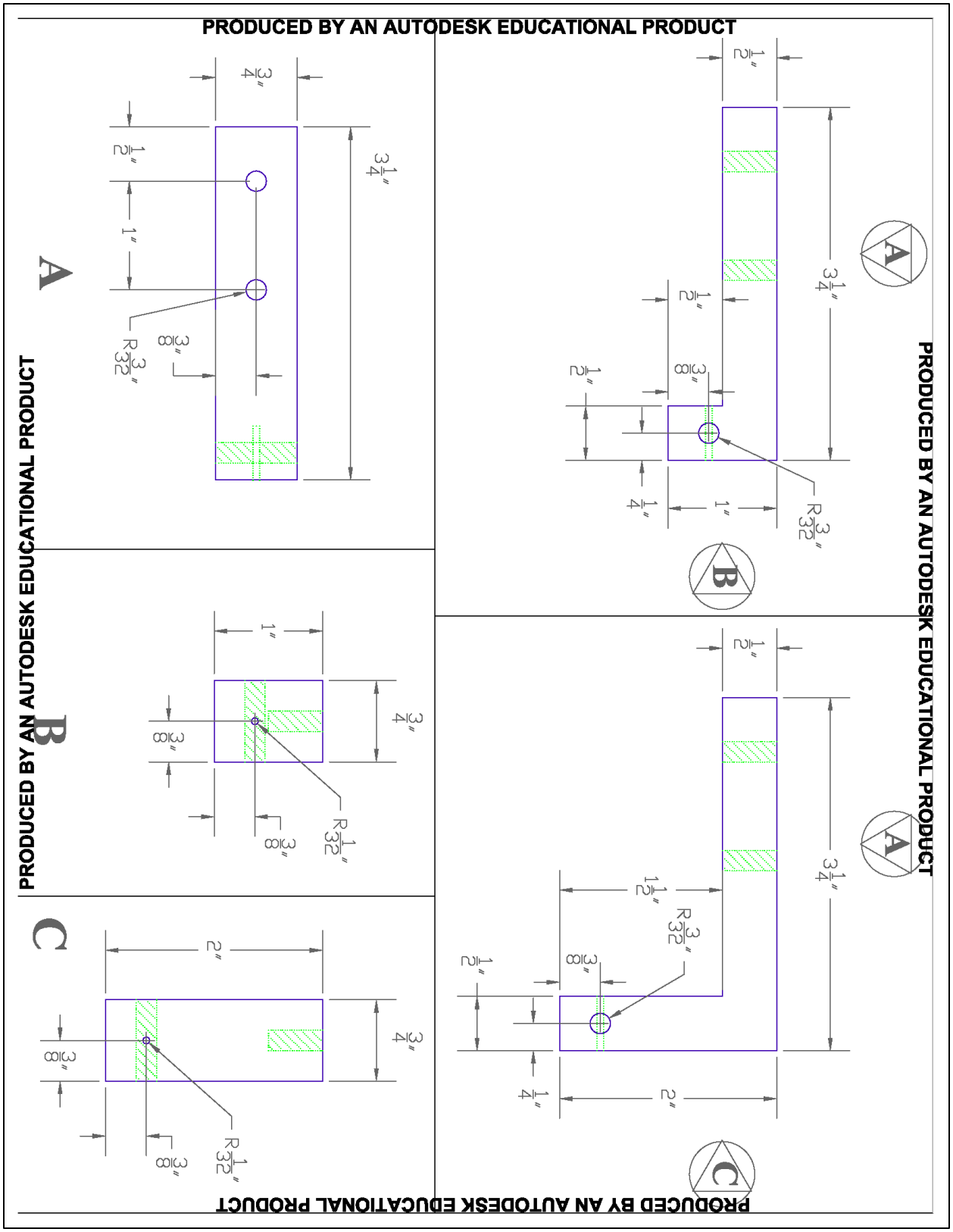
PRODUCED BY AN AUTODESK EDUCATIONAL PRODUCT
PRODUCED BY AN AUTODESK EDUCATIONAL PRODUCT
PRODUCED BY AN AUTODESK EDUCATIONAL PRODUCT
PRODUCED BY AN AUTODESK EDUCATIONAL PRODUCT
A
B
C
A
B
C
3/4"
1/2"
1"
3 1/4"
3/8"
R 3/32"
1/4"
2"
R 1/32"

Electroanalytical measurements

Electroanalytical measurements were performed using a µAUTOLAB (FRA 2, type III) potentiostat, **Figure 3.19**, along with GPES software (Metrohm) to obtain and analyze time dependent current and voltage measurements. The instrument was used in step voltage and sweep voltage modes. The counter and reference electrodes were connected together as one electrode and working electrode was used as the other electrode. GPES software was used to control experiment conditions and to record and preliminary analyze data. Data was exported as CSV files for further analysis with Microsoft Excel.

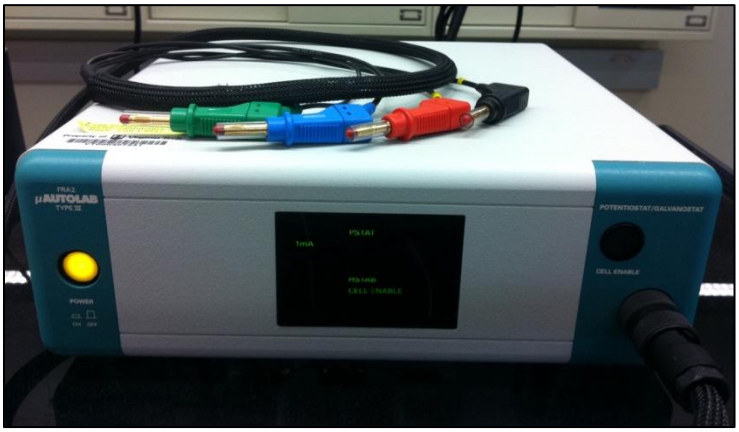

Figure 3.19. µAUTOLAB (FRA 2, type III) potentiostat

Data logger

An Omega® OM-DAQPRO-5300 data logger, **Figure 3.20**, was used to measure and record voltage and current values. The instrument was mainly used in combination with the probe station to record current variations across the electrodes of charging and discharging IEAP actuators. It was also used to monitor voltage across the electrodes of discharging IEAP actuators in some experiments.

Figure 3.20. Omega OM-DAQPRO-5300 data logger

Load cell and signal conditioner

A 10 gram load cell (GS0-10) was used with a 12VDC, 220Hz filter amplifier/ conditioner module (TM0-1), both from Transducer Techniques. The unit generates a voltage between 0-8 V in response to 0 – 10 gram load. The system must first be calibrated.

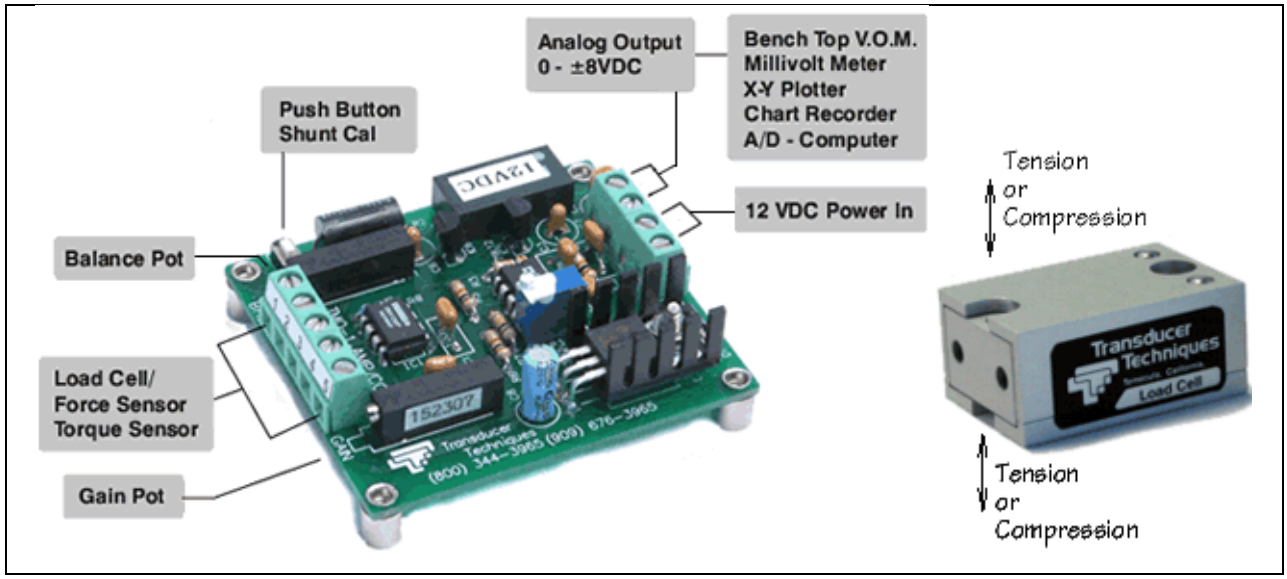

Figure 3.21. Transducer Techniques signal conditioner (left) and load cell (right).

Figure source: Transducer Techniques website

Chapter 4

Preliminary Studies

4.1 Introduction

Prior to systematic study of IEAP actuators, we conducted a wide set of preliminary studies with three primary objectives in mind: first, to choose proper materials for fabrication of CNCs; second, to find means for mechanical and electrical characterization of IEAP actuators; and third, to improve the fabrication process.[1,2]

4.2 Materials

Based on the design for a porous-conductive CNC, spherical metal nanoparticles were chosen as the main structure of CNC layers. The spherical geometry of the nanoparticles would result in formation of nano-channels throughout the CNC and facilitates ion mobility. Metal nanoparticles would also contribute toward electrical conductivity of the CNC, which would increase conductivity and thus reduces charging/discharging times which in turn improves switching speed of the actuators. As shown in **Figure 4.1**, four types of metal nanoparticles with wide size distribution were chosen for preliminary studies. All the nanoparticles were negatively functionalized, thus a PAH polycation was used as the counter ionic solution for LbL ionic self-assembly. Nafion was used as the ionomeric membrane and EMI-Tf as the source of ions. Both of these were chosen based on extensive literature references. Since both materials are very well studied, it would allow us to better understand variations of performance due to the properties of CNC and be able to compare the results with that of IEAP actuators made with different types of CNC.

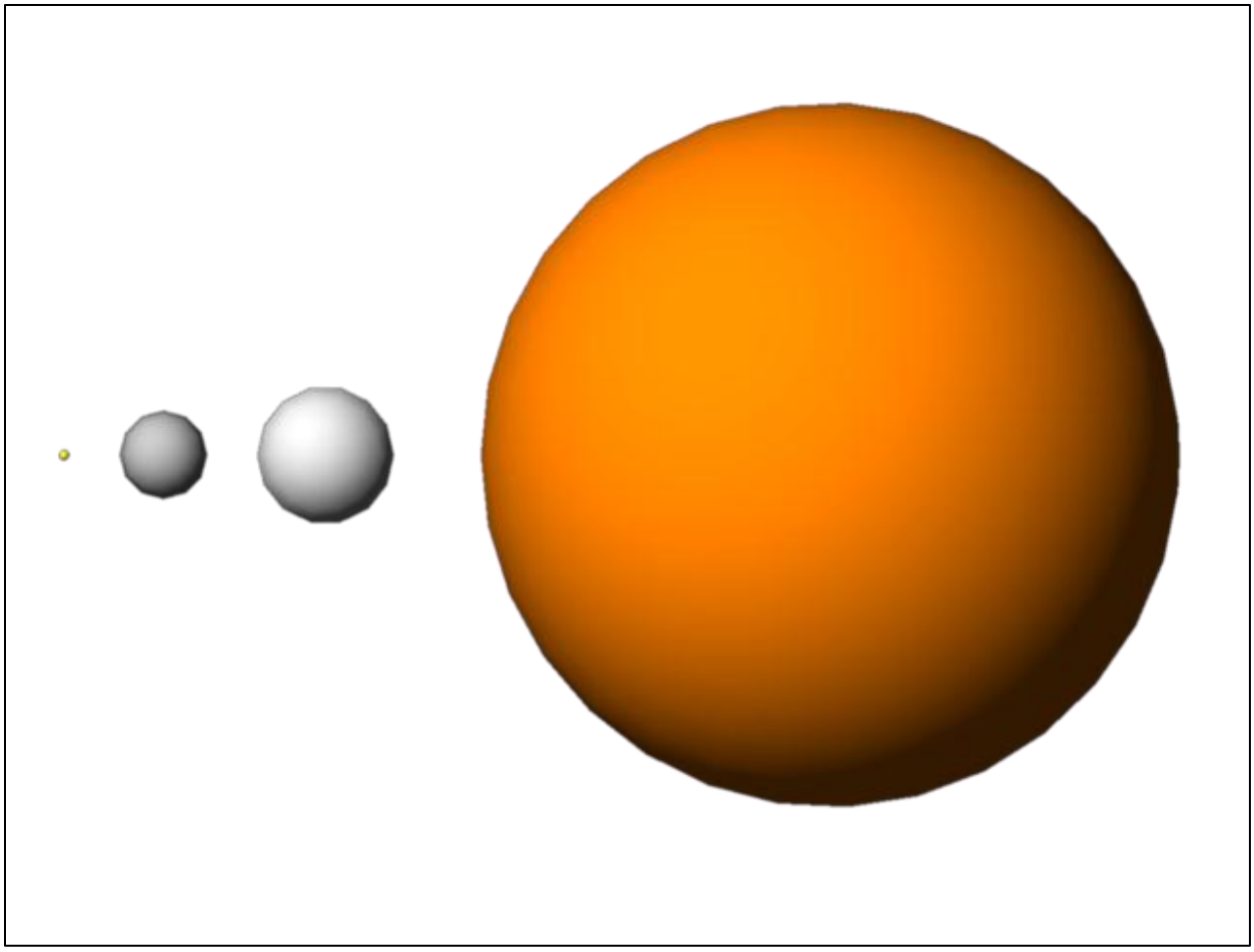

Figure 4.1. To-scale schematic of different nanoparticles used for preliminary studies. Gold nanoparticles of ~3nm diameter, Palladium nanoparticles of ~25nm diameter, Platinum nanoparticles of ~40nm diameter, and Copper nanoparticles of ~ 200nm were chosen

4.2 Characterization

IEAP actuators fabricated based on different metal nanoparticles were characterized for their mechanical properties. First, the actuators were characterized for bending curvature. As shown in **Figure 4.2**, actuators containing larger particles exhibited larger curvature. Under application of 4V, the actuator based on copper nanoparticles exhibited actuation curvature of approximately $0.45mm^{-1}$. The actuation curvature exhibited increase with increase in the diameter of the nanoparticles. Larger nanoparticles form wider nano-channels which facilitates mobility of ions throughout the IPMC. Gold nanoparticles had the largest curvature to particle size ratio.

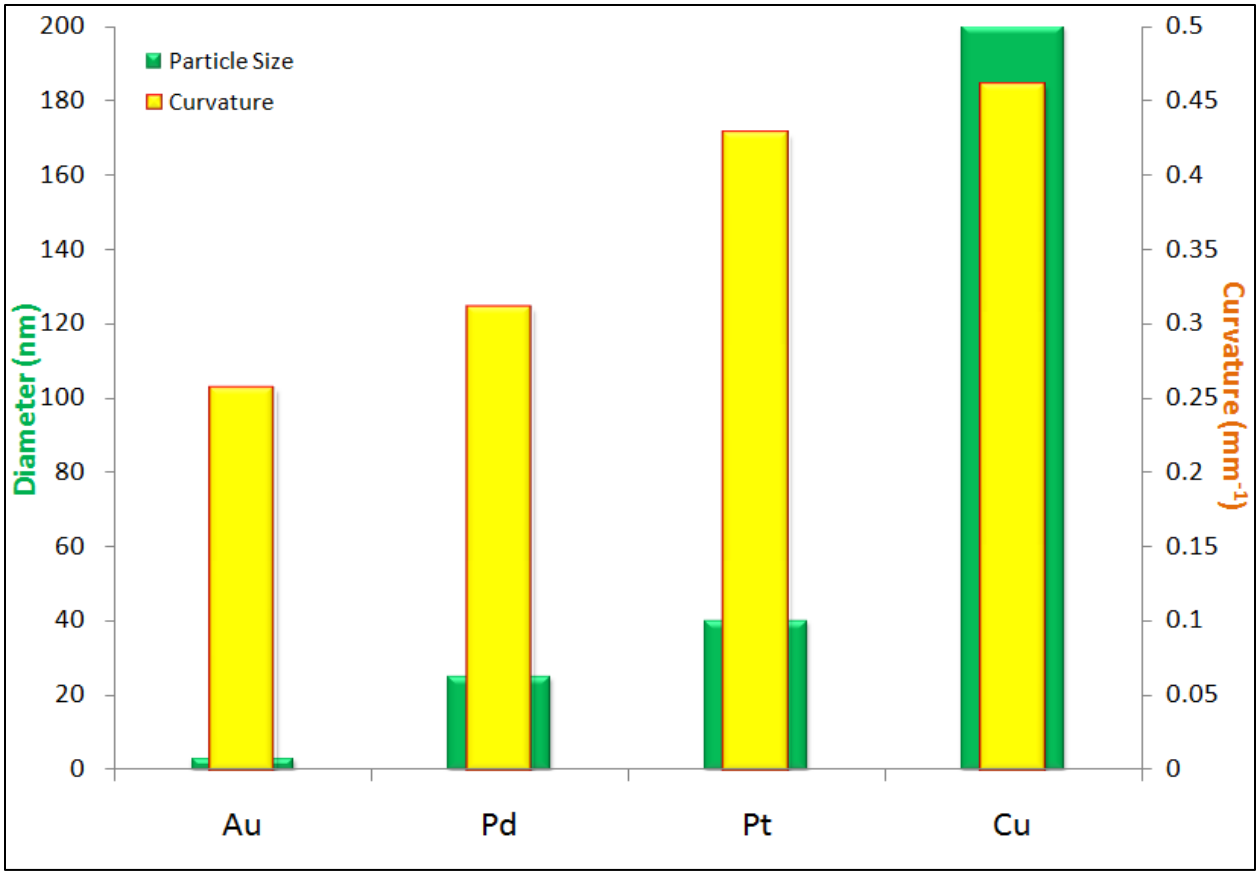

Figure 4.2. Actuation curvature of actuators consisting of different metal nanoparticles. The CNC for each actuator consist of 50 bilayers

To characterize the IEAP actuators for their intrinsic strain, the elastic modulus of each layer along the film surface direction in the IPMC was characterized using a set-up specifically designed to measure the elastic modulus of soft materials.[3,4] In this set-up, the specimen is fixed at two ends and a displacement transducer was used to generate strain in the specimen and the corresponding stress (force/cross section area) was measured by a load cell. In this study, the elastic modulus of the Nafion film with 40 wt% EMI-Tf was measured first (=50 MPa). Then the elastic modulus of the specimen with CNC layers deposited on the Nafion membrane was characterized. From this effective elastic modulus, the elastic modulus of the CNC layer can be deduced. For a bilayer laminate with the length much larger than the other dimensions as illustrated in **Figure 4.3**, the measured elastic modulus Y is related to the elastic modulus of each layer Y^a and Y^b as

$$Y = aY^a + bY^b$$

where a and b are the volume fractions of each layer in the laminate, respectively.

$$a = \frac{t_1}{t_1 + t_2}$$

$$b = \frac{t_2}{t_1 + t_2}$$

The final effective elastic modulus of the five-layered IPCNC (with CNC and gold leaf electrodes) absorbed with EMI-Tf was also measured from which the elastic modulus of the Au layer was deduced (=20 GPa). The modulus of each layer is presented in **Table 4. 1**.

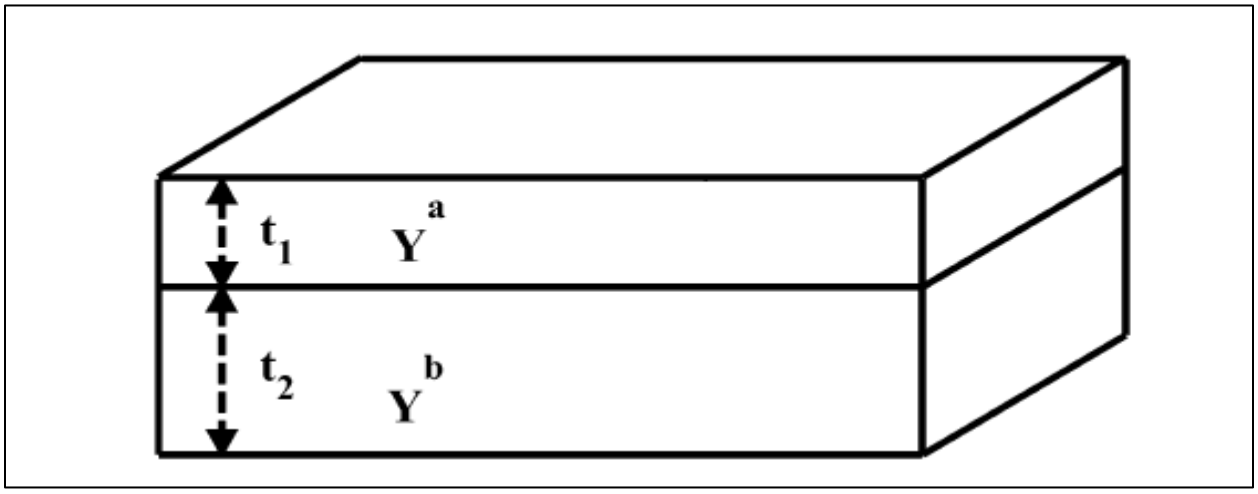

Figure 4.3. Schematic of bilayer laminate for the characterization of the elastic modulus of individual layers

Membrane	CNC	Outer Electrode
50 MPa	780 MPa	20 GPa

Table 4.1. Modulus of each layer in IEAP actuator

Using the modulus and thickness of each layer, the intrinsic strain of actuators was calculated from

$$\boldsymbol{\varepsilon} = \frac{\boldsymbol{Y_m}\left[\left(\frac{\boldsymbol{2t_m^3}}{\boldsymbol{3}}\right) + \boldsymbol{2t_m}\left(\boldsymbol{t_c} + \frac{\boldsymbol{t_i}}{\boldsymbol{2}}\right)^{\boldsymbol{2}} + \boldsymbol{t_m^2}(\boldsymbol{2t_c} + \boldsymbol{t_i})\right] + \boldsymbol{Y_c}\left[\frac{\boldsymbol{2t_c^3}}{\boldsymbol{3}} + \boldsymbol{t_c}\frac{\boldsymbol{t_i^2}}{\boldsymbol{2}} + \boldsymbol{t_c^2 t_i}\right] + \boldsymbol{Y_i}\left[\frac{\boldsymbol{t_i^3}}{\boldsymbol{12}}\right]}{\boldsymbol{r\,Y_c(t_i t_c + t_c^2)}}$$

where Y is the modulus, t is the thickness, r is the radius of curvature, and the subscripts m,c and i correspond to metal, CNC and ionomeric membrane, respectively.

Presented in **Figure 4.4** is the intrinsic strain of IEAP actuators consisting of different types of nanoparticles as a function of applied voltage. The intrinsic strain exhibited an increasing rate with increase in applied voltage and nanoparticle size.

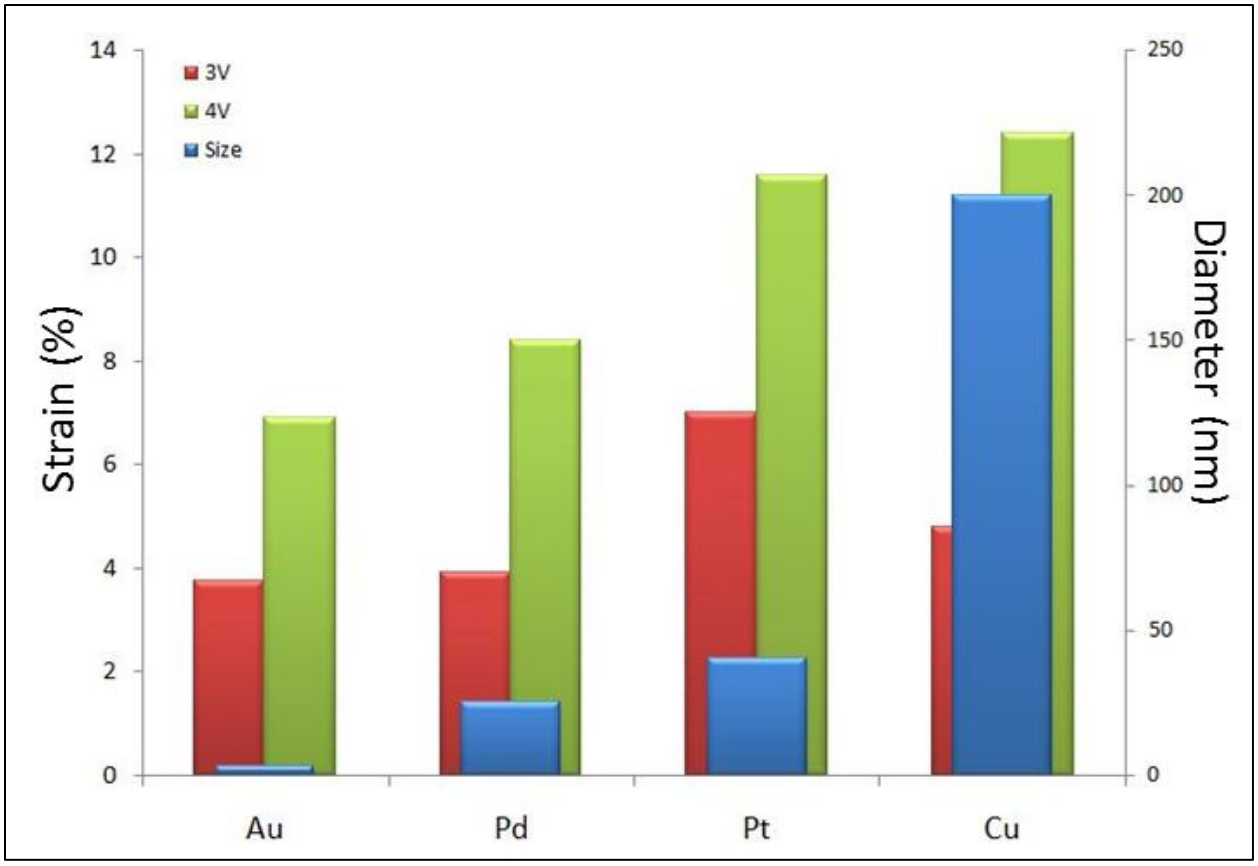

Figure 4.4. Intrinsic strain of actuators consisting of different metal nanoparticles, as a function of applied voltage. Each actuator consists of 50 bilayers

Since using copper nanoparticles in the IPMC would introduce oxidation issues to the system, and smaller nanoparticles form more uniform and homogeneous thin-films and are advantageous in controlling the thickness of CNC, gold nanoparticles of ~3nm diameter were chosen for the systematic studies of IEAP actuators.

The actuation speed of an IEAP actuator based on gold nanoparticles fabricated via LbL ionic self-assembly was characterized and compared to that of an IEAP actuator based on RuO_2 nanoparticles fabricated via conventional method. Presented in **Figure 4.5** is the normalized intrinsic strain as a function of time. The data is fitted with $S = S_0[1-\exp(-t/\tau)]$, which yields τ = 0.18 s for the gold nanoparticle-based IEAP actuator and τ = 1.03 s for the RuO_2-based IEAP actuator. The fast actuation speed of the gold nanoparticle-based actuator is due to the thin CNC layer which is 0.4 μm compared with 3 μm for the RuO_2-based actuator. The results presented

indicate the potential of gold nanoparticle-based CNCs fabricated via LbL ionic self-assembly technique as a class of IEAP actuators for large and fast actuation under low applied voltage.

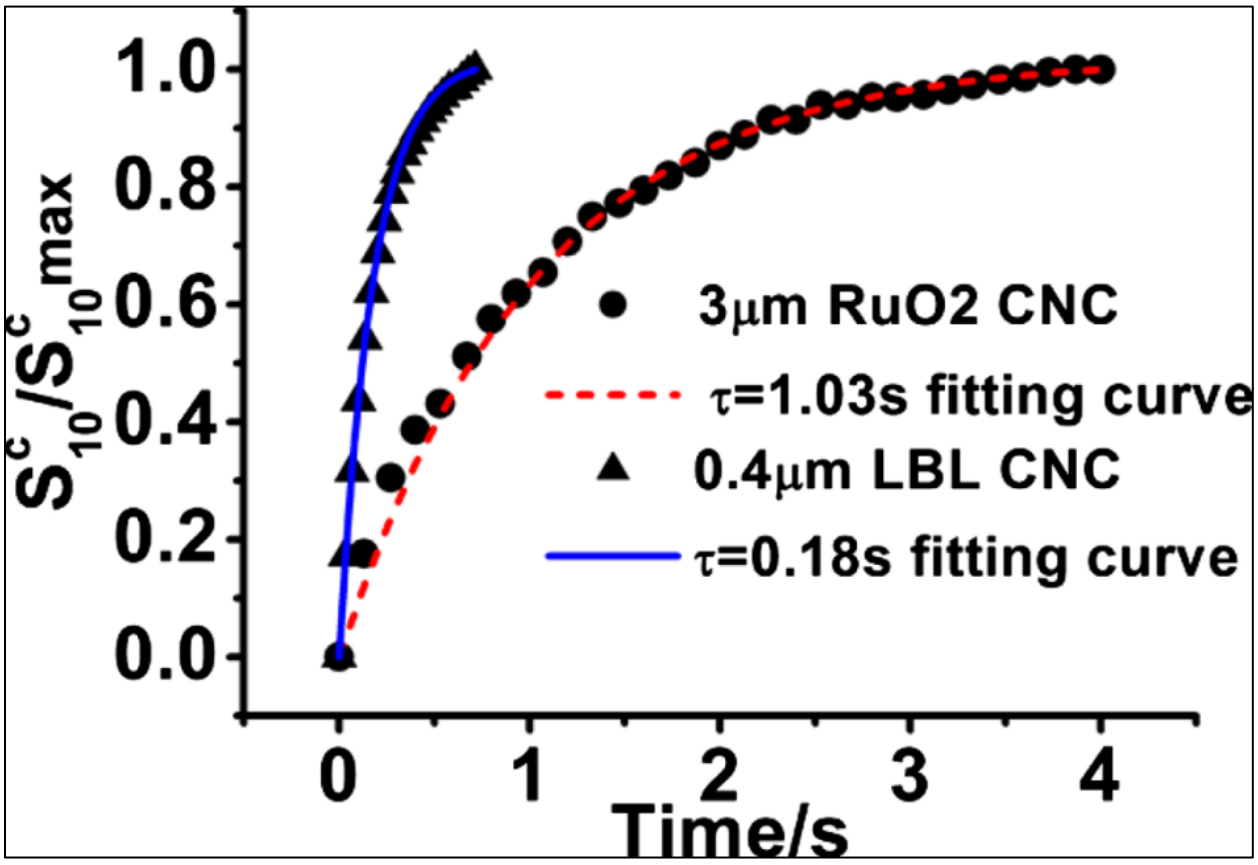

Figure 4.5. The actuator response time as a function of time under a step voltage for the gold nanoparticle-based CNC (25.8 μm total thickness) and RuO_2-based CNC (31 μm total thickness)

Actuators based on gold nanoparticles consisting of CNCs with different number of bilayers were characterized for the intrinsic strain as a function of applied voltage and number of gold nanoparticle/PAH bilayers, as shown in **Figures 4.6** and **4.7**. It was observed that actuators with thicker CNCs exhibit smaller intrinsic strain, which is mainly because of the increased modulus due to added metal nanoparticle in the CNC. The intrinsic strain showed an increasing trend with increasing applied voltage, which is the result of motion of a larger number of ions in stronger electric field.

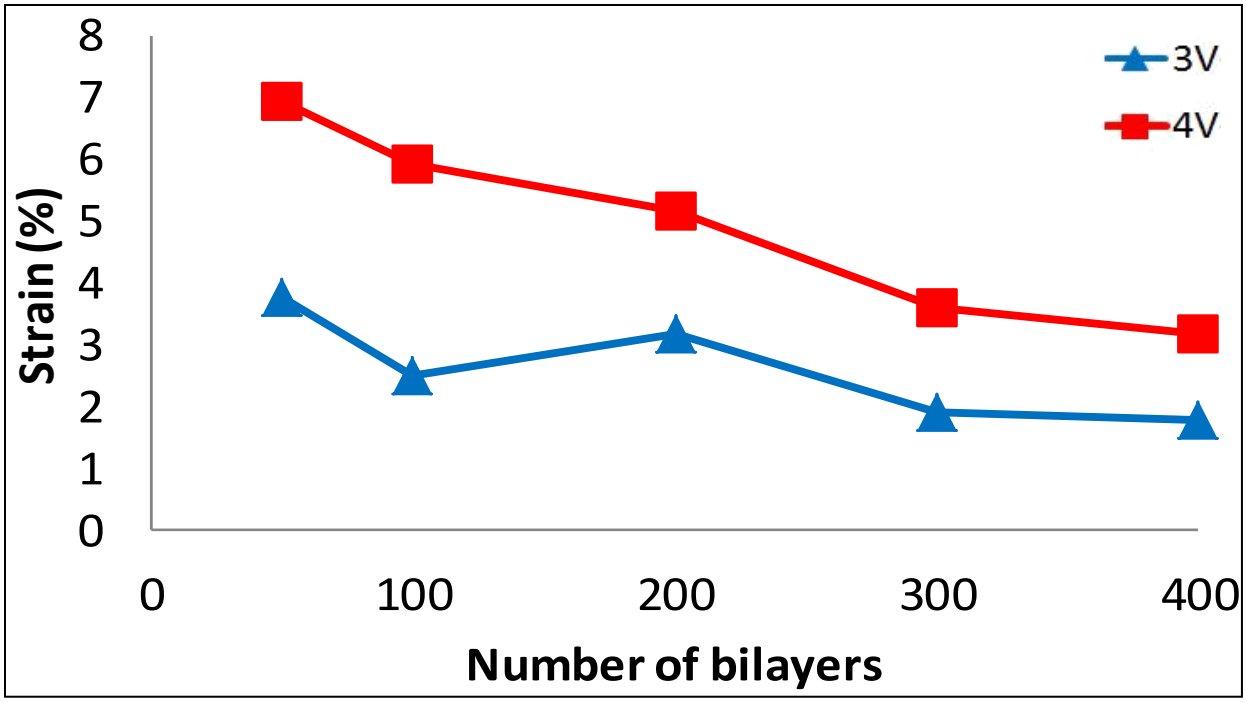

Figure 4.6. Intrinsic strain of gold nanoparticle-based IEAP actuators as a function of the thickness of CNC and applied voltage

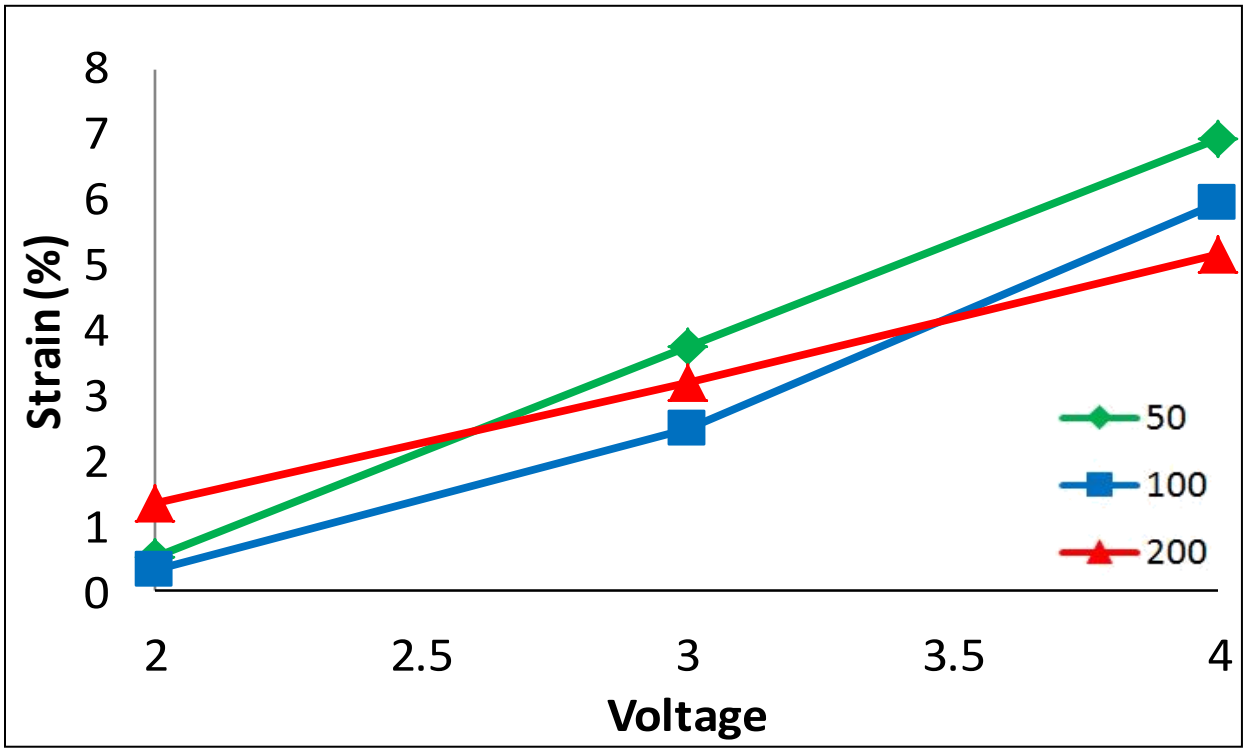

Figure 4.7. Intrinsic strain of gold nanoparticle-based IEAP actuators as a function of the applied voltage and the thickness of CNC

4.3 Fabrication Process

In order to immerse the ionomeric membrane in ionic solutions for LbL fabrication of the CNC, we initially placed the Nafion film between two polycarbonate frames and stapled the frames together. It turned out that immersing the polycarbonate frame and staples into the gold nanoparticle solution results in quick degradation of the solution, so the solution needed to be replaced after every 5 bilayers which increased the cost and also resulted in less homogeneous thin films, **Figure 4.8**.

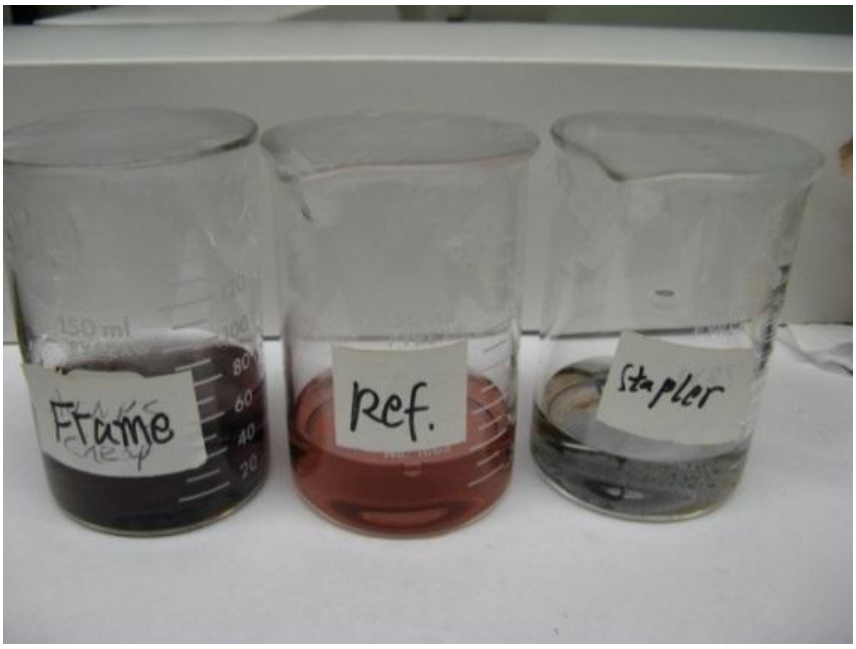

Figure 4.8. Gold nanoparticle solution degrades when in contact with polycarbonate frame (left) or staple (right). The reference solution is shown at the center

To overcome this issue, glass frames were designed and made from 1”×3” microscope glass slides and double-sided tape was used to secure the Nafion film to the frame. The resultant thin-films were of significantly higher quality both in uniformity and thickness. Using the glass frames, the gold nanoparticle solution does not degrade and lasts for more than 15 bilayers until almost all the gold nanoparticles are absorbed and the solution becomes clear. Presented in **Figure 4.9** are schematics of the polycarbonate and glass frames along with pictures of two thin-films consisting of the same number of bilayers fabricated with polycarbonate and glass frames.

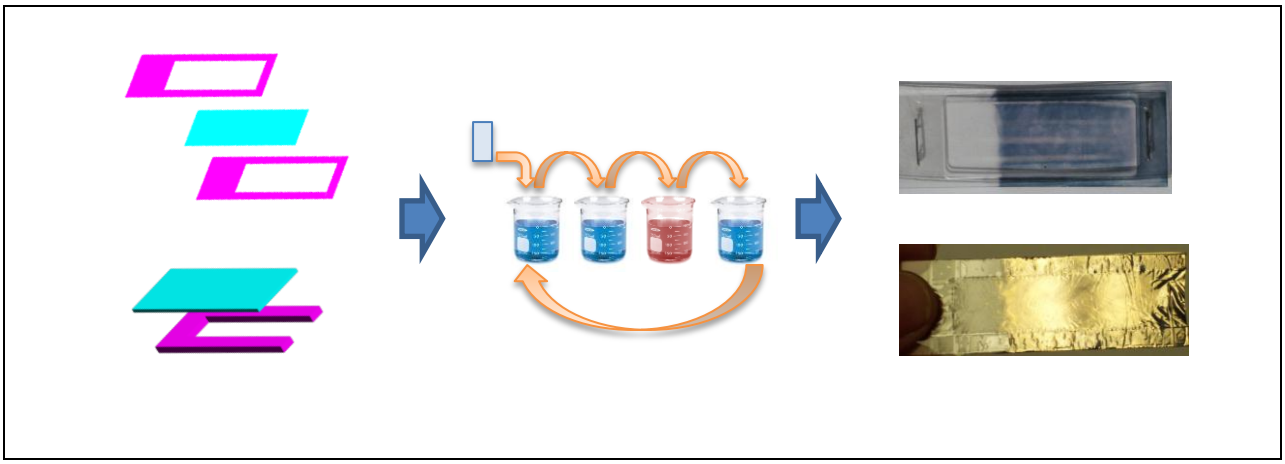

Figure 4.9. Schematics of polycarbonate and glass frames along with pictures of thin-films consisting of the same number of bilayers fabricated with LbL ionic self-assembly technique using two different types of frames

References

1 S Liu, R Montazami, Y Liu, V Jain, M Lin, JR Heflin, and QM Zhang, "Layer-by-layer self-assembled conductor network composites in ionic polymer metal composite actuators with high strain response," Applied Physics Letters **95** (2), 3 (2009).

2 S Liu, R Montazami, Y Liu, V Jain, M Lin, X Zhou, JR Heflin, and QM Zhang, "Influence of the conductor network composites on the electromechanical performance of ionic polymer conductor network composite actuators," Sensors and Actuators A: Physical **157** (2), 267-275 (2010).

3 Kailiang Ren, Sheng Liu, Minren Lin, Yong Wang, and Q. M. Zhang, "A compact electroactive polymer actuator suitable for refreshable Braille display," Sensors and Actuators A: Physical **143** (2), 335-342 (2008).

4 Kailiang Ren, Yiming Liu, H. Hofmann, Q. M. Zhang, and John Blottman, "An active energy harvesting scheme with an electroactive polymer," APPLIED PHYSICS LETTERS **91** (13), 132910-132913 (2007).

Chapter 5

Influence of CNC thickness on the Performance if IEAP Actuators

This chapter is an expansion of work published in the Journal of Applied Physics entitled: "Thickness dependence of curvature, strain, and response time in ionic electroactive polymer actuators fabricated via layer-by-layer assembly", Authored by Reza Montazami, Sheng Liu, Yang Liu, Dong Wang, Qiming Zhang, and James R. Heflin, J. Appl. Phys. **109**, 104301 (2011)

5.1 Introduction

Transport of ions through the CNC and their accumulation at the oppositely charged outer electrodes, under an applied voltage, results in an imbalance of force between the two sides of IEAP actuator and in turn causes a mechanical deformation called actuation. Initially, ions are randomly distributed in the CNC layers and membrane; upon application of an external electric field the ions start to move through membrane and CNC and toward the outer electrode of opposite charge. Thus the physical properties of the CNC layer along with the possible chemical interactions between the ions and CNC are influential and important in defining the performance and properties of the IEAP actuators. Given the high influence of the CNC on performance of IEAP actuators and since it is easier to alter the structure of CNC, in comparison to the ionomeric membrane, structural alterations and modifications of the CNC can be used as a powerful tool to optimize the performance of IEAP actuators, and to tailor them to specific needs and applications. There are several approaches to alter the structure of CNC. One approach is to change the building blocks of the nanocomposite. That is, to use different materials such as gold, silver, platinum, copper, zinc, carbon nanotubes or silica nanoparticles to form the nanocomposite; or to use different polymers for construction of layer-by-layer ISAM films. Another approach is to use nanomaterials of different geometries such as spherical nanoparticles versus nano flakes. Yet another approach is to keep the building blocks fixed and alter the physical properties of the nanocomposite. Physical properties such as thickness, volume density and pore size are some of the factors expected to influence the actuator performance.

In this chapter, several aspects of the performance of actuators are studied as a function of thickness of the CNC and the results are analyzed to deduce performance data. It is shown that one effective method to improve the performance of IEAP actuators is control over the thickness of the CNC layers, without even varying the CNC nanocomposite structure. The thickness of the CNC is important because it is directly proportional to the volume of CNC. In other words, the capacity of the CNC for electrolyte uptake. The thickness also defines part of the path length for ion travel. The amount of electrolyte translates to larger number of ions in the device which directly influences the performance of IEAP actuators; as more ions can result in a larger imbalance in the actuator and generate larger force. Here I show that IEAP actuators containing porous CNC and ionic liquids can result in high strain and fast response times. Incorporation of spherical gold nanoparticles (AuNPs) in the CNC enhances the conductivity and porosity, while maintaining relatively small thickness, which leads to improved mechanical strain and bending curvature of the actuators. It is also shown how the LbL self-assembly technique is a useful tool for fabrication of CNC with precise control over the thickness of nanocomposite. Beside curvature, intrinsic strain and total net strain of IEAP actuators, the net strain generated by the CNC is also analyzed in this study.

5.2 Materials

Commercially-available Nafion films of thickness 25 μm (Ion Power, Inc.) were used as the ionomeric membrane in all IEAP actuators investigated in this chapter. Nanocomposites of the polycation poly(allylamine hydrochloride) (PAH) (Sigma Aldrich) and anionic functionalized gold nanoparticle (AuNP) (~3 nm diameter, Purest Colloids, Inc.) were grown on both sides of the Nafion membrane via LbL deposition of the ionic species. The substrates were alternately immersed for 5 minutes each in aqueous solutions of PAH at a concentration of 10 mM at pH 4.0 and AuNP at a concentration of 20 ppm at pH 9.0 with three rinsing steps for 1 minute each in deionized water after each deposition step. Glass frames were used to support the membrane in the solutions during the deposition process. After deposition of the PAH/AuNP CNCs on the Nafion membrane, the films were soaked with 1-ethyl-3-methylimidazolium trifluoromethanesulfonate (EMI-Tf) (Sigma Aldrich) ionic liquid to approximately 40 wt%. Gold leaf electrodes of thickness 50 nm were then hot-pressed on both sides of the membrane to form IEAP actuators. Other ionic liquids can also be used as sources of mobile ions; however, IEAP

actuators with EMI-Tf have shown the highest strain response.[1] The IEAP actuators were then cut into approximatly1×6 mm^2 strips for testing. The thicknesses of CNCs consisting of different numbers of bilayers were measured using a Veeco Dektak 150 profilometer. An SEM image of a 40-bilayer AuNP surface is shown in **Figure 5.1.**

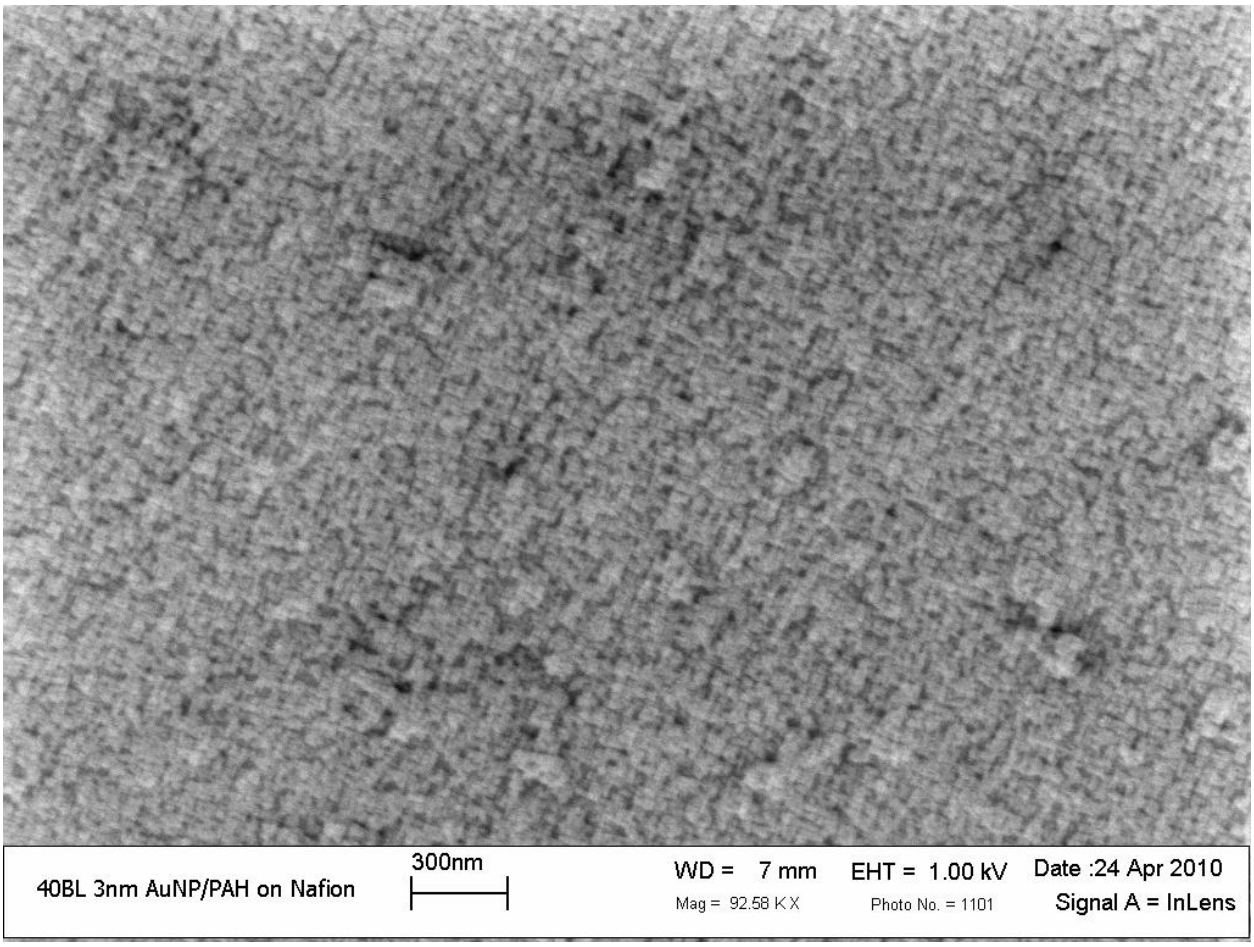

Figure 5.1. SEM image of 40 bilayers of (PAH/AuNPs) on Nafion

5.3 Results and Discussions

As noted in section 2.3, the ISAM technique provides precise control over the thickness of the thin-film nanocomposite. Here we are taking advantage of this factor and using the number of deposoited layers of PAH/AuNPs to control the thickness of the CNC layers. Increase in the thickness of the CNC with respect to number of deposited bilayers (between 10 and 40 bilayers)

exhibited a linear growth of approximately 2 nm/bilayer. The increase in the thickness of the CNC as a function of number of bilayers is shown in **Figure 5.2**. Since the CNCs are fabricated on both sides of the ionomeric membrane, twice the CNC thickness is added to the thickness of the membrane to obtain the total thickness of the IPMC. The thicknesses of different samples are presented in **Table 5.1.**

Sample	CNC (μm)	IPMC (μm)	Actuator (μm)
Bare Nafion	0.000	25.000	25.100
10 BL	0.023	25.046	25.146
15 BL	0.033	25.066	25.166
25 BL	0.051	25.102	25.202
30 BL	0.064	25.128	25.228
40 BL	0.081	25.162	25.262

Table 5.1. Thickness of different components of variety of actuators. Bare Nafion has thickness of 25 μm and each metal electrode is 50 nm thick

As we have shown previously,[2] ionic liquid bending actuators under constant applied voltage exhibit first a motion towards the anode followed by a motion towards the cathode. This is interpreted as a fast motion by the ionic liquid cations followed by a slower motion of the anions. In the devices discussed in this chapter, the faster bending has a fairly small amplitude (with a time constant of ~0.2 s) until the device has undergone several cycles of actuation, while the slower motion (time constant ~1.5 s) towards the cathode remains fairly constant during this conditioning process. In this chapter, we will focus our discussion on the slower motion towards the cathode which is due to motion of anions (or negatively charged clusters of ions). The faster response will be discussed in more detail in **chapter 7**.

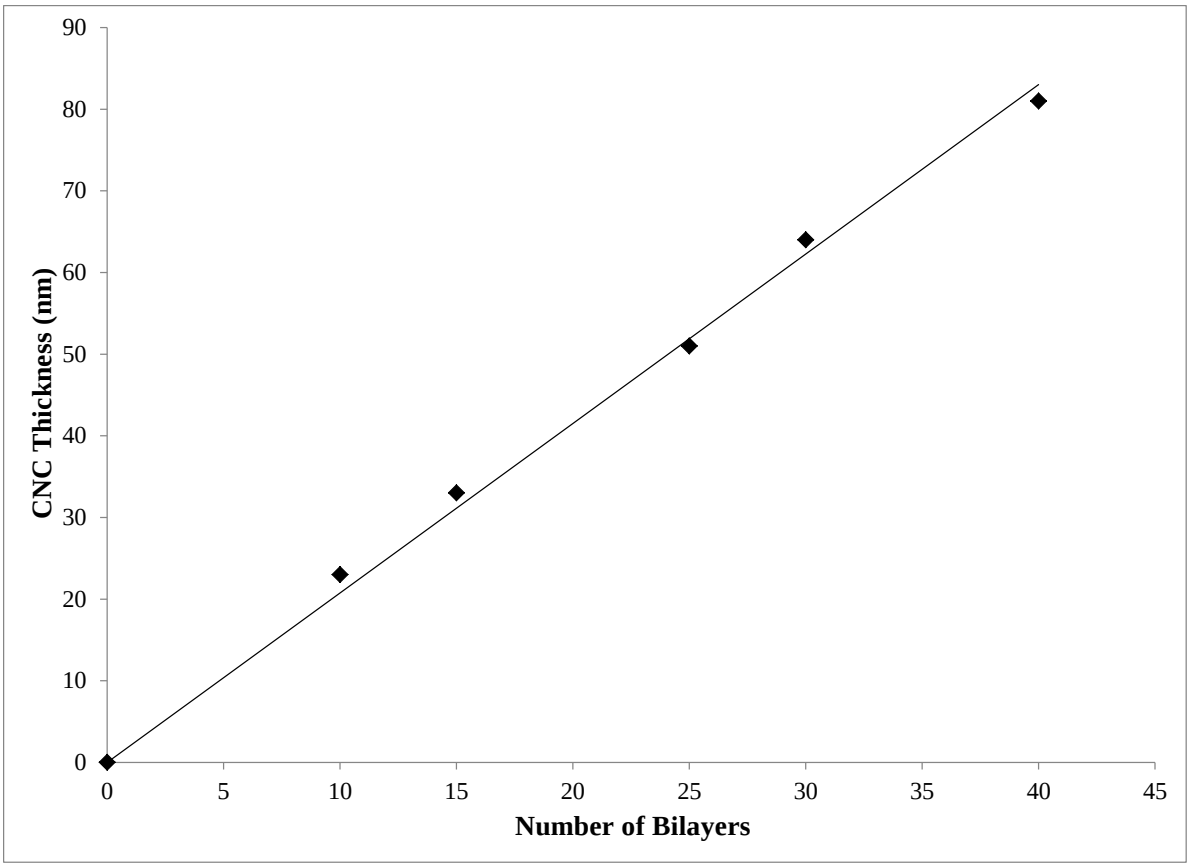

Figure 5.2. CNC thickness vs. number of bilayers. The trend line indicates linear increase in thickness

For the devices discussed in this chapter, the responses of IEAP actuators to an electrical signal of 4 V were monitored and recorded. Monitoring and recording the response of actuators was performed using a charge-coupled device (CCD) video camera at 30 fps. The actuation radius of each actuator as a function of time was determined from the optical images and used to calculate the actuation curvature (Q). **Figure 5.3** shows the maximum actuation curvature towards the cathode as a function of CNC thickness for actuators with different numbers of bilayers comprising the CNC, including the case of bare Nafion (no CNC). The curvature increases linearly with the thickness of the CNC at a rate of 0.0029 mm^{-1}/nm. The increase of actuation curvature as a function of thickness is due to the motion of a larger number of ions into the thicker CNCs, as thicker CNCs are capable of containing more electrolyte and hence more ions accumulate at each electrode in the presence of an electric field due to this higher capacitance.

The largest actuation curvature (0.43 mm^{-1}) corresponds to the sample consisting of 40 bilayers. The curvature of the 40-bilayer device is 2.4 times larger than that of the actuator without a CNC.

In the case of symmetric cantilever actuators with length significantly larger than width and width significantly larger than total thickness, the application of electric field across the thickness of the actuator will cause longitudinal expansion or contraction in the CNC layers which produces mechanical bending. For a free cantilever bimorph actuator, the extensional force (F) and external moment (M) are zero, and only pure bending occurs during the actuation.[3] The intrinsic strain (ε) within the CNC layer can be obtained from **Equation 1**, using the thickness and elastic modulus of each layer along with the radius of curvature.

$$\varepsilon = \frac{Y_m\left[\left(\frac{2t_m^3}{3}\right) + 2t_m\left(t_c + \frac{t_i}{2}\right)^2 + t_m^2(2t_c + t_i)\right] + Y_c\left[\frac{2t_c^3}{3} + t_c\frac{t_i^2}{2} + t_c^2 t_i\right] + Y_i\left[\frac{t_i^3}{12}\right]}{r\,Y_c(t_i t_c + t_c^2)} \qquad (1)$$

where Y is the modulus, t is the thickness, and r is the radius of curvature, and the subscripts m,c and i correspond to metal, CNC and ionomeric membrane, respectively.

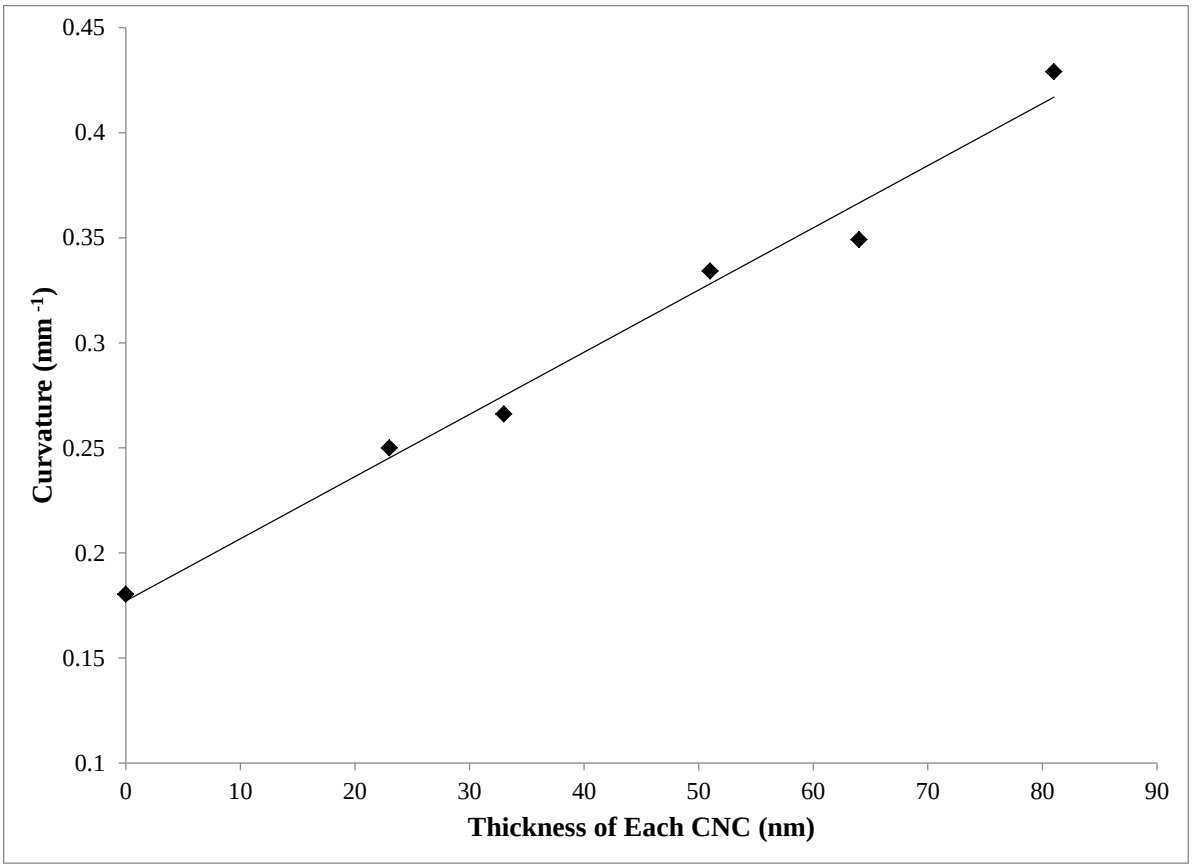

Figure 5.3. Curvature (Q) increases linearly with the increase in the thickness of CNC. The curvature of an actuator consisting of an 80 nm thick CNCs exhibited 2.4 times increase in comparison to actuator consisting of 10 nm CNCs. Data are taken under application of 4V step function

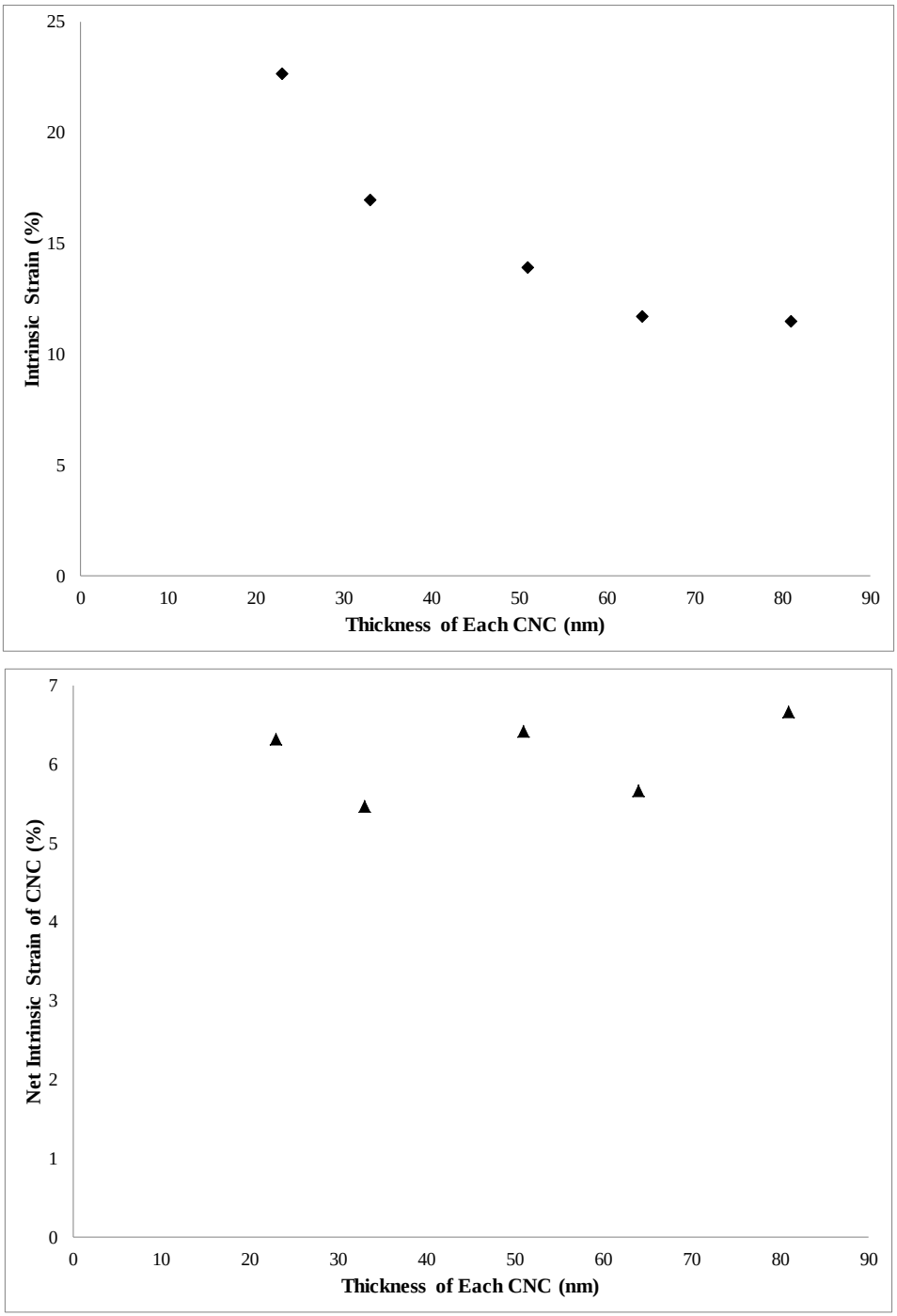

Figure 5.4. Intrinsic strain (top) and net intrinsic strain due to the CNC layer (bottom) as a function of CNC thickness. Samples consisting of thinner CNCs exhibited larger calculated intrinsic strain from Eqn. 1, but the net intrinsic strain due to the CNC layer after subtracting the contribution from bare Nafion is a fairly constant value. Data are taken under application of 4V step function

To quantify the generated intrinsic strain, the elastic modulus of each layer was characterized along the direction of the actuator surface, using a setup specifically designed to measure the elastic modulus of soft materials. Details of the setup and procedures are presented in our previous work.[1] Briefly, the elastic modulus of the Nafion film with 40 wt% EMI-Tf was measured first (=50 MPa). Then the elastic modulus of the specimen with CNC deposited on the Nafion membrane was characterized from which the elastic modulus of the CNC layer is deduced (=739 MPa). The elastic modulus of the five-layer IEAP actuator swollen with EMI-Tf was also measured from which the elastic modulus of the gold electrode was deduced (=20 GPa)
The actuator consisting of 10 bilayers (thinnest CNCs) exhibited the largest intrinsic strain as derived from eqn. 1 compared to other actuators consisting of thicker CNCs. Presented in **Figure 5.4 (top)** is the calculated intrinsic strain as a function of CNC thickness. The mechanical intrinsic strain generated under 4 V was obtained to be 22.65% (45.3% peak-to-peak) for the 10-bilayer actuator and 11.48% (22.96% peak-to-peak) for the 40-bilayer actuator. For comparison, the intrinsic strain of an IEAP actuator based on a 3 μm thick RuO_2 CNCs is 3.3% (6.6% peak-to-peak) under the same voltage. The considerably enhanced strain of the actuators investigated in this work is due to successful formation of uniform and thin CNCs. Such CNCs contain less metal, which lowers the modulus, and uniform structure, which facilitates effective mobility of ions and also increases electrolyte up-take. It is important to note that the actuator without a CNC still exhibits non-negligible curvature. In order to determine the true intrinsic strain of the actuators, this contribution to the curvature should be removed. Thus, the net intrinsic curvature due to the CNC layers for each actuator was derived by subtracting the curvature of the bare Nafion actuator from that of the other actuators. The net curvature was then used to calculate the net intrinsic strain due to the CNC, which was found to be a fairly constant value. The net intrinsic strain has an average value of 6.1% as shown in **Figure 5.4 (bottom)**. The independence of the net intrinsic strain on the CNC thickness indicates that the additional CNC material contributes equally to the bending response over the measured thickness range of 20 to 80 nm.

Net Strain

Intrinsic strain due to the CNC is a value applicable to IEAP actuators and useful in characterizing IPMCs, however it does not translate to a tangible, universal and quantitative

value that can be used to compare IEAP actuators with other sorts of actuators or to give a general, descriptive definition of mechanical deformation of the structure. In order to deduce this universal quantity, which is representative of the actual mechanical deformation of the structure, one should calculate the ratio between the volume of the expanded side of the actuator and its initial volume. This quantity is simply the change in the volume of the expanded layer in reference to the original volume. This quantity is independent of the structural properties of the actuator (number of layers, materials, modulus etc.) and considers the actuator as one uniform, structure of a fixed thickness. **Figure 5.5** and **equations 2 through 6** show an illustration and corresponding equations for calculating the net strain of a bending actuator. The radius of curvature *r* is used with **equation (6)** to obtain the net strain as a function of the thickness *h* of the actuator. The total net strain of an actuator differs from the intrinsic strain of an actuator as the former corresponds to the overall strain generated in the actuator as a whole, while the latter is the strain generated in the CNC layers only. **Figure5.6** illustrates the change in the total net strain as a function of the thickness of CNC layer. The total net strain increases as the thickness of the actuator (i.e. CNC layer) increases; which is due to the significant increase in the bending for a relatively small increase in the thickness of the actuator as a result of the facilitation of the accumulation of charge at the electrodes by the CNC. Since thicker CNC layers are larger reservoirs for intake of free ions, IEAP actuators with thicker CNCs have a larger number of free ions participating in the actuation process. As a result, during actuation a larger imbalance occurs between the two opposite electrodes which results in a larger bending curvature.

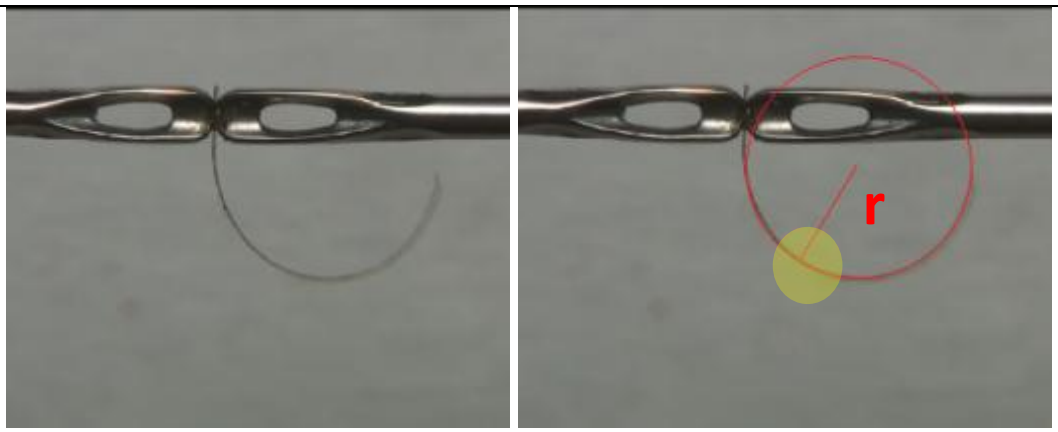

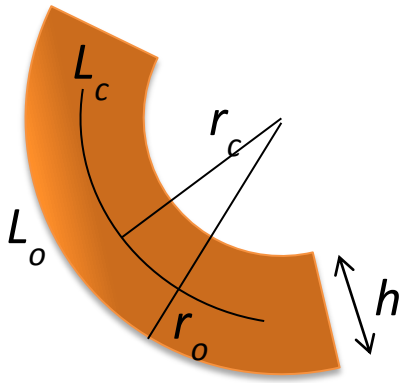

Figure 5.5. Radius of curvature of a bended structure. Center and outer are indicated with "c" and "o" subscripts, respectively. "L" is the length and "h" is the thickness of the structure

$$L_c = a \times r_c \tag{2}$$

$$L_0 = a \times r_0 = a \times (r_c + {}^{h}/_{2}) \tag{3}$$

$$\varepsilon(\%) = \frac{L_o - L_c}{L_c} \times 100 \tag{4}$$

$$\varepsilon(\%) = \frac{a\left(r_c + {}^{h}/_{2} - r_c\right)}{ar_c} \times 100 \tag{5}$$

$$\varepsilon(\%) = \frac{h}{2r_c} \times 100 \tag{6}$$

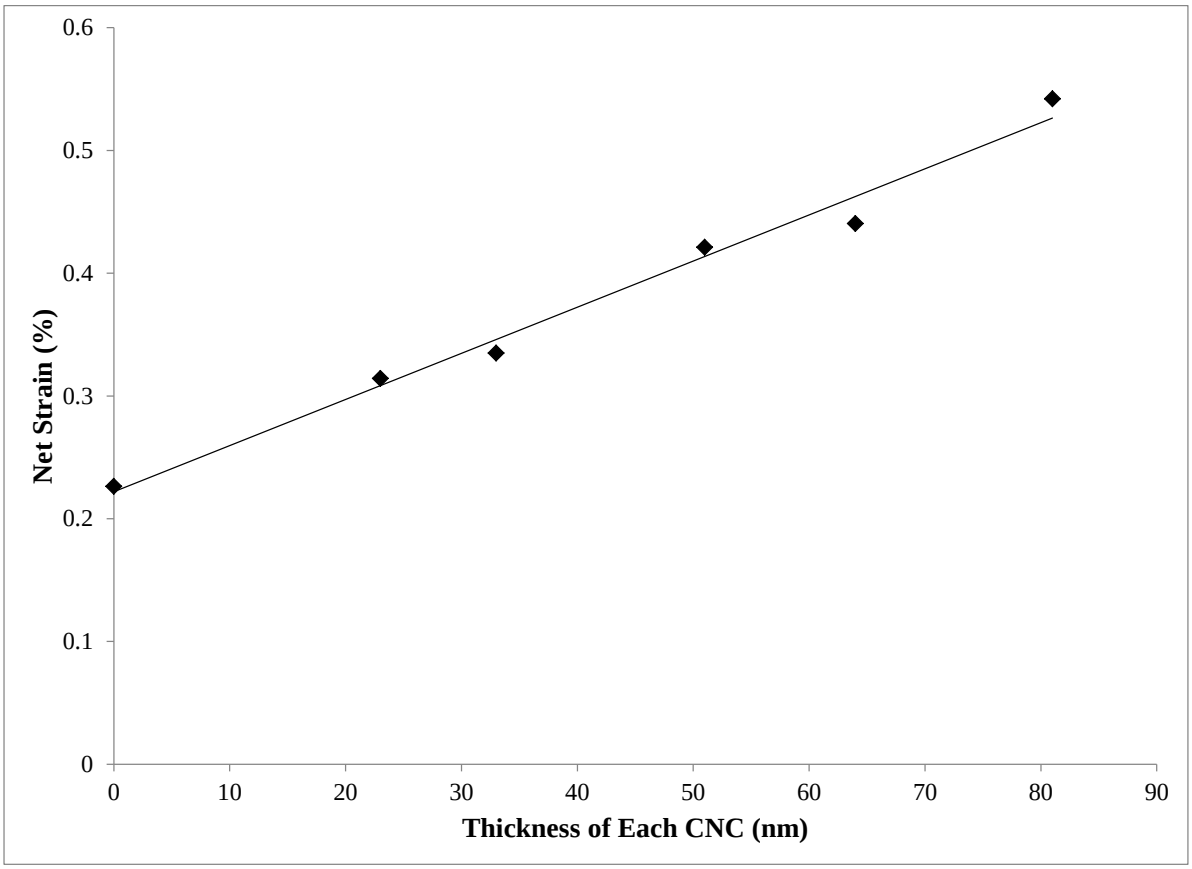

Figure 5.6. Total net strain increases with the increase in the thickness of the CNC. This strain is obtained using the total thickness of the actuator, as shown in Table 1, and the corresponding radius of curvature under application of 4V step function

Response Time

The speed of the actuators was also characterized. The strain generated by each actuator was normalized with respect to the maximum strain and plotted as a function of time. Comparing the normalized strain of different actuators versus time revealed that the response times of all actuators are approximately the same with respect to their normalized strain. In **Figure 5.7** the normalized strain for two of the actuators is shown as a function of time. Data points were fitted with $\varepsilon=\varepsilon_{max}(1-exp(-t/\tau))$ where t is time and τ is the time constant, which yields $\tau = 1.5$ seconds.

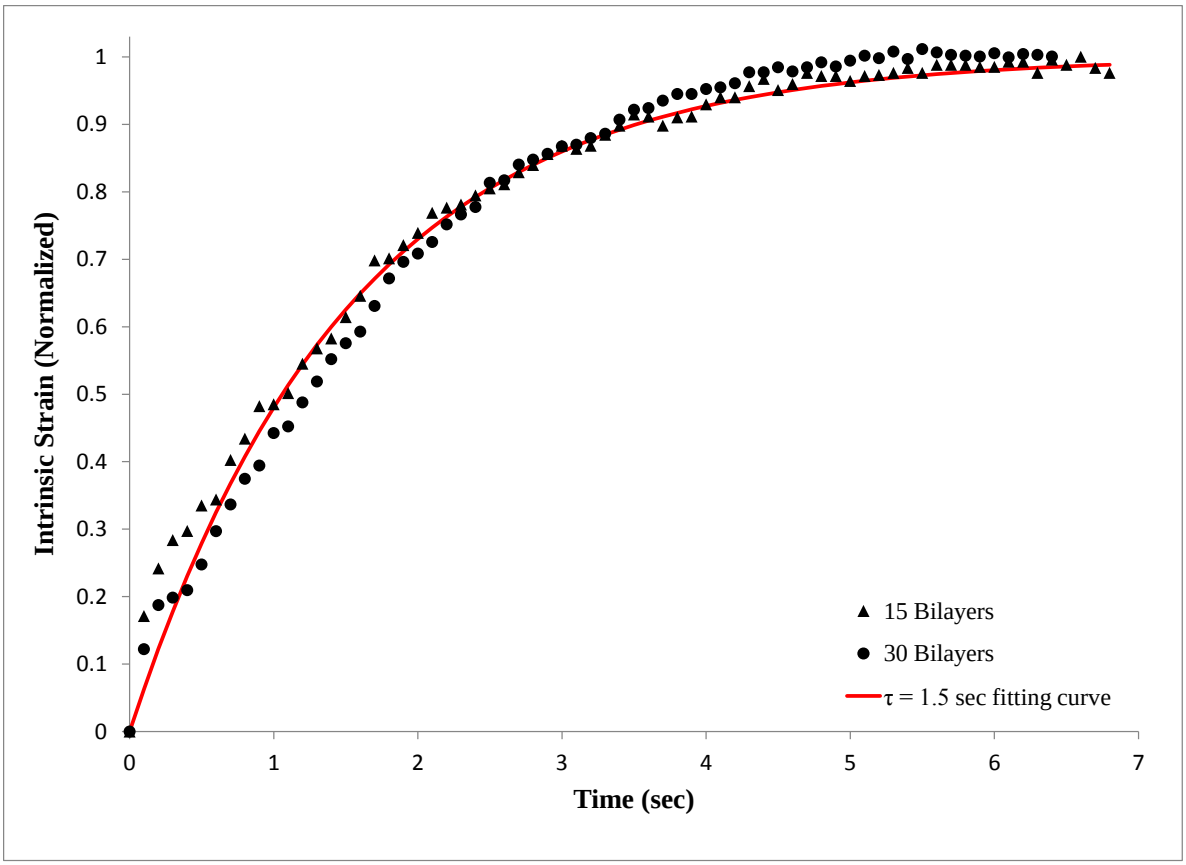

Figure 5.7. Response time of actuators consisting of 15 and 30 bilayer CNCs. It was observed that the change in normalized strain of actuators as a function of time is independent of the thickness of actuators

Conclusion

CNCs consisting of different numbers of bilayers of PAH and AuNPs were fabricated via the LbL assembly technique and used to form IEAP actuators. The resultant actuators exhibited significantly large strain compared to other types of actuators. It was observed that actuators with thicker CNC layers are capable of generating larger bending. The maximum curvature of the actuators towards the anode was found to increase linearly with the thickness of the CNC layer. After accounting for the curvature observed in an actuator with no CNC layer, the net intrinsic strain of the CNC was found to be ~6.1% independent of thickness, which indicates that the entire thickness is equally effective at contributing to the strain as the thickness of the CNC in increased. The response time for actuation was also found to be relatively independent of

thickness with a time constant τ of 1.5 seconds. This suggests that the limiting factor of the speed of the anion motion is the Nafion membrane itself rather than the CNC. The improved actuation curvature and strain are results of successful fabrication of thin and uniform CNCs. Properties and performance of actuators studied in this chapter are summarized in **Table 5.2**.

Sample	**CNC Thickness (μm)**	**IPMC Thickness (μm)**	**Actuator Thickness h (μm)**	**Curvature Q (mm^{-1})**	**Intrinsic Strain (ε_{int}%)**	**CNC Strain (ε_{CNC}%)**	**Net Strain (ε_{net}%)**
Nafion	0.000	25.000	25.100	0.180	N/A	N/A	0.226
10 BL	0.023	25.046	25.146	0.249	22.645	6.308	0.314
15 BL	0.033	25.066	25.166	0.266	16.923	5.458	0.334
25 BL	0.051	25.102	25.202	0.334	13.917	6.407	0.421
30 BL	0.064	25.128	25.228	0.349	11.690	5.652	0.440
40 BL	0.081	25.162	25.262	0.429	11.482	6.657	0.542

Table 5.2. Summary of the properties and performance of actuators consisting of different thicknesses

References

1 S Liu, R Montazami, Y Liu, V Jain, M Lin, JR Heflin, and QM Zhang, "Layer-by-layer self-assembled conductor network composites in ionic polymer metal composite actuators with high strain response," Applied Physics Letters **95** (2), 3 (2009).

2 Y Liu, S Liu, J Lin, D Wang, V Jain, R Montazami, JR Heflin, J Li, L Madsen, and QM Zhang, "Ion transport and storage of ionic liquids in ionic polymer conductor network composites," Applied Physics Letters **96**, 3 (2010).

3 QM Wang and LE Cross, "Performance Analysis of Piezoelectric Cantilever Bending Actuators," Ferroelectrics **215**, 27 (1998).

Chapter 6
Influence of the Volume Density of the Conductive Network Composite

This chapter is an expansion on the work to be submitted to Sensors and Actuators A

6.1 Introduction

Typically, the high performance (large actuation) IEAP actuators contain an ionic polymer-metal composite (IPMC) which consists of two conductive network composite (CNC) layers formed on the surfaces of an ionomeric membrane (very often Nafion®) containing an electrolyte.[1-3] The CNCs are added to the ionomeric membrane to act as reservoirs for electrolyte (aqueous or ionic liquid) solution, thus they have a significant interface and interaction with ions in the electrolyte, and their properties directly influence the mobility of ions in the IPMC. The mechanical response of most ionic liquid-containing IEAP actuators to an external electric field can be divided into two separate steps: fast response and slow response. The fast response is typically smaller in magnitude and is generated by cations that rush toward the cathode rapidly once the voltage is applied and cause the actuator to bend toward the anode. Depending on the thickness of the IPMC and the CNC-ion interface area, the fast response can have a time constant as low as 0.18 second.[4] The slow response is generated by motion of anions (or ion clusters with negative net charge). It is larger in magnitude and consists of bending of the actuator toward the cathode, canceling the fast response completely. Presented in **Figure 6.1** is the response of an IEAP actuator, consist of 20-bilayer CNCs and 25 μm Nafion, to a 4 V step voltage. Response to step voltage is usually slower that response to a waveform as the system stars from a neutral state rather than a charged state in case of waveform. There are applications in which fast cationic response is preferred, yet a large magnitude of bending is also desired. Operating the actuator at a fast enough frequency, the anionic response can be eliminated (see **chapter 7**). And the magnitude of bending can be maximized by optimizing CNC layers. Most electrical and mechanical properties of CNC layers, such as conductivity, volume density, porosity and pore size, can be optimized by variation of the composite materials, fabrication technique and

thickness of the thin-film composite. [5] The speed and extent of response of ions to an external electric field depends on several factors including CNC-ion interface area and conductivity of the CNC layer. Previous studies have demonstrated the great influence of CNC layers on the electromechanical behavior of IEAP actuators.[6-8] Moreover, it is well known that the dynamics of mobility and diffusion of ions in IPMC and their interaction with CNC layers has a vital rule in defining electromechanical properties of ionic devices.[9,10]

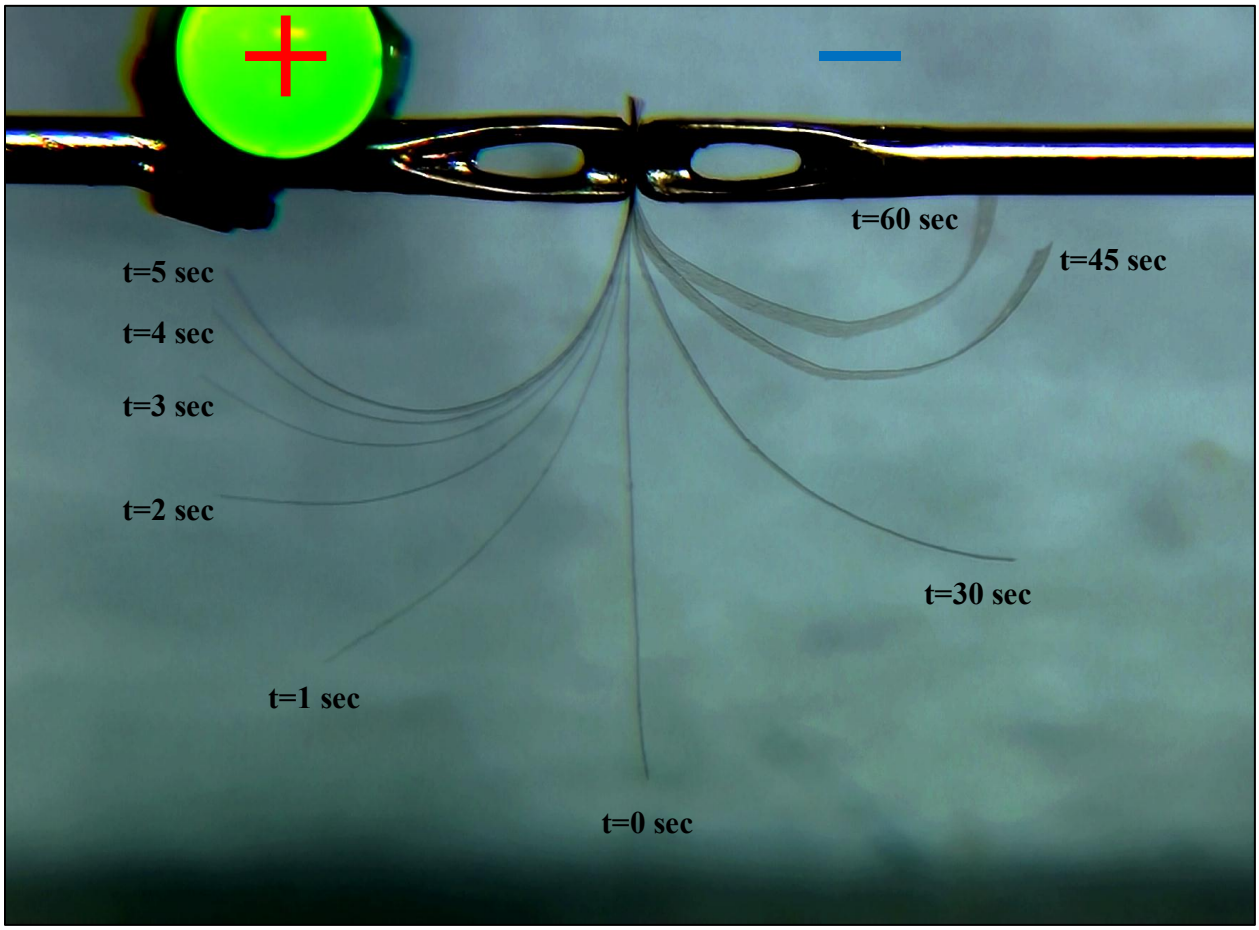

Figure 6.1. Overlaid photographic images of an IEAP actuator responding to a 4V step voltage

One of the main advantages of using LbL technique is the ability to construct electrically conductive porous CNCs while keeping the thickness in nanometer range.[11,12] Such ultra-thin composites do not interfere with the desired mechanical properties of Nafion membrane, that is, the modulus is not changed by a large amount, while significantly increasing CNC-ion interface and facilitate mobility of ions through CNC. Moreover, IPMCs with porous CNC layers have

larger electrolyte uptake capacity due to the porous structure of the nanocomposite. In the previous chapter, we showed that the thickness of CNC is highly influential on the performance of IEAP actuators. There we demonstrated that increasing the thickness of the CNC results in larger strain and bending curvature, which are the results of the increased electrolyte uptake, without significantly increasing the overall thickness of the IPMC.

In this work, we investigate the mobility of ions in a series of IEAP actuators consisting of CNCs with different gold nanoparticle (AuNP) densities fabricated via the LbL assembly technique and demonstrate that the cationic response can be maximized by tuning the nanostructure of CNC layers. Control over the density of the CNC is achieved directly through varying the concentration of AuNPs in the aqueous immersion solution. We have quantified the sheet resistance, anionic strain, cationic strain and frequency dependence of the cationic strain of the resultant actuators with different density CNCs, and have also characterized the charging and discharging of the actuators as a function of time.

6.2 Experimental

Commercially-available Nafion film of thickness 25 μm (Ion Power, Inc.) was used as the ionomeric membrane in all IEAP actuators investigated in this work. Nanocomposites of the polycation poly(allylamine hydrochloride) (PAH) (Sigma Aldrich) and anionic functionalized gold nanoparticles (AuNPs) (~3 nm diameter, Purest Colloids, Inc.) were grown on both sides of the Nafion membrane via LbL deposition of the ionic species. The substrates were alternately immersed for 5 minutes each in aqueous solutions of PAH at a concentration of 10 mM at pH 4.0 and AuNPs at 2, 4, 10 and 20 ppm concentrations at pH 9.0 with three rinsing steps for 1 minute each in deionized water after each deposition step. Glass frames were used to support the membrane in the solutions during the deposition process to eliminate frame-solution chemical reactions. After deposition of the PAH/AuNP CNCs on the Nafion membrane, the IPMCs were soaked with 1-ethyl-3-methylimidazolium trifluoromethanesulfonate (EMI-Tf) (Sigma Aldrich) ionic liquid to approximately 40 wt%. Gold leaf electrodes of thickness 50 nm were then hot-pressed on both sides of the membrane to form IEAP actuators. The IEAP actuators were then cut into approximatly1×6 mm^2 strips for testing. The thicknesses of CNCs fabricated by different AuNP concentration were measured using a Veeco Dektak 150 profilometer. The surface resistance was measured using a Jandel four-point-probe measurement system equipped with a

cylindrical probe head. Actuation motion was recorded at the rate of 30 fps by a charge-coupled device (CCD) mounted to an in-house fabricated probe station. Step voltage was derived from an HP 6218A and square waveforms were generated using an HP 3312A function generator. Current flow was measured and recorded using a FRA2 μAutolab type III potentiostat.

Strain was calculated from the radius of curvature *r* and thickness *h* of the actuators, using **equation (1)**. Strain calculated with this method is the net strain exhibited by that particular geometry and it does not take into account the intrinsic properties of the actuator such as materials, moduli, composite structure etc.

$$\boldsymbol{\varepsilon}(\%) = \frac{\boldsymbol{h}}{\boldsymbol{2r}} \times \mathbf{100} \quad \textbf{(1)}$$

6.3 Results and discussion

6.3.1 IPMC characteristics

Electrical conductivity and ionic permeability of CNC thin-films largely depend on the concentration of the metallic component and the size of pores formed in the structure of the nanocomposite respectively. Decreasing the concentration of AuNP solution, as shown in **Figure 6.2a-b** results in formation of nanocomposite structure with lower gold densities per layer. Films with reduced AuNP density have low electrical conductivity yet large pores. Although pore size is increased in samples with lower AuNP concentration, the density of ions that move into the CNC under applied voltage is expected to be low due to the reduced electrode surface area. As a result, response of ions to electric field is limited and so is the generated strain. On the other hand, increasing the AuNP concentration results in formation of closely packed metallic structures, which is more effective in establishing an electric field to attract/repulse ions and hence generated strain. **Figure 6.2c-d** shows an SEM image of CNCs consisting of higher concentration of AuNPs. The porosity of the composite allows ions to easily move through the nanocomposite, while the high concentration of AuNPs provides large gold-ion interfacial area. It is important to note that pores that are too small (on the order of the size of the mobile ions) will also reduce performance of the actuators by limiting mobility of ions. An optimum structure

has large enough pores to easily allow transport of ions and a dense enough electrically conductive structure to maximize the CNC-ion interface and thus increase participation of ions in the actuation process.

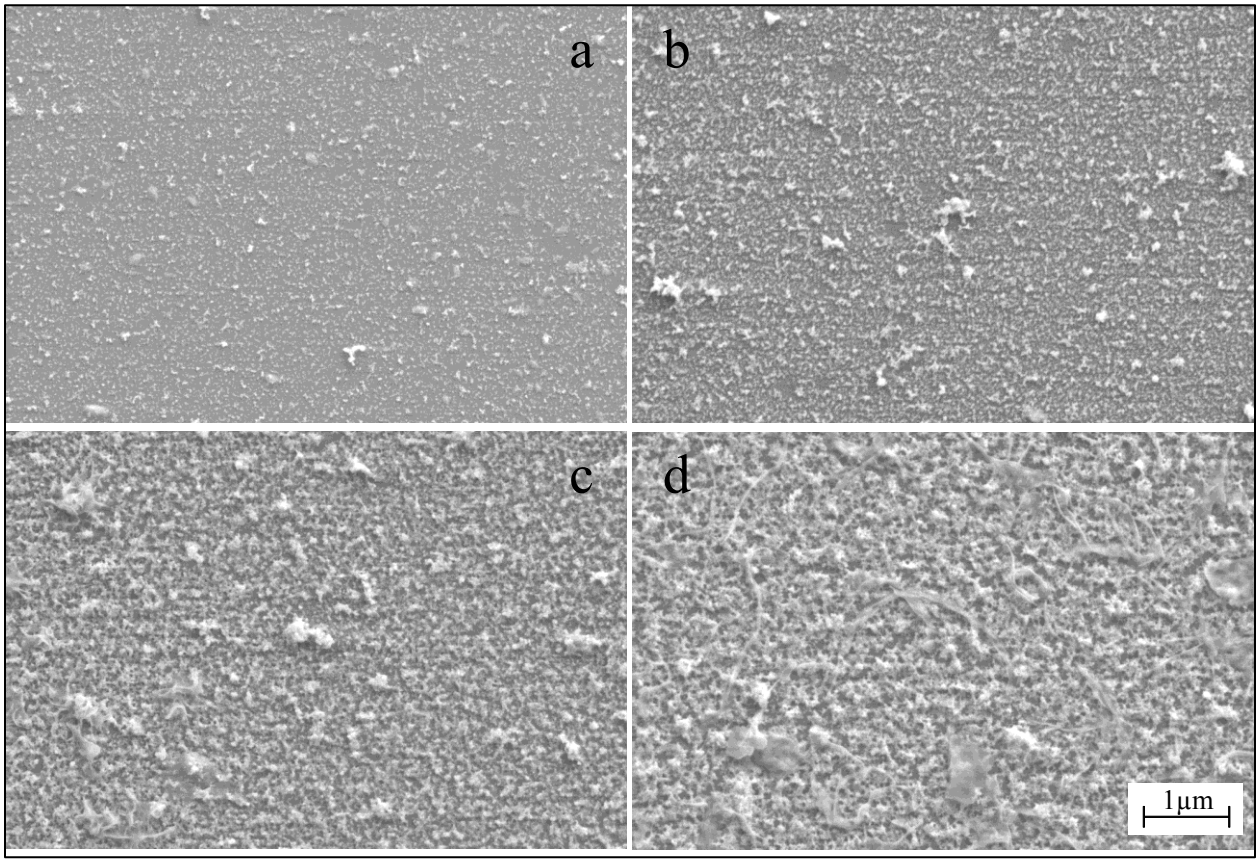

Figure 6.2. SEM images of 20-bilayer (PAH/AuNP) CNCs containing a) 2, b) 4, c) 10 and d) 20 ppm concentration of AuNPs

Taking into account the approximate two-dimensional geometry of the IPMCs, with thickness significantly smaller that width and length, the sheet resistance of IPMCs containing different volume ratios of AuNPs was measured using the four-point-probe method. The measurements were carried out under 20-120mV, using very low current flow (10-100nA) to compensate for relatively high resistance of the thin-films. As expected, we found that the sheet resistance decreased as the concentration of colloidal gold was increased. **Figure 6.3** shows sheet resistance for IPMCs containing different concentrations of AuNPs. It is clear from these data that at relatively low concentration of AuNPs, the sheet resistance of the IPMCs is approximately equal

to that of bare Nafion (no CNC) since the nanoparticles are too separated to allow electron transport between them.

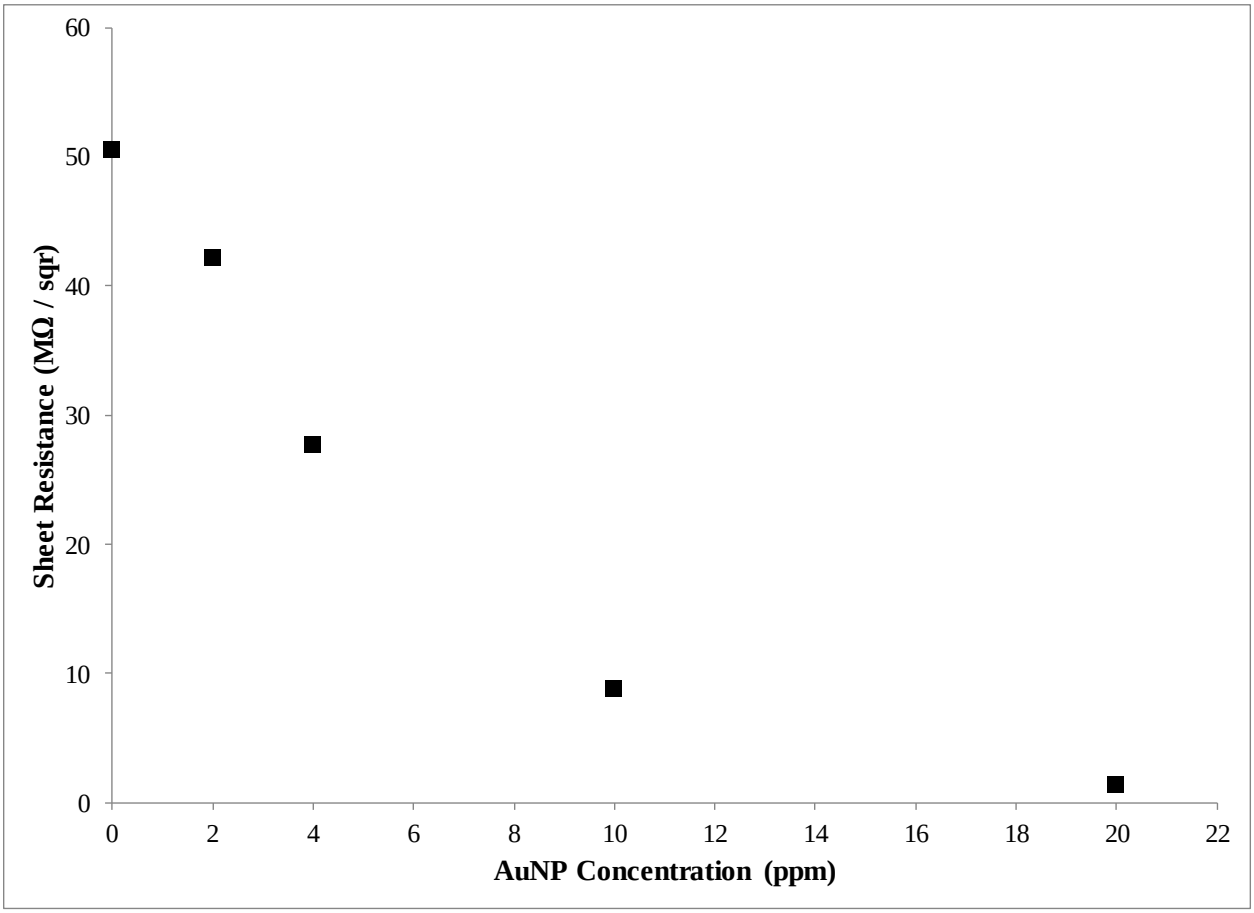

Figure 6.3. Sheet resistance decreases significantly as concentration of AuNPs is increased. The sheet resistance of bare Nafion is shown as 0 AuNP concentration

6.3.2 Mechanical response to electric field

In IPMC based actuators, the largest portion of strain is generated within the CNC layers. Fast motion of EMI^+ cations toward the cathode quickly generates a relatively small strain and causes the actuator to bend toward the anode. This quick and small cationic strain is then canceled by the slow moving Tf^- anions that are more effective in generating strain and bend the actuator toward the cathode. Given the larger Van der Waals volume of EMI^+ cations, compared to Tf^- anions, it is believed that charge clusters of negative net charge (eg. $Tf^- EMI^+ Tf^-$) arepresent in the electrolyte and participate in the actuation process which causes anions to be more effective in generating strain. Presented in **Figure 6.4** are the cationic and anionic strains generated by

actuators consisting of CNCs of different AuNP concentrations, in response to a step voltage of 4 V. The cationic strain is quiet small since EMI^+ cations are not as effective as Tf^- anions in generating strain, yet they show an increasing trend as the AuNP concentration is increased in the CNC. Since bending due to cationic motion is limited by the time required for anions to generate opposite strain, the larger cationic strain generated by CNCs with higher AuNP concentration (denser nanostructure) indicates that EMI^+ cations move quicker in denser CNCs. Although denser CNCs have higher capacitance, they also have significantly lower resistance which reduces the time required (time constant τ=RC) for charging. Moreover, the larger CNC-ion interface in the denser CNCs reduces the screening of electric field by ions that have already moved into the CNC at any given time. Therefore, in the dense CNCs, during the first few seconds that the electric field is applied, a larger number of EMI^+ cations respond to the electric field and participate in the actuation process. Thus, generated strain is larger compared to that in less dense CNCs for the same duration of time, which is the time before the cationic strain is canceled by the anionic strain. As can be seen from **Figure 6.4**, the magnitude of the anionic strain is fairly constant for the different samples, implying that all samples get fully charged by the same amount after significant time, also suggesting that there are approximately equal amounts of mobile ions in each sample.

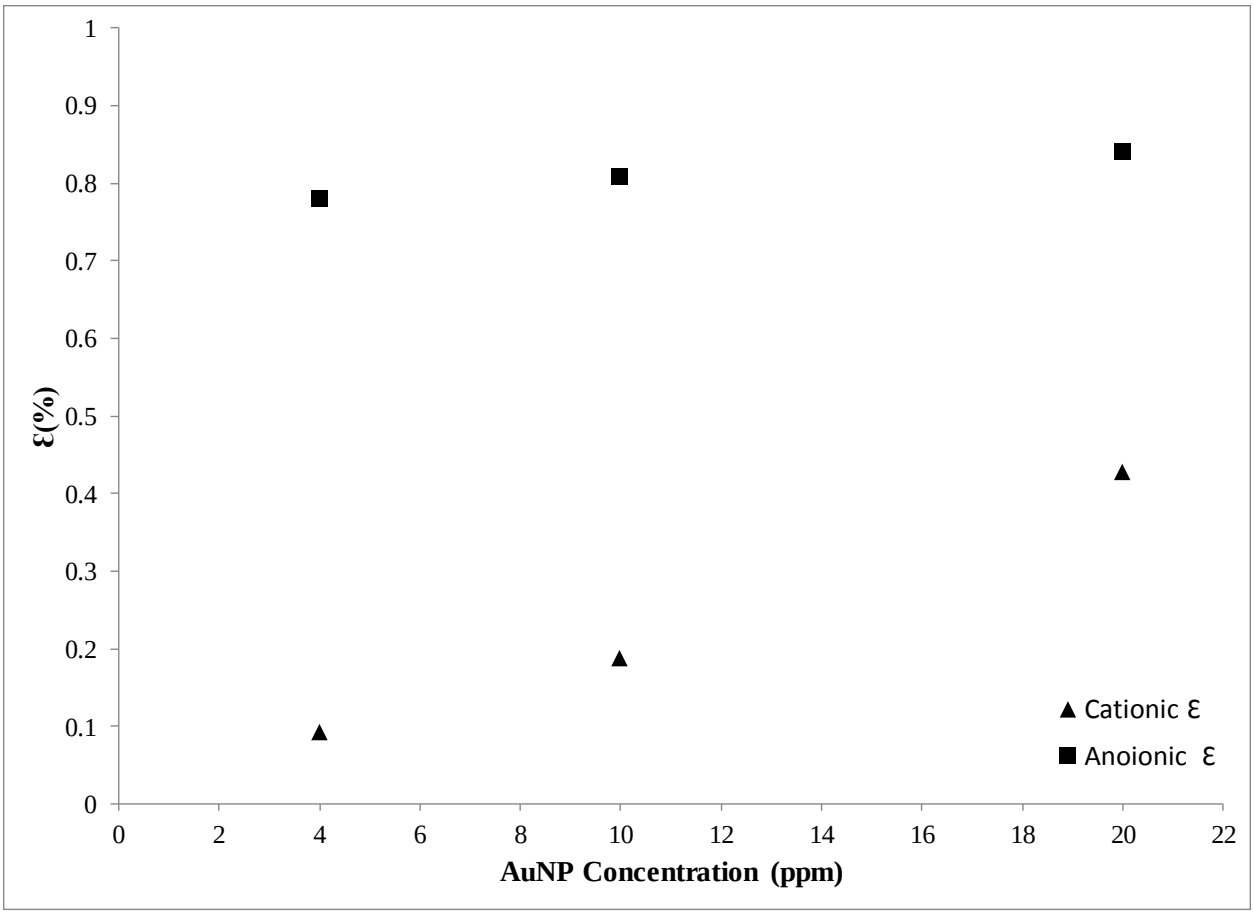

Figure 6.4. Strain due to cations and anions as a function of AuNP concentration. Anionic strain is fairly constant, while cationic strain increases with increasing AuNP concentration

To further scrutinize the effect of the CNC density on the charging process, we measured and recorded the current flow during charging and discharging of the actuators as a function of time, to compare the charging/discharging times for actuators with different density CNCs. The mobility of ions within IPMC can be modeled by complex resistor-capacitor (RC) circuits,[13] in which the charging/discharging time constant depends on the product of corresponding capacitance and internal resistance of different types of ions in the system. As shown in **Figure 6.5**, charging and discharging time constants are shorter for denser CNCs and time constant is increased as the density of CNC is reduced. The observation that denser CNCs charge and discharge at a faster rate which is in agreement with experimental strain measurements.

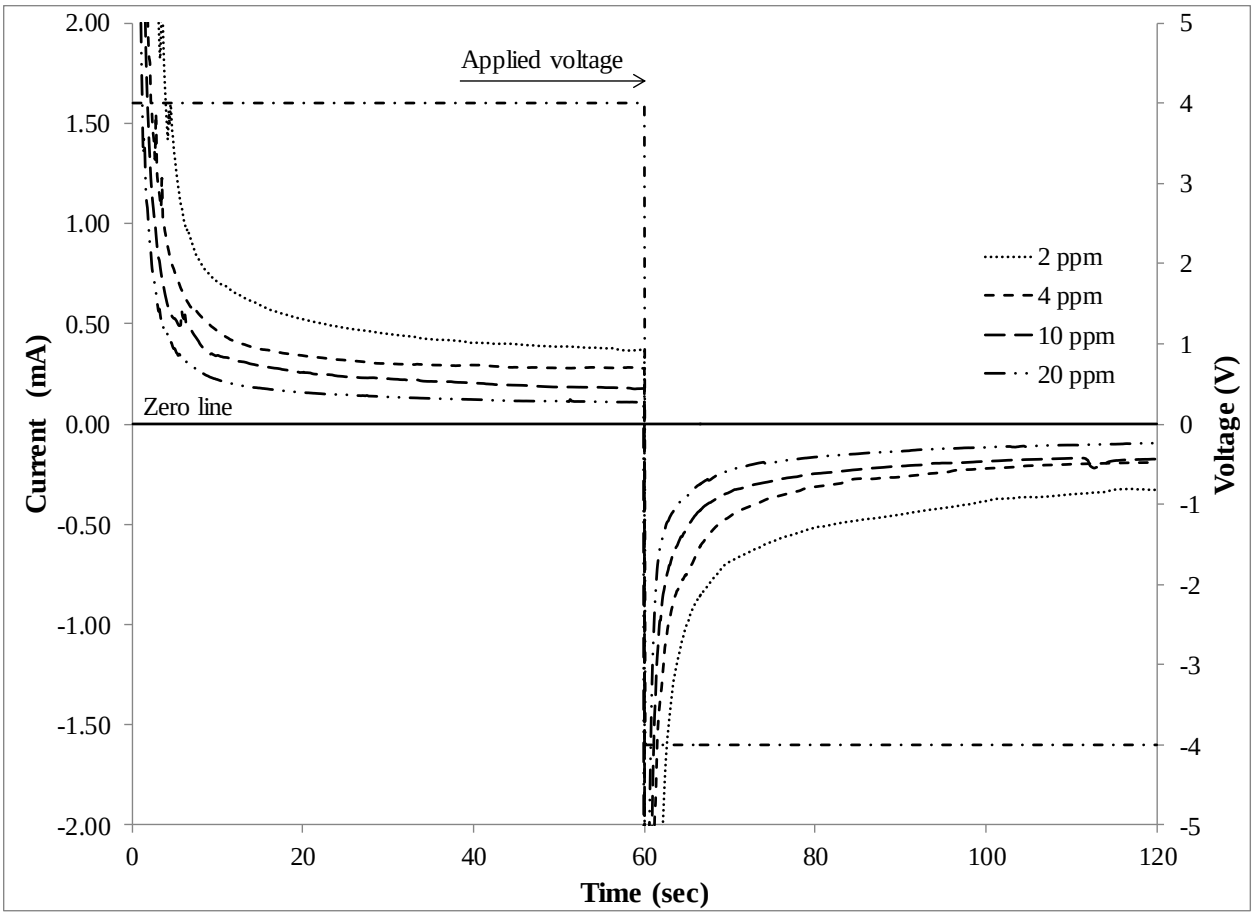

Figure 6.5. Charging and discharging currents for samples containing different AuNP concentrations are recorded as a function of time under 4V square wave

6.3.3 Frequency dependence of cationic strain

The frequency dependence of the electromechanical strain of the actuators was characterized under 4V square wave to study the influence of the density of AuNPs in the CNC layers on the time dependence performance of actuators. Actuators with different CNC densities were subjected to a range of frequencies and the mechanical strain was deduced from either the radius of curvature or the tip displacement (when the radius of curvature was insufficient to be measured). Since the bending is quite small under 1 and 10Hz frequencies, the tip displacement was recorded, instead of the radius of curvature, and was used along with the thickness and free length of the actuator to calculate the strain using **equation (2)**

$$\boldsymbol{\varepsilon}(\%) = \frac{\boldsymbol{\delta h}}{\boldsymbol{L^2}} \times \mathbf{100} \quad \textbf{(2)}$$

where δ is tip displacement, h is the thickness and L is the free length of actuator.[14] It is important to note that strains generated at all these frequencies are cationic strain as, in this set of actuators, anionic strain begins to dominate at a time longer that 10 seconds from application of the electric field. Presented in **Figure 6.6** is the peak-to-peak cationic strain of actuators with different CNC densities in response to a range of frequencies. The strain is increased for lower frequencies as the cations are given more time to accumulate at the electrodes. Also, denser CNCs show larger strain at any frequency, again suggesting that denser CNCs charge at a faster rate and thus can be used to fabricate faster actuators with larger strain generated per unit time.

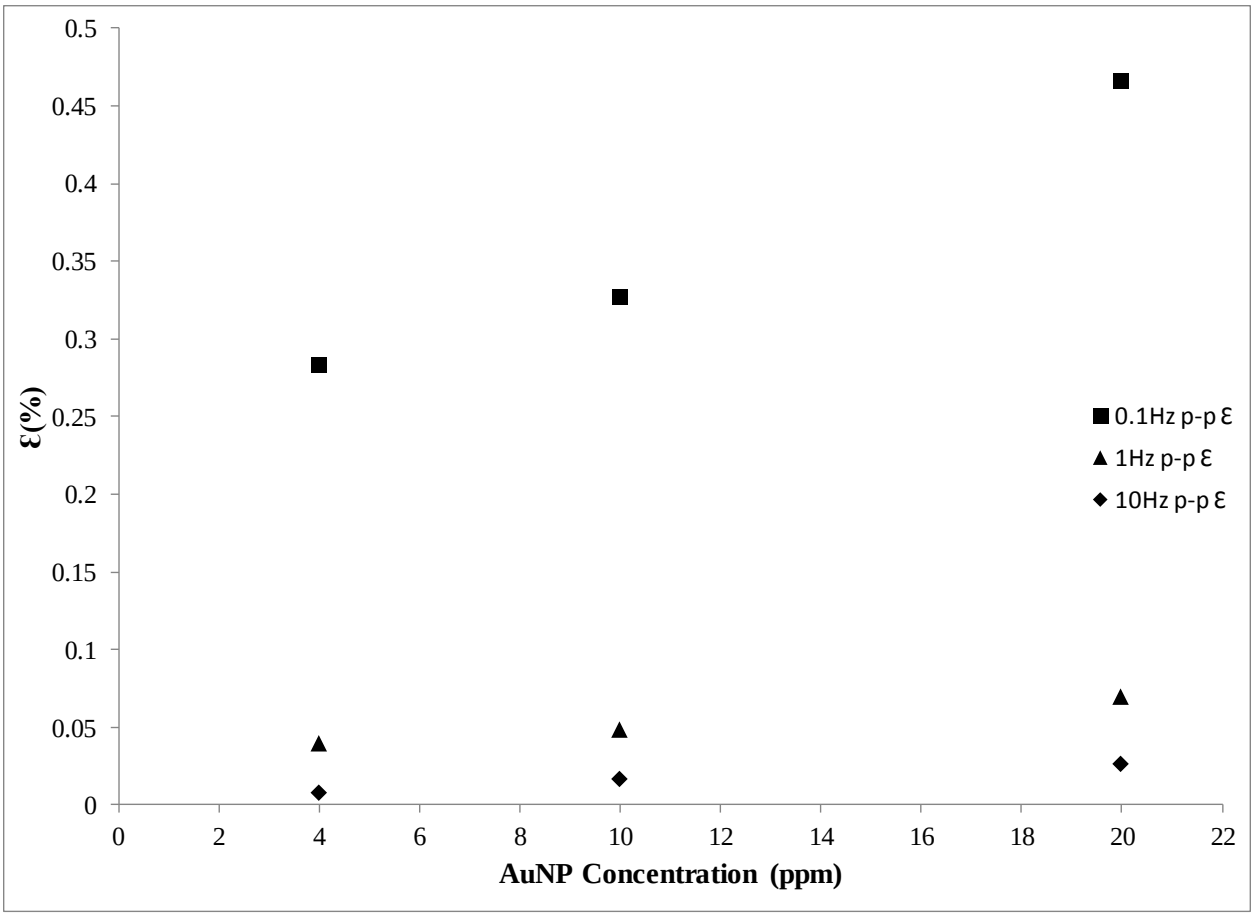

Figure 6.6. Cationic strain of actuators with different AuNP concentration is shown at different frequencies. Cationic strain increases with increasing AuNPs concentration and decreasing frequency

6.4 Summary

We have studied ionic electroactive polymer actuators consisting of conductive network composites (CNCs) with different volume densities of gold nanoparticles (AuNPs). We have successfully controlled and varied the AuNP concentration in CNC thin-films with minimum thickness fluctuation (~ 25 nm) and minimum effect on the mechanical properties of IPMCs. Varying the AuNP concentration provides a means to control the resistance and the CNC-ion interfacial area in IEAP actuators, which in turn influences charging/discharging times. Increasing the concentration of AuNPs in CNC thin-films increases the CNC-ion interface and lowers the electrical resistance of the CNC. Actuators with higher concentration of CNC exhibited faster charging/discharging and generated larger cationic strain. The larger cationic

strain in denser CNCs is due to quicker charging in such systems, which results in accumulation of more cations at the cathode before cationic strain is canceled by anionic strain. We have demonstrated that cationic strain in an actuator with denser CNC (20 ppm AuNP solution) is increased by more than a factor of four compared to that of an actuator with less dense CNC (4 ppm AuNP solution). Also, the time dependence response is improved by increasing the AuNP concentration in CNC. Under 0.1Hz frequency, the actuator with denser CNC (20 ppm AuNP solution) generates more than 164% strain compare to an actuator with less dense CNC (4 ppm AuNP solution). Improvement is less, yet still obvious, in case of faster frequencies. Such systems can be used in applications where fast response and optimum strain are desired, such as mimicking the wing motion in microrobotic insects.

References

1 R Toniolo, N Comisso, G Bontempelli, G Schiavon, and S Sitran, "A Novel Assembly for Perfluorinated Ion-Exchange Membrane-Based Sensors Designed for Electroanalytical Measurements in Nonconducting Media," Electroanalysis **10** (14), 942-947 (1998).

2 BJ Akle, 2005.

3 GS Virk, DR Harvey, I Chochlidakis, S Dogramadzi, and A Dehghani, (unpublished).

4 S Liu, R Montazami, Y Liu, V Jain, M Lin, JR Heflin, and QM Zhang, "Layer-by-layer self-assembled conductor network composites in ionic polymer metal composite actuators with high strain response," Applied Physics Letters **95** (2), 3 (2009).

5 Tatsuhiro Okada, Gang Xie, Oddvar Gorseth, Signe Kjelstrup, Norito Nakamura, and Tomoaki Arimura, "Ion and water transport characteristics of Nafion membranes as electrolytes," ELECTROCHIMICA ACTA **43** (24), 3741-3747 (1998).

6 M Shahinpoor and KJ Kim, "Novel ionic polymer-metal composites equipped with physically loaded particulate electrodes as biomimetic sensors, actuators and artificial muscles," Sensors and Actuators A: Physical **96** (2-3), 125-132 (2002).

7 BJ Akle, DJ Leo, MA Hickner, and JE McGrath, "Correlation of capacitance and actuation in ionomeric polymer transducers," J. Mater. Sci. **40** (14), 3715-3724 (2005).

8 BJ Akle, MD Bennett, and DJ Leo, "High-strain ionomeric-ionic liquid electroactive actuators," Sensors and Actuators A: Physical **126** (1), 173-181 (2006).

9 Md Abu Bin Hasan Susan, Taketo Kaneko, Akihiro Noda, and Masayoshi Watanabe, "Ion Gels Prepared by in Situ Radical Polymerization of Vinyl Monomers in an Ionic Liquid and Their Characterization as Polymer Electrolytes," JOURNAL OF THE AMERICAN CHEMICAL SOCIETY **127** (13), 4976-4983 (2005).

10 M. Terrones, J. M. Romo-Herrera, E. Cruz-Silva, F. López-Urías, E. Muñoz-Sandoval, J. J. Velázquez-Salazar, H. Terrones, Y. Bando, and D. Golberg, "Pure and doped boron nitride nanotubes," Materials Today **10** (5), 30-38 (2007).

11 Gero Decher, "Fuzzy Nanoassemblies: Toward Layered Polymeric Multicomposites," Science **277** (5330), 1232-1237 (1997).

12 PT Hammond, "Form and Function in Multilayer Assembly: New Applications at the Nanoscale," Advanced Materials **16** (15), 1271-1293 (2004).

13 Y Liu, S Liu, J Lin, D Wang, V Jain, R Montazami, JR Heflin, J Li, L Madsen, and QM Zhang, "Ion transport and storage of ionic liquids in ionic polymer conductor network composites," Applied Physics Letters **96**, 3 (2010).

14 BJ Akle, MD Bennett, DJ Leo, KB Wiles, and JE McGrath, "Direct assembly process: a novel fabrication technique for large strain ionic polymer transducers," J. Mater. Sci. **42** (16), 7031-7041 (2007).

Chapter 7
Ion Transport in IEAP Actuators

This chapter is an expansion on the work to be submitted to Sensors and Actuators A

7.1 Introduction

The focus of this chapter is on investigations of ion transport in IPMCs. Ion sources, both ionic liquids and aqueous electrolytes, consist of two types of ions: cations and anions. These two ions have different masses and volumes, thus their mobility under applied electric field is different. **Figure 7.1** presents strain generated by an IEAP actuator, consist of 30-bilayers CNC (PAH/AuNP) CNCs, at different frequencies. As can be seen from this figure, the time constant of actuation is fixed for faster frequencies and slows down beyond a certain frequency. Since transport of both types of ions begins simultaneously, it is challenging to distinguish between their motion and effect on actuation, yet it is very important to develop a good understanding of the transport of ions in the system as it is directly influential on the performance of actuators.

Understanding the dynamics of mobility and diffusion of ions within, and through, ionic membranes in ionic devices has become increasingly important and interesting due to their vital rule in defining the properties of those devices.[1,2] Ionic devices, such as ionic polymer actuators, fuel cells, batteries, super-capacitors, dye-sensitized solar cells and ionic polymer sensors, are conceptually similar to electronic devices but function based on motion of ions rather than electrons.[3] Understanding the dependence of the mobility of ions on operation conditions, such as voltage and frequency, can help to improve the efficiency and performance of ionic devices, and also provides a means to improve the design of such devices.[4]

The functionality of IEAP actuators is due to transfer of ions through the ion-exchange membrane and CNCs and their accumulation at the CNC-electrode interfaces.[5-7] Compared to other types of electromechanical actuators, such as piezoelectric materials, IEAP actuators are significantly more efficient and have the advantage of low operating voltage (~ 4 V) and high-strain output (> 15%).[8,9] The mobility of ions within the CNC layers and their transport through

the ion-exchange membrane are highly influential in defining the properties of IEAP actuator. The structure of a typical IEAP actuator is illustrated in **Fig. 7.2(top).**

In this chapter, we investigate the transport anisotropy of cations and anions within IEAP actuators by measuring the time constant of each type of ion from experimental results, and have theoretically quantified the turnover frequency for each type of ion based on its time constant. Moreover, we have verified the theoretical findings via studying the response of IEAP actuators to applied square waves of turnover frequencies.

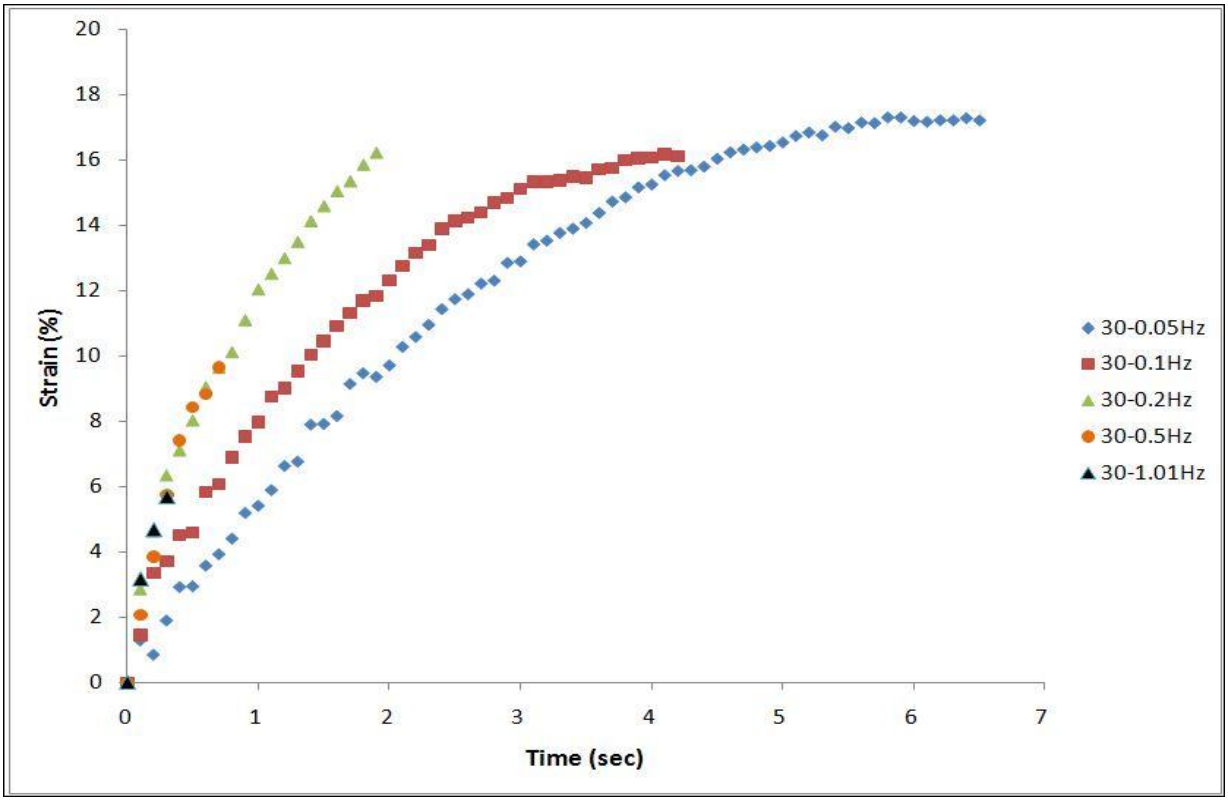

Figure 7.1. Strain of an IEAP actuator in response to a 4 V square wave at different frequencies

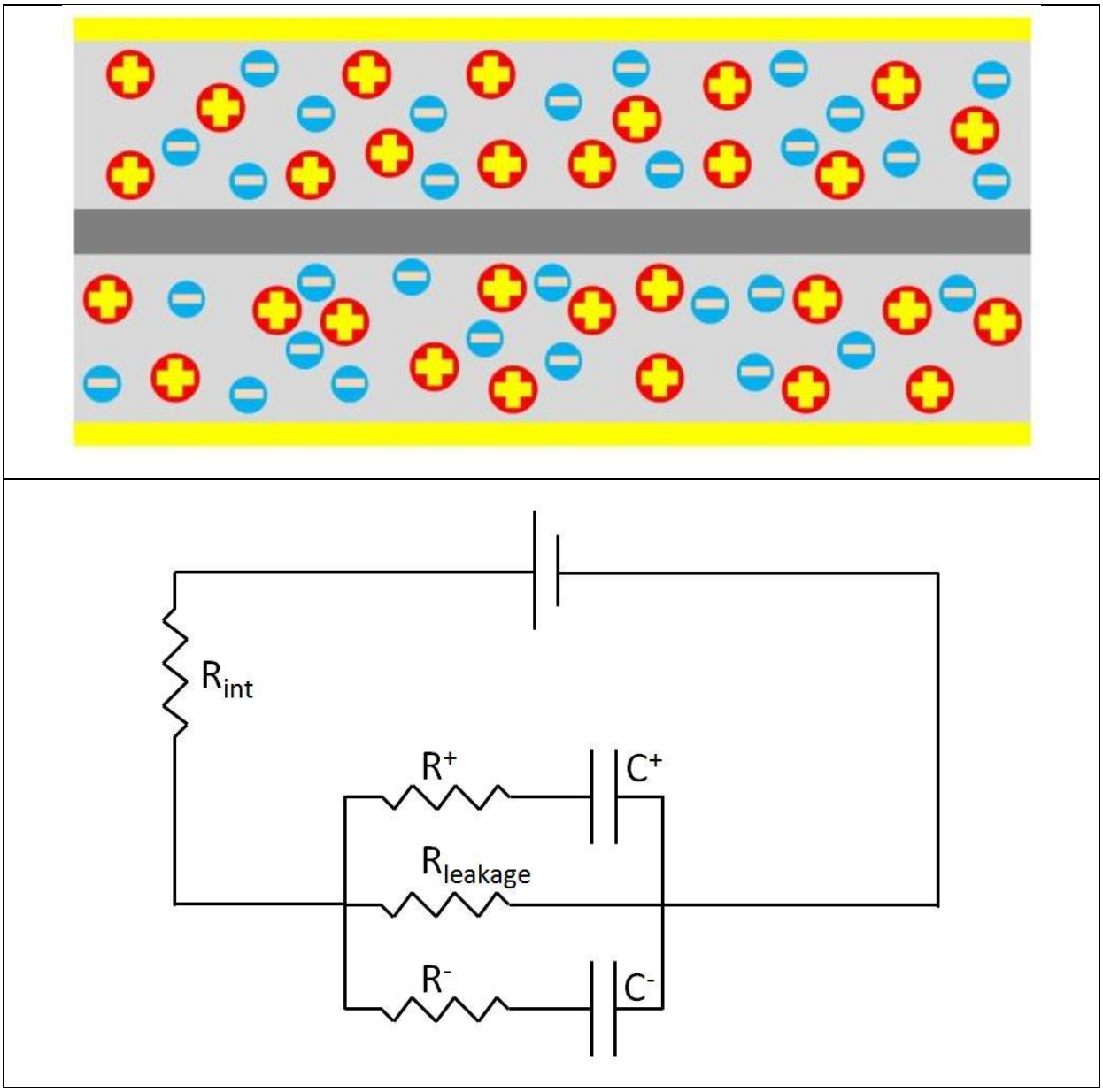

Figure 7.2. Top: Not-to-scale schematic of a typical IEAPA. Bottom: Three-loop equivalent circuit, illustrating electrical behavior of IEAPAs

7.2 Materials and Methods

The layer-by-layer (LbL) self-assembly technique was used to fabricate the CNC layers.[10,11] Consecutive deposition of anionic gold nanoparticles, AuNPs (3nm diameter, Purest Colloids inc.) and Poly(allylamine hydrochloride), PAH (M_w 70,000, Sigma Aldrich) polycation on both sides of Nafion (N111-IP, extruded, Ion Power) membrane of thickness 25μm resulted in growth of 20-bilayer thin-film nanocomposite structures. Homogeneous coverage of the thin-film was

confirmed both visually and by measuring the sheet resistance at several points of the thin-film. The membrane were then soaked with approximately 40 wt% 1-ethyl-3-methylimidazolium trifluoromethanesulfonate (EMI-Tf) (Sigma Aldrich) ionic liquid at 80°C and hot-pressed between two gold electrodes of 50nm thickness each at 95°C and 800 pound-force. Thickness of CNC layer was measured using a profilometer (Veeco Dettak 150) and found to be 32.5 nm. The mechanical response of the actuator to electric field was monitored and recorded as a function of time by a probe station equipped with a charge-coupled device (30 frames/sec) high definition camera.

7.3 Experimental results and discussions

Presented in **Figure 7.3** is the bending curvature Q (where Q is the inverse of radius of curvature) of an IEAPA under application of a 4 V step voltage. The initial response is a slight bending toward the anode, which is due to higher EMI^+ cation concentration at the cathode. The EMI^+ cation concentration at the cathode increases more quickly because cations, although spatially larger, move more easily within the ionic device. Yet, as time elapses, enough Tf^- anions reach the anode to cancel the mechanical strain generated by EMI^+ cations, and eventually bend the actuator toward cathode. Although Tf^- anions are spatially smaller than EMI^+ cations, they are more massive; as a result, have smaller drift velocity V_d. The drift velocity of each ion, regardless of the electric field, can be calculated from the following equation:

$$\boldsymbol{V_d = 2\sqrt{\frac{KT}{3m}}} \qquad \textbf{(1)}$$

where *K* is Boltzmann constant, *T* is absolute temperature and *m* is the mass of ion. The observation of ultimate bending toward the cathode indicates that Tf^- anions, although smaller in size, are more efficient in generating mechanical strain. One possible explanation for this is that they exist as aggregates (eg. $Tf^-EMI^+Tf^-$). Moreover, their transfer at a slower rate is perhaps due to existence of aggregates and/or strong interaction with the surrounding environment.

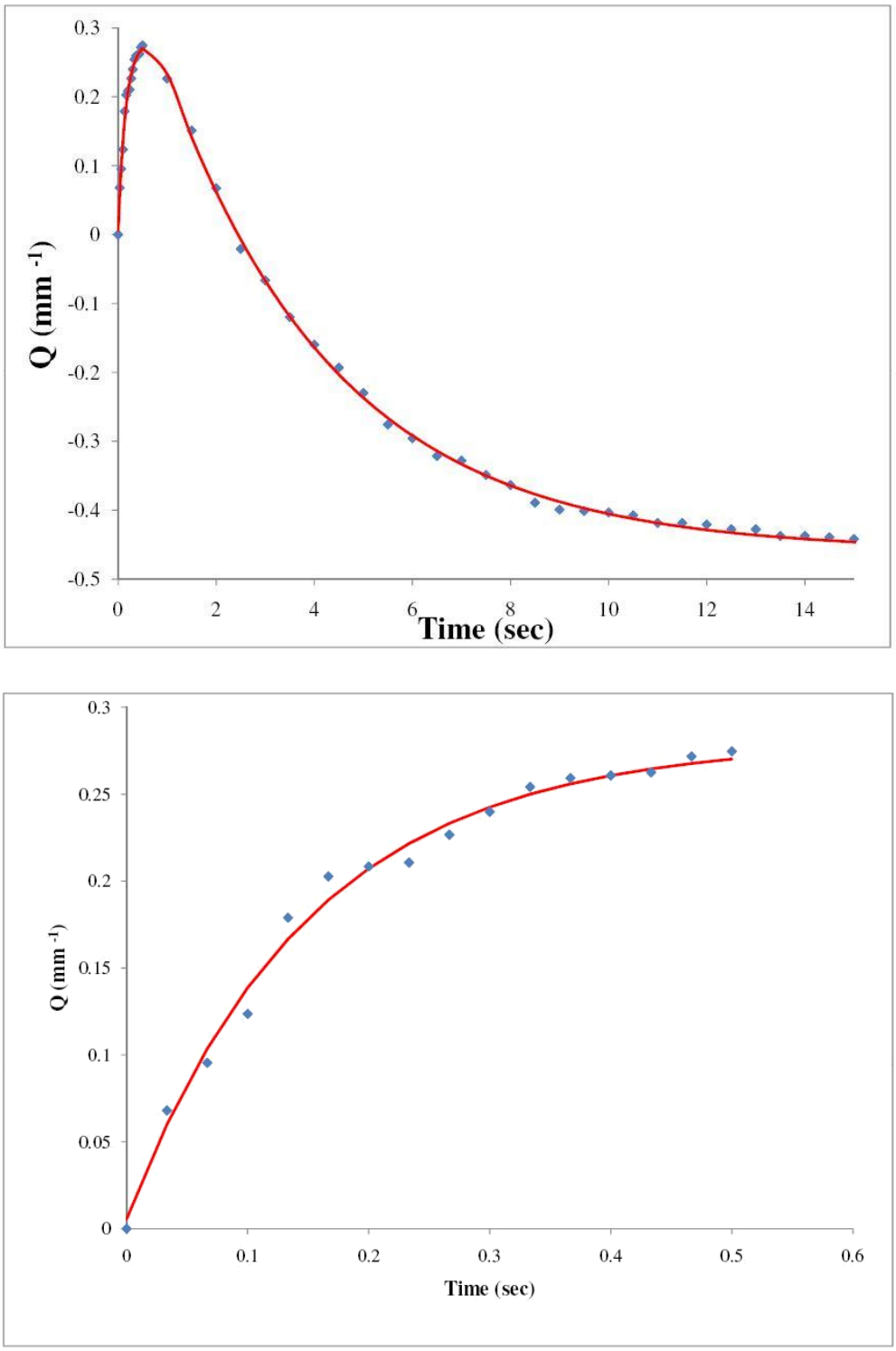

Figure 7.3. Top: Data and fitting of the electromechanical response of an IEAPA to a 4 V step function. Curvature generated by EMI^+ cations (bending toward anode) is indicated as (+) and curvature generated by Tf^- anion (bending toward cathode) is indicated as (-). Bottom: Magnified actuation data and fitting generated by cations

The curvature of IEAP actuator can be discussed and understood using a two-carrier model[12] that takes into account the anisotropy of cation and anion motion within IEAP actuators. **Figure 7.2 (bottom)** illustrates a three-loop equivalent RC circuit including two separate, yet interacting, RC branches for cations and anions, and one loop for internal resistance of the ionic device. The internal resistance of the ionic device was detected from electrical measurements that indicate a leakage current, not shown here. The curvature of the actuator can be fitted in two separate steps, for cation dominated and anion dominated motion, with the following equations:

$$\boldsymbol{Q_{fit}^{+} = Q^{+}\left(1 - e^{-t/\tau^{+}}\right) + n} \quad \textbf{(2)}$$

$$\boldsymbol{Q_{fit}^{-} = c\left[\left(Q^{-}e^{-t/\tau^{-}}\right) + m\right]} \quad \textbf{(3)}$$

where Q^{+} and Q^{-} are maximum absolute curvatures generated by cations and anions respectively, τ^{+} and τ^{-} represent the time constants of cations and anions respectively, and *m*, *n* and *c* are correcting constants.

As EMI^{+} cations and Tf^{-} anions have different time constants when in an electric field, they respond differently to wave functions with different frequencies. The turnover frequency (frequency at which each type of ion dominates the actuation) of each type of ion can be calculated from the following equation, by using the time constant of each type of ion.

$$\boldsymbol{f_{turnover} = (2\pi RC)^{-1} = (2\pi\tau)^{-1}} \quad \textbf{(4)}$$

Equations (2) and (3) were used to fit the experimental data, as shown in **Fig. 7.3 (bottom)**. The fitting parameters are shown in **Table 7.1**. The time constants τ^{+} and τ^{-} are found to be 0.15 s and 3.52 s respectively. This indicates that, as expected, EMI^{+} cations are significantly faster than Tf^{-} anions, which results in initial fast bending toward the anode, and as time progresses Tf^{-} anions which are slower but more efficient in generating strain ($Q^{+} < Q^{-}$) take over and generate

enough strain to bend the actuator toward the cathode. The turnover frequencies for each type of ion were then deduced from equation (4) and are shown in **Table 7.1**. The turnover frequency of EMI^+ cations is determined to be 1.06 Hz; that is at frequencies 1.06 Hz and faster EMI^+ cations dominate the actuation, and the curvature generated by EMI^+ cations is optimum (maximized) at the turnover frequency. At frequencies between the two turnover frequencies the curvature efficiency of the actuator is not optimum as strain generated by cations and anions tend to work against each other, as a result performance is decreased to different extents depending on the frequency. When the frequency drops to or below turnover frequency of Tf^- anions, 0.045 Hz, Tf^- anions are given enough time to generate maximum strain, thus the efficiency is again optimized.

	EMI^+ Cation	Tf^- Anion
τ	0.15 s	3.52 s
Q	0.275 mm^{-1}	0.452 mm^{-1}
n	0.005	N/A
m	N/A	0.26
c	N/A	-2.03
f	1.06 Hz	0.045 Hz
V_d	170.66 $m.s^{-1}$	149.36 $m.s^{-1}$

Table 7.1. Characteristic parameters of EMI^+ cation and Tf^- anion

Presented in **Figure7.4** is the actuation curvature of an IEAP actuator in response to a 4 V square-wave function at 1 Hz frequency. The bending is only and always toward the anode, which implies domination of EMI^+ cations in generating strain. The wave function is also shown, solid line, to verify that the bending is always toward the anode. Similar data is taken for frequencies equal to or smaller than 0.045 Hz to verify that net bending is toward the cathode and Tf^- anions are dominating the bending. The plot would be a cyclic repetition of **Figure 7.3**, not shown here.

A comparison of τ^+ and τ^- reveals that EMI^+ cations, although spatially larger, move at a significantly faster speed compared to more massive Tf^- anions. The bending pattern of the actuator suggests that Tf^- anions are more efficient in generating strain, yet at frequencies equal or higher than the cation's turnover frequency, bending is dominated by the fast EMI^+ cations. This suggests that the bending can be manipulated by control of operation conditions, particularly frequency.

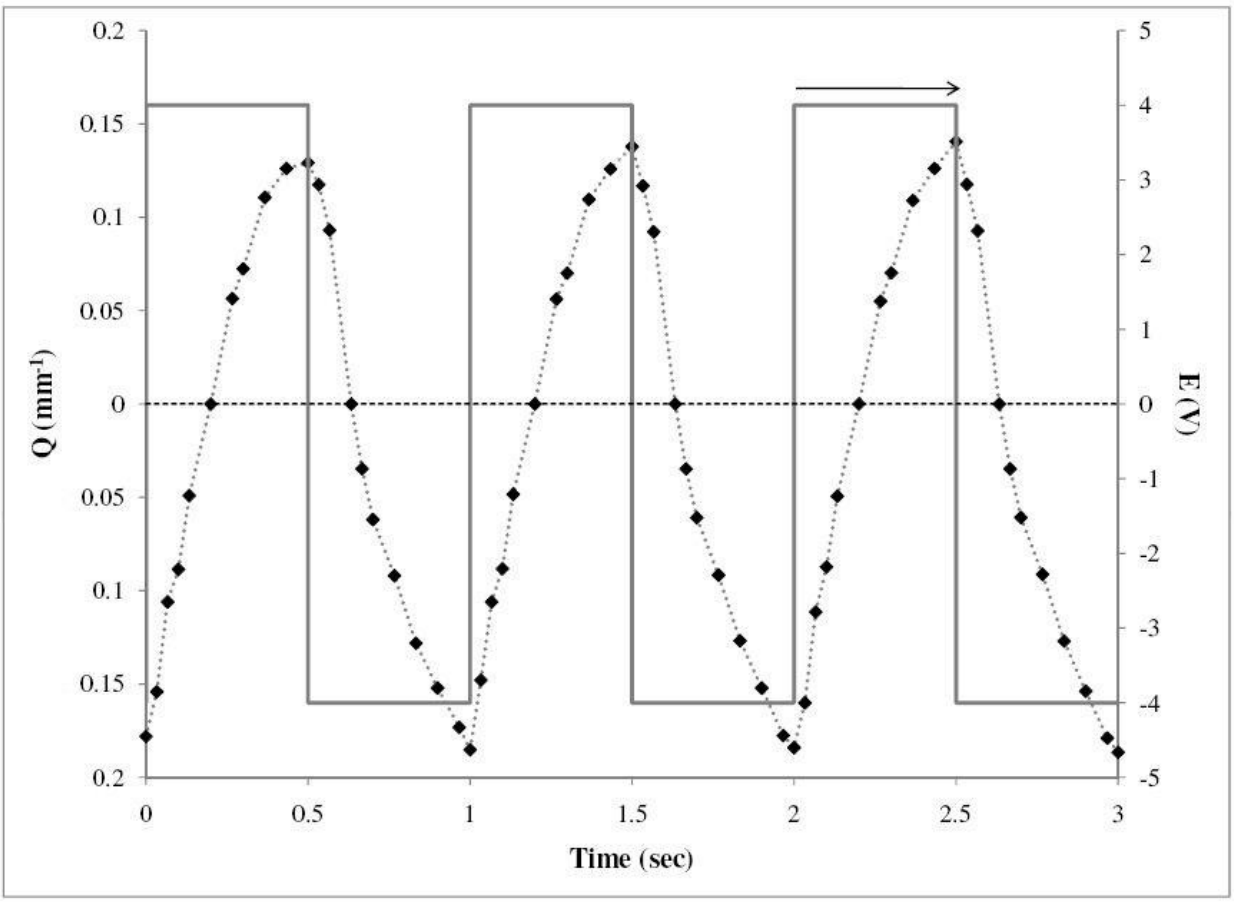

Figure 7.4. Electromechanical response of an IEAPA to a 4 V, 1 Hz square wave, EMI^+ cations dominate the actuation. The dotted line is to guide the eye and the dashed line indicates the zero-line

7.4 Summary

Ionic electroactive polymer actuators exhibit electromechanical coupling in response to an applied electric voltage. The mobility of ions in this type of actuator is important and influential

on the efficiency of the actuator. Understanding dependence of the mobility of ions on operation conditions is of vital importance in improving the design and efficiency of the actuators. Here we presented a study of frequency dependence of actuation in ionic electroactive polymer actuators and have quantified time constants of cations and anions. We have also theoretically quantified and experimentally confirmed the turnover frequencies of the system, at which the actuation is dominated by cations or anions. Our findings provide critical feedback for optimizing performance of actuators, and ionic devices in general, via control of the operation conditions.

References

1 Md Abu Bin Hasan Susan, Taketo Kaneko, Akihiro Noda, and Masayoshi Watanabe, "Ion Gels Prepared by in Situ Radical Polymerization of Vinyl Monomers in an Ionic Liquid and Their Characterization as Polymer Electrolytes," JOURNAL OF THE AMERICAN CHEMICAL SOCIETY **127** (13), 4976-4983 (2005).

2 M. Terrones, J. M. Romo-Herrera, E. Cruz-Silva, F. López-Urías, E. Muñoz-Sandoval, J. J. Velázquez-Salazar, H. Terrones, Y. Bando, and D. Golberg, "Pure and doped boron nitride nanotubes," Materials Today **10** (5), 30-38 (2007).

3 W Weppner, "Interfaces in ionic devices," Ionics **7** (4), 404-424 (2001).

4 J Li, KG Wilmsmeyer, J Hou, and LA Madsen, "The role of water in transport of ionic liquids in polymeric artificial muscle actuators," Soft Matter **5** (13), 2596-2602 (2009).

5 BJ Akle, MD Bennett, and DJ Leo, "High-strain ionomeric-ionic liquid electroactive actuators," Sensors and Actuators A: Physical **126** (1), 173-181 (2006).

6 Sia Nemat-Nasser, "Micromechanics of actuation of ionic polymer-metal composites," Journal of Applied Physics **92** (5), 2899-2915 (2002).

7 BJ Akle, MD Bennett, DJ Leo, KB Wiles, and JE McGrath, "Direct assembly process: a novel fabrication technique for large strain ionic polymer transducers," J. Mater. Sci. **42** (16), 7031-7041 (2007).

8 E Smela, "Conjugated polymer actuators for biomedical applications," Advanced Materials **15** (6), 481-494 (2003).

9 S Liu, R Montazami, Y Liu, V Jain, M Lin, JR Heflin, and QM Zhang, "Layer-by-layer self-assembled conductor network composites in ionic polymer metal composite actuators with high strain response," Applied Physics Letters **95** (2), 3 (2009).

10 JL Lutkenhaus and PT Hammond, "Electrochemically enabled polyelectrolyte multilayer devices: from fuel cells to sensors," Soft Matter **3** (7), 804-816 (2007).

11 K Ariga, JP Hill, and Q Ji, "Layer-by-layer assembly as a versatile bottom-up nanofabrication technique for exploratory research and realistic application," Physical Chemistry Chemical Physics **9** (19), 2319-2340 (2007).

12 Y Liu, S Liu, J Lin, D Wang, V Jain, R Montazami, JR Heflin, J Li, L Madsen, and QM Zhang, "Ion transport and storage of ionic liquids in ionic polymer conductor network composites," Applied Physics Letters **96**, 3 (2010).

Chapter 8
Motion of Different Ions in IEAP Actuators

The functionality of IEAP actuators is due to mobility of ions within the IPMC. The ions are sourced by uptake of electrolyte (aqueous or ionic liquid) into the IPMC. Nafion has a sulfonate end group with a proton counterion. To further understand the extent of the importance and influence of ions on the performance of IEAP actuators, we have used different ionic liquids as the ion source and have also substituted Nafion's proton counterion. To slow down the full motion of the ions in the IPMC, so that we can better observe the behavior of the actuators, a 90 μm thick Nafion membrane was used instead of the 25 μm thick Nafion used in the other studies in this dissertation. Also, a CNC thin-film was not fabricated on these membranes. The actuators used for this study consist of Nafion, the ionic liquid electrolyte, and outer gold leaf electrodes. This chapter presents results and discussion of this study.

8.1 Ionic Liquids

We have used EMI-Tf for our previous studies presented in this work, and thus use it as a reference ionic liquid here. In addition, we used two other ionic liquids that have different cations but the same anion, 1-Butyl-1-methylpyrrolidinium bis(trifluoromethylsulfonyl)imide (BMP-TFSI) and Triethylsulfonium bis(trifluoromethylsulfonyl)imide (TES-TFSI). Presented in **Figure 8.1** are the 3D chemical structures of the three ionic liquids we used in this study.

The samples of 90 μm thick Nafion were soaked in the ionic liquids solutions diluted with ethanol. The solution was heated to 80°C expedite the uptake process. The details of the process are presented in chapter 3.

Samples consisting of Nafion, in its proton form, and different ionic liquids were tested under 4 V electric field. The bending occurred rather slowly due to large thickness of the ionomeric membrane. The strain is shown as a function of time in **Figure 8.2**. As expected, the sample with EMI-Tf first bends toward the anode, and the bending is then slowly canceled and changes direction toward the cathode. In the case of the other two samples, no bending due to cationic motion was observed, and bending was only toward the cathode. Given that net strain is in fact

the difference of cationic and anionic strains, this result suggests that BMP and TES cations have very limited mobility in this case and thus do not generate significant strain. The strain generated by TFSI dominates the net strain.

Since even in the case of EMI-Tf the anionic strain eventually dominates, the difference is probably that the TES and BMP cations do not move quickly enough to provide initial cation-induced strain. For EMI-Tf, the EMI cation moves more quickly than the Tf anion so that there is an initial bending due to the cation motion that then gets canceled by the anion-induced strain.

It is also seen in **Figure 8.2** that the strain for the BMP-TFSI sample is less than that of the TES-TFSI samples. Since the BMP cation is larger in volume than the TES cation, this result is consistent with a larger cancelation of the TFSI induced bending by BMP than by TES.

Dual motion (cationic followed by anionic) of IEAP actuators is one of the areas that receives the most criticism, as it makes it difficult to use the actuators in practical applications. These results suggest that the dual motion problem can be eliminated using proper electrolytes.

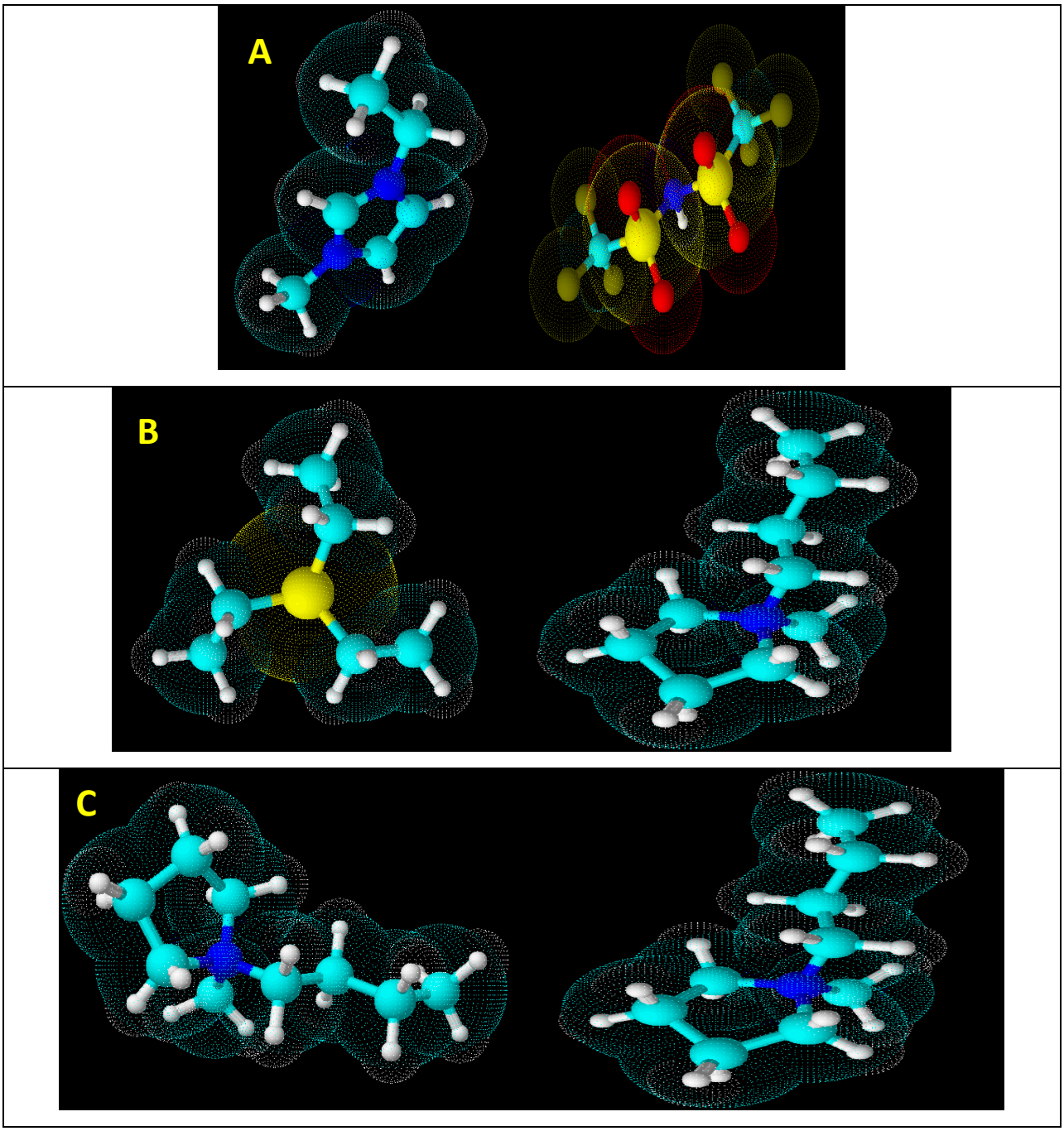

Figure 8.1. A) 1-Ethyl-3-methylimidazolium trifluoromethanesulfonate (EMI-Tf) (molecular formula: $C_7H_{11}F_3N_2O_3S$), B) Triethylsulfonium bis(trifluoromethylsulfonyl)imide (TES-TFSI) (molecular formula: $C_8H_{15}F_6NO_4S_3$), C) 1-Butyl-1-methylpyrrolidinium bis(trifluoromethylsulfonyl)imide (BMP-TFSI) (molecular formula: $C_{11}H_{20}F_6N_2O4S_2$)

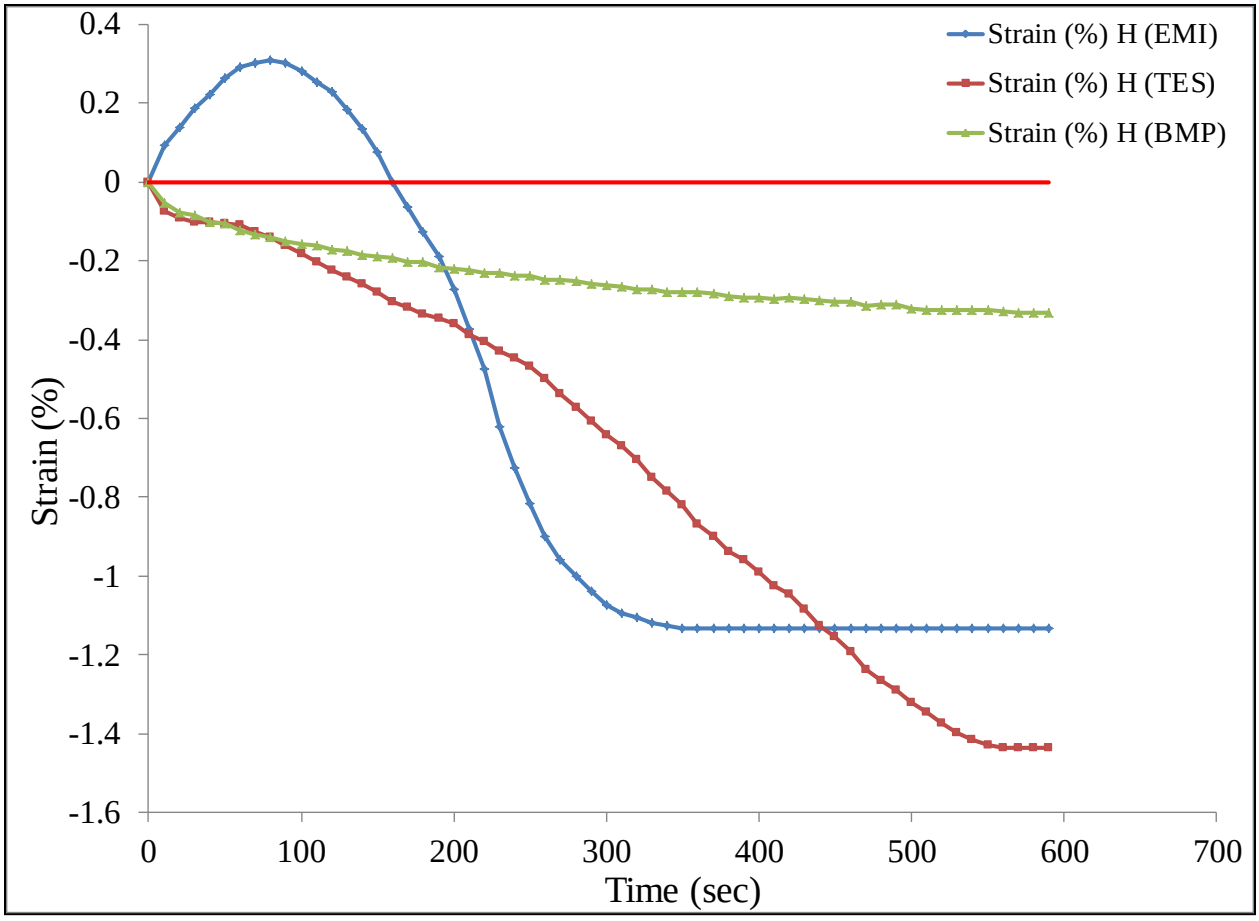

Figure 8.2. Net strain of IEAP actuators with ionic liquids, EMI-Tf, TES-TFSI and BMP-TFSI. Sample with EMI-Tf ionic liquid is the only one exhibiting bending due to cationic motion. 90 µm thick Nafion, in its proton form, is used as the ionomeric membrane

8.2 Counterion exchange

Nafion is provide commercially in acid form. That is, it has a proton counterion at its sulfonate end group, **Figure 8.3**. It has been shown previously that exchanging the proton counterion can result in variations in the actuation behavior of IEAP actuators.[1]

In this study, the proton counterion was replaced with the EMI cation through an ion exchange process (see **chapter 3**) to scrutinize the influence of the counterion on the behavior of IEAP actuators containing different ionic liquids.

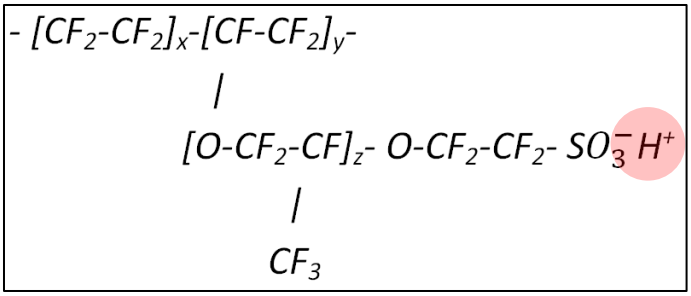

Figure 8.3. Nafion is shown in its acid form. The proton is highlighted

Replacing the proton with EMI and repeating the set of experiments in section 8.1, it was observed that in all cases the actuation behavior of the IEAP actuators is influenced, as shown in **Figure 8.4**. The most significant variation was in the case of the IEAP actuator with BMP-TFSI ionic liquid, which had only exhibited bending due to anionic motion when the proton was the counterion. In the presence of the EMI counterion, only bending due to cationic motion was observed in this case, which shows a strong influence from the counterion in the actuation process.

Presented in **Figures 8.5**, **8.6** and **8.7** are the strain of IEAP actuators with the same ionic liquid and different counterion. Comparison of the strain between the samples with proton and EMI counterions shows that in all cases, but to different extents, the net strain is shifted toward cationic motion. This suggests that EMI, which is a larger cation compared to a proton, participates in the actuation process and generation of strain. Furthermore, the reversal in the case of BMP-TFSI from anion-dominated bending to cation-dominated bending is consistent with the fact that the ultimate anionic bending is significantly less for BMP-TFSI than for EMI-Tf and TES-TFSI (see **Figure 8.2**). Thus, the additional cationic contribution from EMI Nafion counterion is sufficient to reverse the bending direction for BMP-TFSI.

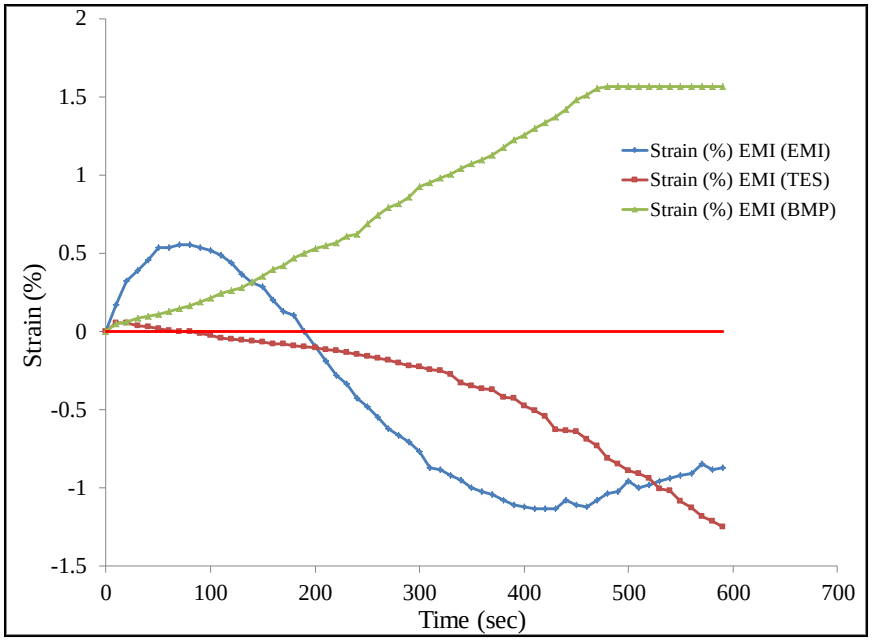

Figure 8.4. Net strain of three IEAP actuators with different ionic liquids and EMI counterion for Nafion. A 90 µm thick Nafion with EMI counterion, is used as the ionomeric membrane

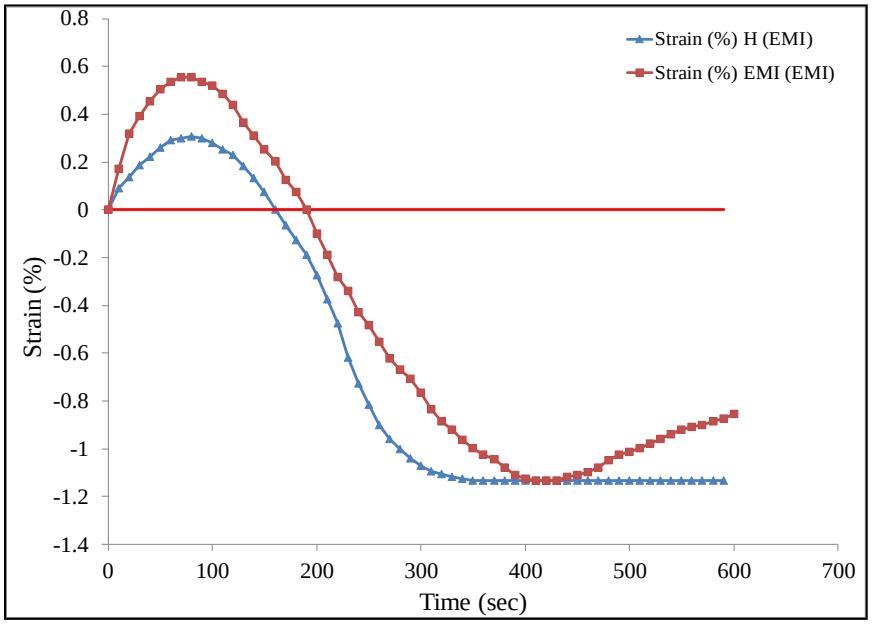

Figure 8.5. IEAP actuators with proton and EMI counterions, containing EMI-Tf. The net strain in the sample with EMI counterion is shifted toward cationic motion, indicating the influence and participation of the larger EMI counterion in generation of cationic strain

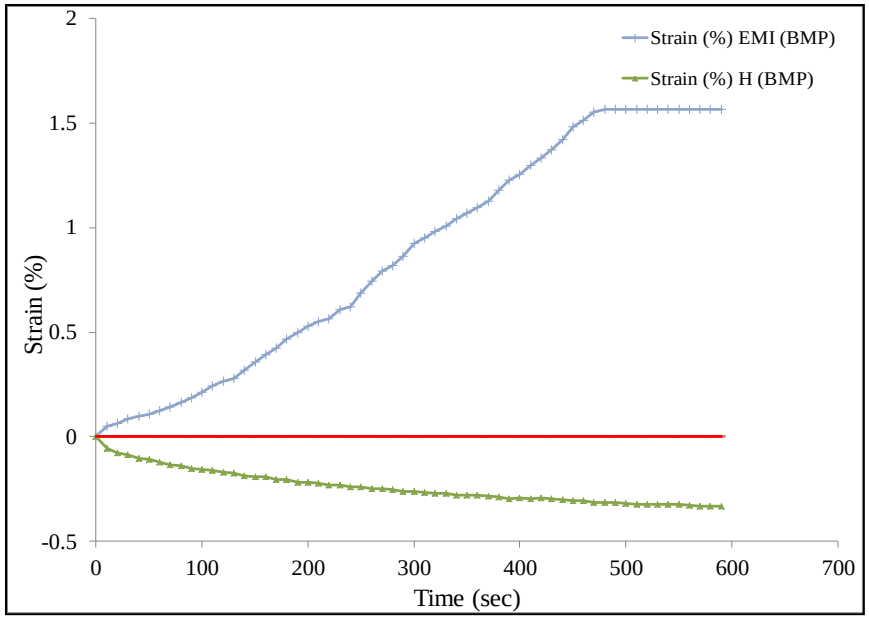

Figure 8.6. IEAP actuators with proton and EMI counterions, containing BMP-TFSI. The net strain in the sample with proton counterion is only anionic whereas the net strain in the sample with the EMI counterion shifts direction completely and only exhibits cationic motion

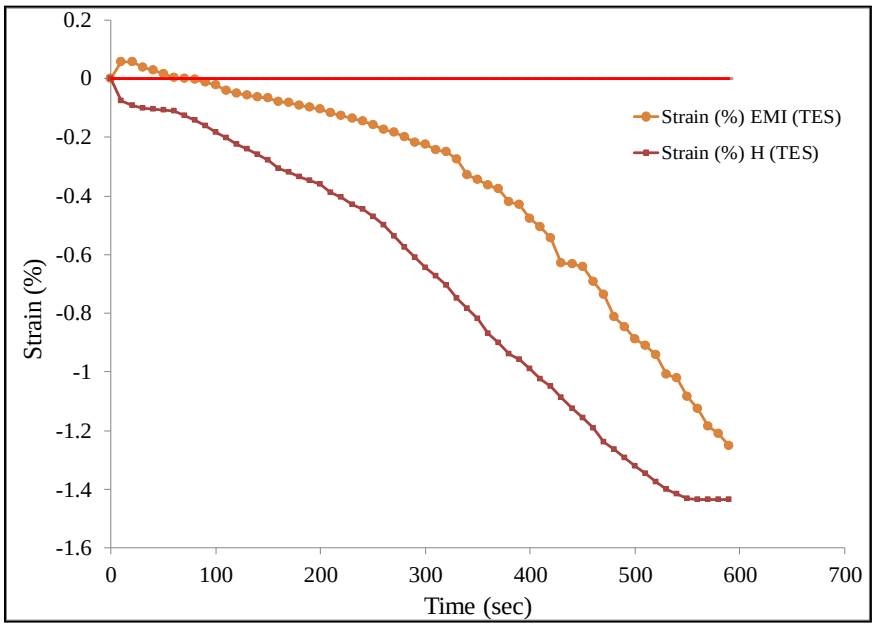

Figure 8.7. IEAP actuators with proton and EMI counterions, containing TES-TFSI. The net strain in the sample with EMI counterion is shifted toward cationic motion, yet is still dominated by anionic motion. The results indicate the strength of TFSI anions in generating strain compared to TES cations.

Reference

1 M.D. Bennett, D.J. Leo, G.L. Wilkes, F.L. Beyer, and T.W. Pechar, "A model of charge transport and electromechanical transduction in ionic liquid-swollen Nafion membranes," POLYMER **47** (19), 6782-6796 (2006).

Chapter 9
Nematic Liquid Crystal Elastomer Thermomechanical Actuators

The work described in this chapter was done during a summer internship at Naval Research Laboratory. This work is submitted to Sensors and Actuators A.

9.1 Introduction

Development of biomimetic, stimuli responsive, smart materials has attracted significant experimental[1-7] and theoretical[8-12] interest from the materials research community. There have been considerable efforts to mimic the fiber structure of skeletal muscle by developing soft linear electromechanical and/or thermomechanical actuators as the building blocks of artificial muscles.[13,14] Liquid crystal elastomers (LCEs) have been shown to exhibit a linear, anisotropic mechanical response to electrical and/or thermal stimulation due to a reversible change in orientation of the liquid crystal director, which is tightly coupled to the underlying polymer network.

Polymer liquid crystals are ordered super molecules with excellent framework for functionality. Cross-linking of polymeric liquid crystals results in elastomers with similar properties to conventional elastomers. Liquid crystal elastomers have some advantages over ordinary elastomers, one of which is response to external stimuli. The mechanical response of LCEs can be tuned by optimization of cross-linking density, flexibility of the polymer backbone, coupling between the backbone and liquid crystal group and coupling within the liquid crystal group.

In the early 2000's nematic LCE materials were developed for actuator applications. In the nematic phase, mesogens have orientational order which forces the backbone of polymer chains to align along the average direction of mesogens; this results in elongation of the elastomer. Upon heating, the nematic order is disturbed and eventually lost which results in disappearance of the alignment force which in turn results in relaxation of the backbone of polymers to their coil-like conformation, and contraction of the elastomer. This process can be reversed by cooling the elastomer and repeated by thermal cycles.

Nematic LCEs are particularly attractive for biomedical applications since they are soft, elastic materials. Nematic LCE actuators are axial actuators. When the actuator is stimulated, mechanical deformation appears in all three spatial dimensions. When the actuator is expanding, the thickness and width decrease to compensate the increase of length of the actuator. The reverse occurs when the actuator in contracting. Nematic LCE actuators have been shown to exert stress and strain comparable to that of human skeletal muscle (σ= 350kPa and ε= 25%).

LCE actuators have possible applications in biomimetic actuators, as they have close mechanical properties and performance to biological muscles. LCEs can also be used in design of temperature sensitive mechanical valves which can operate autonomously with no need for an external energy source.

Nematic LCEs consist of pendant liquid crystal mesogens attached to a polymer network. Previous studies have demonstrated that the actuation properties of LCEs may be enhanced by doping these materials with colloidal particles. Addition of micron-sized particles was shown to produce defects in the elastomer network that may deform the director, causing the formation of complex structures.[15-17] Effective dispersion of submicron particles in LCEs is a delicate task, yet provides a means to improve the material response to external stimuli while preserving the elastomer network. Incorporating a high concentration of submicron particles disturbs the elastic network of the elastomer and creates rigid compounds,[18,19] while embedment of low concentrations introduces several interesting properties to the LCEs.[20-22] For instance, Reznikov *et al.* embedded ferroelectric thiohypodiphosphate particles in nematic LCE matrices and enhanced the dielectric anisotropy without significantly perturbing the director field.[20] Matuo *et al.* studied the dynamic behavior of nematic LCEs doped with ferromagnetic particles using linear optical techniques and verified that ferromagnetic particles reduced the volume fraction of the magnetic material in the sample.[21] Courty *et al.* induced a large electromechanical response in nematic LCEs filled with very low (~0.01%) concentration of carbon nanotubes aligned along the director, which is particularly significant since pure nematic LCEs do not respond to electric field.[22]

In this work, we embed dispersed AuNPs in nematic LCEs. Due to the high thermal conductivity of gold (300 W/m·K), the presence of AuNPs in the elastomer was expected to enhance the

inherently low thermal conductivity of the nematic LCE.[14] We report the effects of incorporating low amounts of AuNPs into a nematic LCE and quantify the mechanical properties, thermoelastic properties and response time of the resultant material at different AuNP concentrations. Presented in **Figure 9.1** is a schematic illustration of the AuNPs in liquid crystal elastomer network.

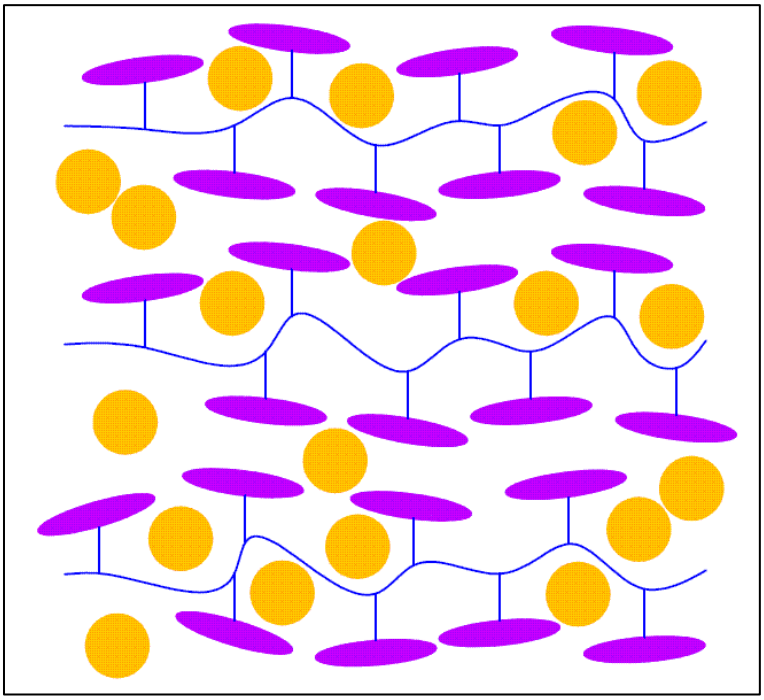

Figure 9.1. Schematic illustration of the AuNPs in liquid crystal elastomer network

9.2 Materials

2,5-Dihydroxybenzoic acid, benzyl bromide, 4-pentylcyclohexylcarboxylic acid, 4-hydroxybutyl acrylate, and anhydrous dichloromethane were purchased from Sigma Aldrich. 1,6-Hexanediol diacrylate (HDA) was purchased from Scientific Polymer and the photoinitiator Irgacure 369 was purchased from Ciba-Geigy. AuNPs (3nm diameter) were obtained from Purest Colloids. Further purification and/or synthesis have been described previously[23].Materials obtained from Sigma Aldrich were used to synthesize two liquid crystal monomers, LCM-1($C_{36}H_{40}O_{10}$) and LCM-2 ($C_{38}H_{56}O_8$). The synthesis of these two materials has been previously reported.[23] **Figure 9.2** illustrates the structure of the liquid crystal monomers.

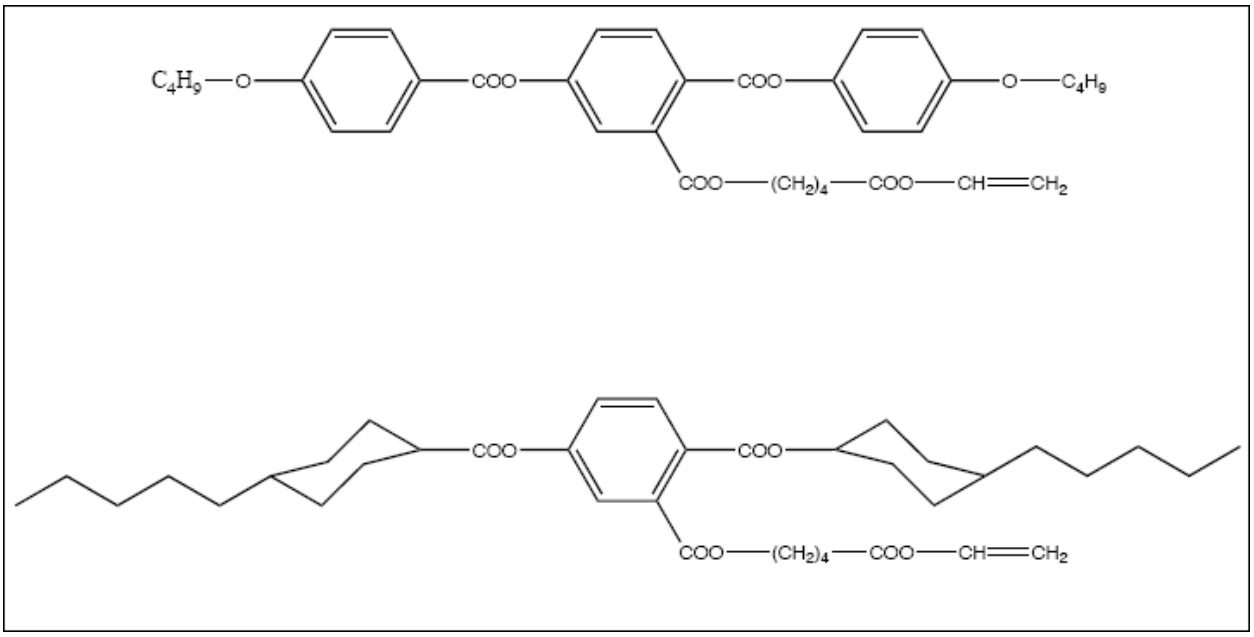

Figure 9.2. Chemical structures of two liquid crystal monomers LCM-1 (top) and LCM-2 (bottom)

9.3 Samples preparation

Nematic compound

LCM-1 and LCM-2 were mixed at equal parts by weight. To this was added 10 mol% of the cross-linking agent HDA and 0.1 mol% of Irgacure 369. The mixture was diluted in dichloromethane.

9.3.1 Incorporation of AuNP

To bring the colloidal metal from an aqueous suspension, the AuNPs were centrifuged at 16K×g for 5 minutes and the supernatant was then carefully removed. Equal amount of nematic LCE solution was added to vials containing 0, 10, 20, and 40µg of AuNPs to obtain concentrations of 0, 0.024, 0.048 and 0.096 mol% respectively. The samples were then placed under vacuum for 72 hours to evaporate the solvent. After drying, 1 mL of dichloromethane was added to each sample and sonicated for 3 hours to create a homogeneous dispersion of nanoparticles and to break up any possible aggregates. The samples were again placed under vacuum for 24 hours to evaporate the solvent.

9.3.2 Fabrication of free-standing films

The procedure of creating the free-standing elastomer films has been described elsewhere.[7] In brief, the monomeric mixture was filled at 100°C into 100 μm thick glass templates coated with a mechanically rubbed layer of polyvinyl alcohol (PVA). The mixture was then aligned by slow cooling to ambient temperature and photopolymerized under UV light. The sacrificial PVA coating was then dissolved in hot water and the elastomer film was carefully extracted from the cell. The resultant elastomer films were highly birefringent, confirming the alignment of the material.

9.4 Mechanical and thermoelastic studies

All mechanical and thermoelastic measurements were done on a TA Instruments Q800 Dynamic Mechanical Analyzer (DMA) equipped with a liquid nitrogen cooling accessory using a tension (film) clamp. The clamp consists of a fixed upper clamp and a moveable lower clamp positioned on an air bearing. Three types of experiments were performed on the DMA: isothermal stress/strain, thermoelastic, and response time. *Isothermal* experiments were performed at 70°C under application of 8kPa preload and applying a static force at the rate of 2mN/min. Young's moduli (*E*) were then calculated from the slope of the stress vs. strain plot. *Thermoelastic* experiments were conducted by applying repeated heating and cooling cycles to samples at several constant applied stresses ranging from 5kPa to 40kPa. The temperature was cycled between 50°C to 130°C at a rate of 0.5°C/min. Each cycle was performed after an initial 10 minute isothermal hold. *Response time* measurements were performed by applying various heating rates while the elastomer film was held under a preload of approximately 10kPa. The changes in the strain of the elastomer were recorded as a function of time. Presented in **Figure 9.3** is the elastomer under cross-polarizers, the high birefringence of the elastomers under cross-polarizers confirms good alignment of the directors along the rubbing direction.

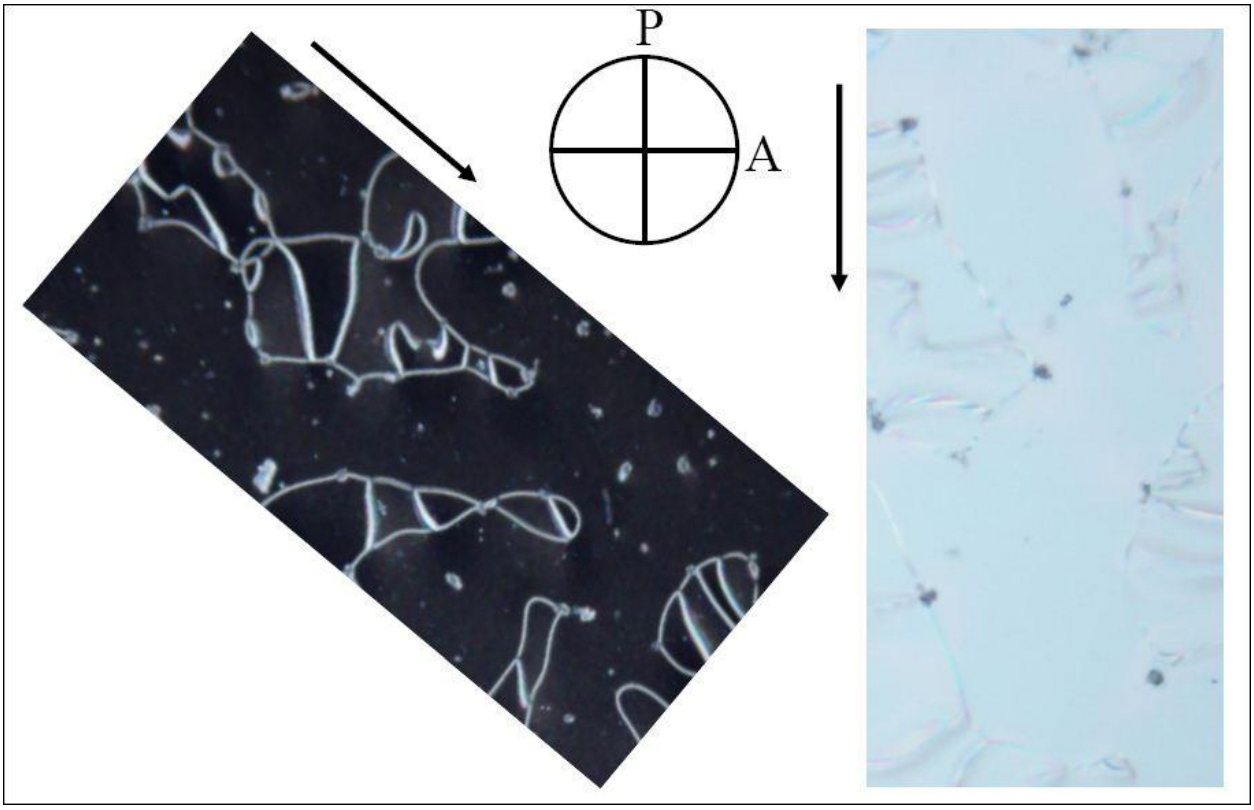

Figure 9.3. High birefringence of the elastomers under cross-polarizers confirms good alignment of the directors along the rubbing direction

9.5 Results and discussion

The strain of elastomers containing different concentrations of AuNPs was measured as a function of stress applied parallel to the long axis of the films and the liquid crystal director. The measurements were carried out at a rubbery plateau in the nematic phase at 70°C with a static force applied at 2 mN/min and a preload stress of 10kPa. Taking into account the cross-sectional area of each LCE, which was ~0.5 mm^2, the Young's moduli of the LCEs were determined from the stress-strain curve. It was found that the modulus increased as the concentration of colloidal gold was increased in each elastomer. **Figure 9.4 (top)** shows stress/strain curves for samples containing different concentrations of AuNPs and **Figure 9.4 (bottom)** illustrates the change in the Young's moduli of the elastomers as a function of the concentration of AuNPs dispersed in the elastomer network. It is clear from these data that at relatively low concentrations of colloidal gold, the material stiffened. Thermomechanical properties of elastomers also change with embedment of AuNPs. As shown in **Figures 9.5 (top)** and **9.5 (bottom)**, samples with embedded

gold exhibit a better structural integrity when subjected to heating. **Figure 9.5 (top)** presents sequential images of a pure sample heated from 30°C to 110°C. The sample starts to lose its mechanical integrity at around 100°C and it completely degraded at 110°C. On the other hand, the sample doped with 0.096 mol% AuNPs, **Figure 9.5 (bottom)**, is starting to degrade at 110°C yet it is not fully degraded up to 125°C. These results suggest that embedment of AuNPs in ionic liquid elastomer networks influences their thermomechanical properties.

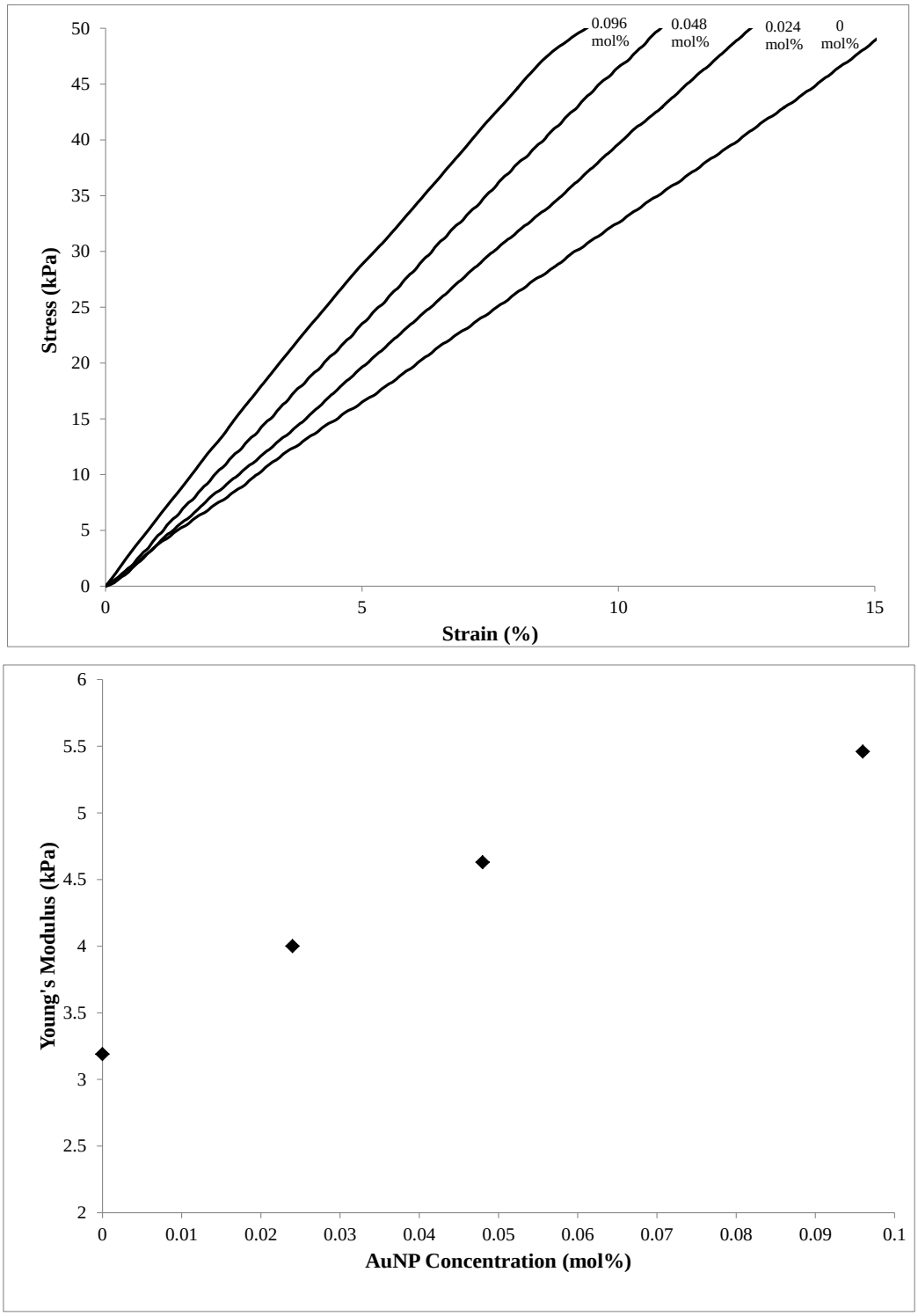

Figure 9.4. The Young's modulus exhibited an increase with an increase in the concentration of AuNPs in elastomers. Top: Stress-strain plots for elastomers containing different concentrations of AuNP. Bottom: The Young's moduli of the elastomers increase with the concentration of AuNPs.

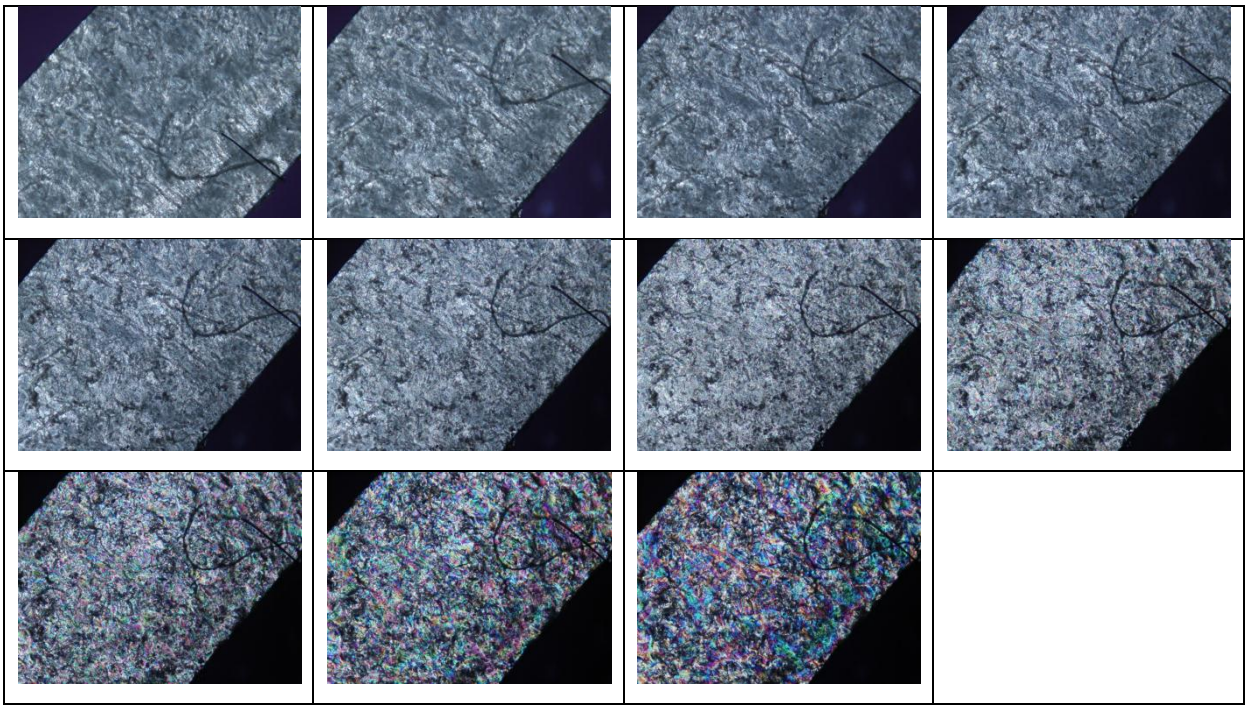

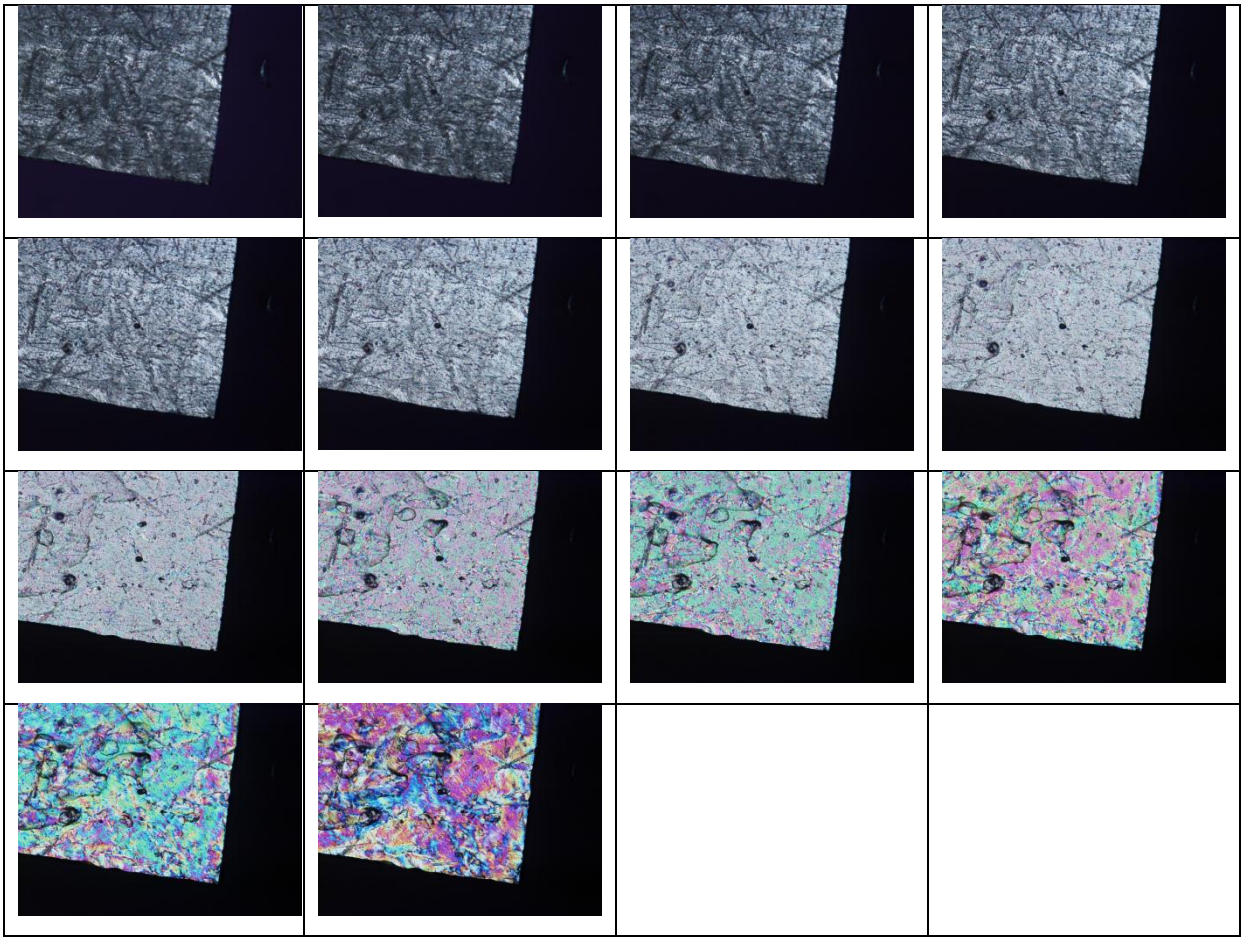

Figure 9.5. Samples with embedded gold nanoparticles exhibit a better structural integrity when subjected to heating. (Top): Sequential images of a pure samples heated from 30°C to 110°C and (Bottom) samples doped with 0.096 mol% gold nanoparticle heated from 30°C to 125°C. The images are taken at 30,45,60,75,80,85,90,95,100,105,110,* 115,120,125*°C. (Temperatures shown in* italic *only apply to doped sample)

Resistance of an LCE to applied stress largely depends on the type and concentration of the crosslinker.[6] The cross-linking density, *n*, of each elastomer was estimated at the rubbery plateau based on the deduced value of its Young's modulus, using the equation $E=3nRT$, [23] where E is the Young's modulus, R is gas constant and T is temperature. Although all the elastomers investigated in this study contain 10 mol% of the HDA cross-linker, elastomers with higher concentrations of colloidal gold exhibited higher cross-linking densities. The calculated cross-linking densities of elastomers along with the associated Young's moduli are shown in **Table 9.1**. It can be concluded form these data that AuNPs are affecting the cross-linking density of the elastomers and consequently increase their elastic moduli. The highest calculated cross-linking density of 6.31×10^{-5} mol/cm^3, corresponding to the LCE with 0.096 mol% AuNPs, is still lower than the expected value of 2.01×10^{-4} mol/cm^3 for 10 mol% of HDA. Lower than expected cross-linking density of the elastomers is likely due to the partial participation of the cross-linking units in the polymer network.

AuNP (mol%)	E (MPa)	n×10^{-5} (mol/cm^3)	$\overline{T_{NI}}$ (°C)
0	0.31	3.62	82.93
0.024	0.40	4.67	84.41
0.048	0.46	5.37	86.90
0.096	0.54	6.31	90.28

Table 9.1. Young's modulus, cross-linking density and mean phase transition temperature of elastomers containing different concentrations of AuNPs

The thermoelastic behavior of the LCEs containing different concentrations of AuNPs were studied through heating and cooling cycles between 50 and 130°C and ramped at a rate of 0.5°C/min through the nematic to isotropic phase transition (T_{NI}). At a fixed static force, the strain was measured as a function of temperature. Multiple cycles were applied to the samples under increasing static forces. As expected, the rate of the change of the length was greatest near the T_{NI}. At temperatures > 100°C the length of the film remained approximately constant. A similar pattern was observed for the cooling cycle. **Figure 9.6** shows the thermoelastic plots for the film containing 0.048 mol% of AuNPs under application of different preloads ranging from 5 to 40kPa. Embedment of AuNPs in LCEs resulted in an upward shift in the mean phase transition temperature ($\overline{T_{NI}}$). As presented in **Table 9.1**, $\overline{T_{NI}}$ has increased about 7°C between the film without any AuNPs and the one doped with 0.096 mol% AuNPs.

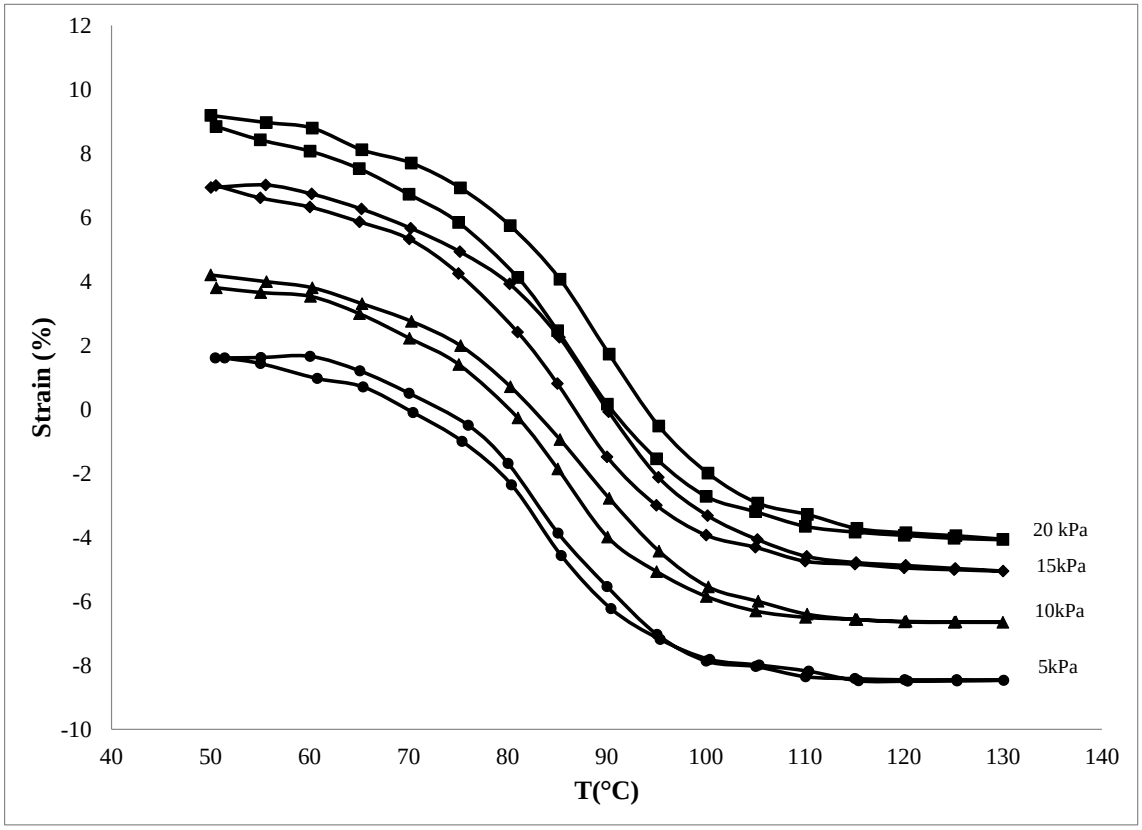

Figure 9.6. Thermoelastic measurements of elastomer doped with 0.048 mol% AuNPs at 0.5°C/min heating and cooling rate under application of different static forces from 5 to 40kPa. Negative and positive strain values indicates contraction and expansion of the elastomer respectively

We then tested the hypothesis that embedded AuNPs, which have high thermal conductivity, increased the thermal conductivity of the elastomer, thereby enhancing the actuation speed. To accomplish this, the change in the rate of mechanical strain of the elastomers with respect to time (Δε%) was measured at different temperature rates. Applying heating rates of 20°C/min revealed no change in the strain rate of elastomer samples with or without AuNPs. When the temperature was increased to a faster rate of ~50°C/min, the LCE elastomers doped with AuNPs exhibited greater change in their strain rate. As shown in **Figure 9.7**, LCE films doped with 0.096 mol% AuNPs exhibited more than a 100% improvement in their actuation speed compared to samples without any AuNPs or those containing lower AuNP concentrations. This enhanced response of LCEs doped with metallic nanocolloids is due to improved thermal conductivity, allowing more efficient transfer of heat into the elastomer.

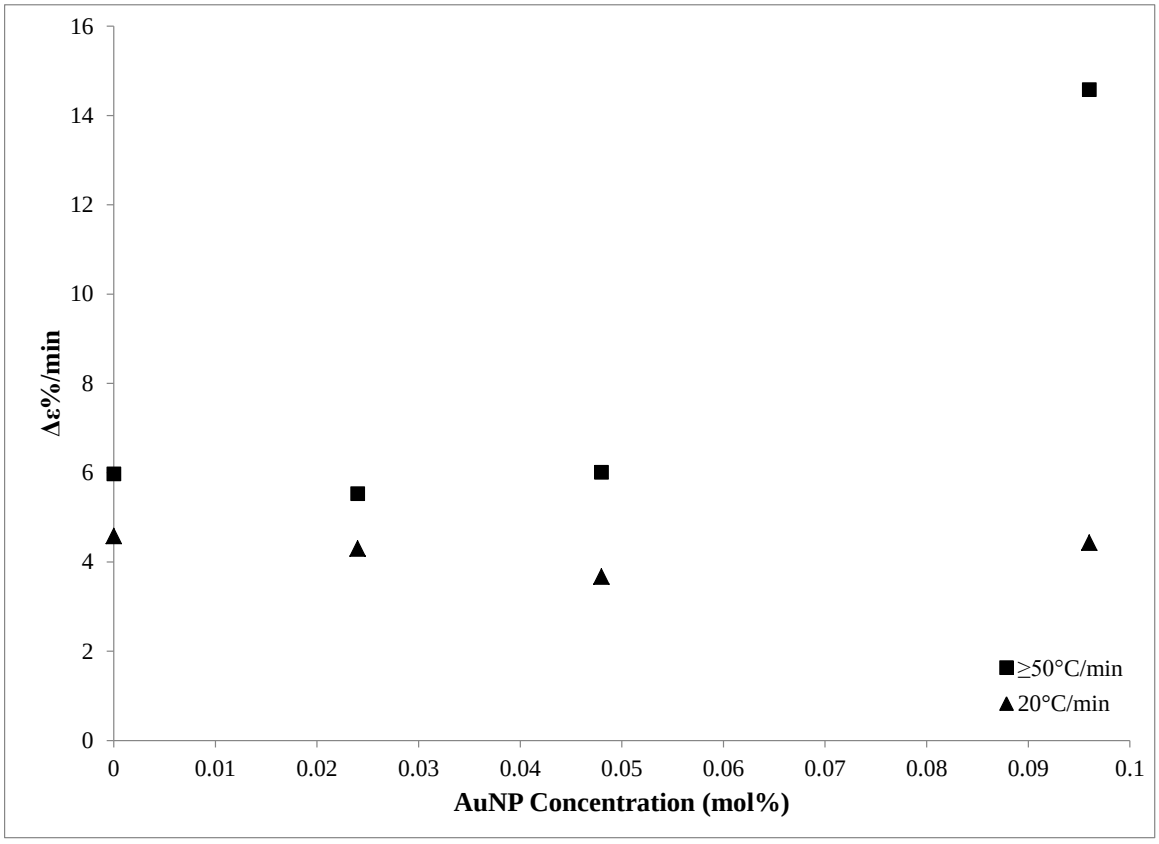

Figure 9.7. Actuation speeds of LCE actuators doped with different concentrations of AuNPs under slow and fast heating conditions. Under fast heating, the elastomer doped with 0.096 mol% AuNPs exhibited >100% faster actuation speed compared to other elastomers

9.6 Conclusion

We have successfully dispersed AuNPs in thermomechanical nematic LCE actuators and have significantly improved the material response to a thermal stimulus. Embedment of AuNPs in LCEs stiffened the elastomers, resulting in a slight decrease in the strain of the actuators, but this effect was more than compensated by a significant improvement in the actuator strain rate in response to an external stimulus. Incorporating a fractional amount of metal nanoparticles in these thermomechanical actuators can result in a pronounced enhancement of the thermal conductivity. Doping LCEs with AuNPs provides a means to improve the material response time to external stimuli. Under fast heating conditions, the AuNP-doped LCE actuators exhibited more than a 100% increase in the rate of change of strain with respect to time. The improved efficiency further develops the material response in this unique class of soft linear actuators for use in a wide range of applications.

References

1 SM Clarke, AR Tajbakhsh, EM Terentjev, C Remillat, GR Tomlinson, and JR House, "Soft elasticity and mechanical damping in liquid crystalline elastomers," Journal of Applied Physics **89**, 6530 (2001).

2 G. G. Barclay and C. K. Ober, "Liquid crystalline and rigid-rod networks," Progress in Polymer Science **18** (5), 899-945 (1993).

3 R Pelrine, R Kornbluh, Q Pei, and J Joseph, "High-speed electrically actuated elastomers with strain greater than 100%," SCIENCE **287** (5454), 836 (2000).

4 S Hashimoto, Y Yusuf, S Krause, H Finkelmann, PE Cladis, HR Brand, and S Kai, "Multifunctional liquid crystal elastomers: Large electromechanical and electro-optical effects," Applied Physics Letters **92**, 181902 (2008).

5 CM Spillmann, JH Konnert, JR Deschamps, J Naciri, and BR Ratna, "Molecular Packing in Electroclinic Liquid Crystal Elastomer Films," Chemistry of Materials **20** (19), 6130-6139 (2008).

6 CM Spillmann, J Naciri, MS Chen, A Srinivasan, and BR Ratna, "Tuning the physical properties of a nematic liquid crystal elastomer actuator," Liquid Crystals **33** (4), 373-380 (2006).

7 CM Spillmann, BR Ratna, and J Naciri, "Anisotropic actuation in electroclinic liquid crystal elastomers," Applied Physics Letters **90**, 021911 (2007).

8 H. Finkelmann, I. Kundler, E.M. Terentjev, and M. Warner, "Critical Stripe-Domain Instability of Nematic Elastomers," J. Phys. II France **7** (8), 1059-1069 (1997).

9 T.C. Lubensky, E.M. Terentjev, and M. Warner, "Layer-network coupling in smectic elastomers," J. Phys. II France **4** (9), 1457-1459 (1994).

10 Peter D. Olmsted and Eugene M. Terentjev, "Mean-field nematic–smectic-A transition in a random polymer network," Physical Review E **53** (3), 2444 (1996).

11 M. J. Osborne and E. M. Terentjev, "Elasticity of rubber with smectic microstructure," Physical Review E **62** (4), 5101 (2000).

12 E.M. Terentjev and M. Warner, "Continuum theory of elasticity and piezoelectric effects in smectic A elastomers," J. Phys. II France **4** (1), 111-126 (1994).

13 EA Kottke, LD Partridge, and M Shahinpoor, "Bio-potential neural activation or artificial muscles," Journal of Intelligent Material Systems and Structures **18** (2), 103-109 (2007).

14 DK Shenoy, D Laurence Thomsen III, A Srinivasan, P Keller, and BR Ratna, "Carbon coated liquid crystal elastomer film for artificial muscle applications," Sensors & Actuators: A. Physical **96** (2-3), 184-188 (2002).

15 O. V. Kuksenok, R. W. Ruhwandl, S. V. Shiyanovskii, and E. M. Terentjev, "Director structure around a colloid particle suspended in a nematic liquid crystal," Physical Review E **54** (5), 5198 (1996).

16 Martin Zapotocky, Laurence Ramos, Philippe Poulin, T. C. Lubensky, and D. A. Weitz, "Particle-Stabilized Defect Gel in Cholesteric Liquid Crystals," SCIENCE **283** (5399), 209-212 (1999).

17 V. G. Nazarenko, A. B. Nych, and B. I. Lev, "Crystal Structure in Nematic Emulsion," PHYSICAL REVIEW LETTERS **87** (7), 075504 (2001).

18 S. P. Meeker, W. C. K. Poon, J. Crain, and E. M. Terentjev, "Colloid–liquid-crystal composites: An unusual soft solid," Physical Review E **61** (6), R6083 (2000).

19 V. J. Anderson and E. M. Terentjev, "Cellular solid behaviour of liquid crystal colloids 2. Mechanical properties," The European Physical Journal E: Soft Matter and Biological Physics **4** (1), 21-28 (2001).

20 Yurii Reznikov, Olexander Buchnev, Olexander Tereshchenko, Victor Reshetnyak, Anatoliy Glushchenko, and John West, "Ferroelectric nematic suspension," Applied Physics Letters **82** (12), 1917-1919 (2003).

21 C. Y. Matuo and A. M. Figueiredo Neto, "Time dependence of the magnetic grain concentration and secondary grain aggregation in ferronematic lyotropic liquid crystals subjected to magnetic field gradients," Physical Review E **60** (2), 1815 (1999).

22 S Courty, J Mine, AR Tajbakhsh, and EM Terentjev, "Nematic elastomers with aligned carbon nanotubes: New electromechanical actuators," Europhysics Letters **64** (5), 654-660 (2003).

23 DL Thomsen III, P Keller, J Naciri, R Pink, H Jeon, D Shenoy, and BR Ratna, "Liquid crystal elastomers with mechanical properties of a muscle," Macromolecules **34** (17), 5868-5875 (2001).

Chapter 10
Closing Remarks

This dissertation has focused on design, fabrication and characterization of smart polymer ionic liquid electromechanical actuators, consisting of gold nanoparticle-based IPMCs. More specifically, the work presented here is focused on the influence of the CNC layer on the mechanical and electrical properties of IEAP actuators, with the goals of improving the mechanical properties to make IEAP actuators suitable for microrobotic applications. Also included in this work is study on a class of thermomechanical actuators based on liquid crystal elastomers doped with gold nanoparticles.

In the following paragraphs I summarize the achievements and contributions of this work to the area of smart polymers and IEAP actuators. And in the last section I will discuss future studies and applications.

10.1 Porous and conductive CNC nanocomposites

CNC nanocomposites are designed to increase intake of free ions and facilitate mobility of ions through the IPMC. Two critical characteristics for CNC layers to fulfill these designated tasks are electrical conductivity and porosity. Electrical conductivity allows uniform distribution of electric charge across the CNC and subjects ions to a fairly uniform electric field. This results in participation of more ions in the actuation process and also more uniform bending. The porosity of the CNC increases the CNC-ion interfacial area and also facilitates mobility of ions by providing nano channels that allow ion travel through the CNC. It is important to note that there is expected to be an optimum size and number of nano channels, values below or above the optimum values would result in decrease of performance.

Our approach to construct a porous and conductive nanocomposite was to form layers of gold nanoparticles on ionomeric membrane via the layer-by-layer self-assembly technique. The LbL self-assembly technique was chosen because it allows fabrication of nanocomposites with nanometer-scale thickness with precise control over the thickness. Also a wide range of materials

can be used with this method. Hypothetically, any dispersed charged species can be used with the LbL self-assembly technique to form nanocomposite thin-films. Gold nanoparticles were chosen among other metallic nanoparticles because of the good electrical conductivity of gold and its environmental stability compared to other metals. Spherical nanoparticles were chosen because of their geometry which allows formation of porous network with significant void volume in between. Moreover, gold nanoparticles are widely available.

10.2 Influence of CNC on mechanical properties of IEAP actuators

In this research I presented two methods for manipulating the mechanical structure of CNC thin films based on changing the thickness of CNC thin-films and changing the volume fraction of gold nanoparticles in CNC thin films. These methods provided the means to study the influence of the mechanical properties of the CNC layers on the performance of IEAP actuators.

In the first approach, thickness of CNC thin-films was controlled by varying the number of deposited bilayers of gold nanoparticles and PAH. In this method, the thickness of CNC layers were varied from approximately 20 nm to approximately 80 nm by depositing 10 to 40 bilayers of gold nanoparticles and PAH. The resultant CNCs were then made into actuators and were characterized for their curvature, strain and actuation speed due to mobility of ions in the actuator.

First, it was observed that actuators made with this method generate significantly large strain compared to other types of actuators which suggests that incorporation of spherical gold nanoparticles in the CNC enhances conductivity and porosity. One key advantage of CNCs fabricated via LbL self-assembly is maintaining a relatively small thickness, which leads to improved mechanical strain and bending curvature of the actuators. It was also observed that actuators with thicker CNC layers are capable of generating larger bending and net strain. The maximum curvature of the actuators towards the anode and the net strain were found to increase linearly with the thickness of the CNC layer. The intrinsic strain of actuators as calculated from a theoretical five-layer model exhibited a decreasing trend with increasing thickness such that actuator with CNC consisting of 40 bilayers generated an intrinsic strain of 11.48% while one with CNC consisting of 10 bilayers generated intrinsic strain of 22.6%. However, it was observed that there was a measurable curvature even for an actuator with no CNC. After

accounting for the curvature observed in an actuator with no CNC layer, the net intrinsic strain of the CNC was deduced and found to be ~6.1% independent of thickness. This indicates that the full volume of the CNC is equally effective in generating the strain. The normalized response time for actuation as a function of intrinsic strain was found to be relatively independent of thickness with a time constant τ of 1.5 s, suggesting that traversal through the Nafion membrane is the limiting factor in the anion motion.

The improved actuation curvature, intrinsic strain and net strain are results of successful fabrication of thin and uniform CNCs, while maintaining a porous and conductive nanostructure.

In the second approach, the surface density of gold nanoparticles in CNC layers was varied by using diluted dispersed gold nanoparticle solutions. Colloidal solutions with concentrations of 20, 10 and 4 ppm gold nanoparticles were used to form CNC thin-films. SEM images confirmed that decreasing surface density of gold nanoparticles results in a less dense thin-film with partial coverage of the substrate, where the thickness of IPMC was kept at fairly constant value. Sheet resistance of CNC thin-films was measured by four-point probe method and exhibited a significant drop as the volume fraction of gold nanoparticles was increased in the thin-films; which is of course due to high electrical conductivity of the connected network gold nanoparticles. The resultant actuators were then characterized for their cationic and anionic strain and charging/discharging time. It was observed that anionic strain is independent of the density of gold nanoparticle; however cationic strain is strongly dependent on density of gold nanoparticles. Charging/discharging times suggest that denser CNCs charge and discharge at a faster rate compared to ones with less dense CNCs. Increasing density of gold nanoparticles in CNC increases the CNC-ion interfacial area and thus the capacitance of the device, which would increase the time constant; however, it also significantly increases conductivity which in this case compensates the increased capacitance and reduces the time constant. The larger cationic strain in denser CNCs is due to quicker charging in such systems, which results in accumulation of more cations at cathode before the cationic strain is canceled by anionic strain.

The improved cationic strain in denser CNCs is due to increased electrical conductivity in the system, which reduces the RC time constant. Such systems can be used in applications where

fast response and optimum strain are desired, such as the wing motion in nature-inspired microrobotic insects.

10.3 Ionic Motion in IEAP actuators

It is highly valuable and interesting to develop a fuller understanding of the ionic motion within the IPMC. It was observed that the actuation performance and bending direction of IEAP actuators is strongly depended on the frequency of the applied waveform. This further confirms that there is more than one simple ion motion in the IPMC. Given that there are two types of ions provided by the ionic liquid, and the fact that cations and anions are of different volume and mass, it is logical to presume that different ions respond differently to variations in electric field. To test and confirm this hypothesis, I modeled the equivalent electric circuit of the system to predict the bending direction of the IEAP actuators as a function of applied frequency. It was observed that a turnover frequency can be calculated based on the response time of the faster ion, which is representative of a frequency at which the effects of the motion of the slower ion are essentially eliminated. The phenomenon was confirmed with supporting experiments.

To better understand the influence of type of ions on the performance of IEAP actuators, as well as the ionic interactions within the IPMC I also studied the performance of actuators as a function of ionic liquid type and the counterion of Nafion membrane. I took two approaches to this subject; one was to use ionic liquids other EMI-Tf as the source of ions and the other was to substitute the proton counter-ion of Nafion with a cationic molecule.

The first approach was aimed on understanding the effects of different cation and anions in the system as free ions. It was observed that anion-cation types strongly influence the performance of actuators. For instance, using BMP-TFSI or TES-TFSI eliminates the cationic motion that is observed in the EMI-Tf case. This suggests that the BMP and TES cations diffuse much more slowly in the Nafion membrane. Furthermore, substitution of the proton counter-ion of Nafion with the larger EMI cation results in stronger cationic motion, suggesting that the counter-ion itself participates in the actuation process. In one case, where BMP-TFSI was used as the ion source, the motion of the actuator was reversed from completely anionic with proton counter-ion to completely cationic with EMI counter-ion.

One of the most significant criticisms to IEAP actuators is the double motion, which is not desired in most applications. This study confirmed that the problem can be eliminated by modifications of the Nafion's counterion and/or by using alternative ionic liquids.

10.4 Thermomechanical Liquid Crystal Elastomers

Nematic liquid crystal elastomers (LCEs) consist of pendant liquid crystal mesogens attached to a polymer network. Thermomechanical LCEs respond to temperature changes in the environment. The actuation speed, or response time, in thermomechanical LCEs depends on heat propagation throughout the actuator. Since these actuators are usually very small and thin, heat propagates quickly and it is usually not a limiting factor when the heating rate is slow. However, when the heating rate is increased, heat propagation can become a limiting factor. To overcome this issue, the thermal conductivity of LCEs should be improved, without disturbing the elastomeric network. To improve the thermal conductivity of the LCEs without disturbing the elastomeric network, I embedded a low concentration of gold nanoparticles in the elastomeric network. Embedment of gold nanoparticles slightly stiffened the actuators; however the effect was more than compensated by increased thermal conductivity and strain rate in response to an external stimulus. Under fast heating conditions, the AuNP-doped LCE actuators exhibited more than a 100% increase in the rate of change of strain with respect to time.

The improved efficiency further develops the material response in this unique class of soft linear actuators for use in a wide range of applications.

10.5 Future Studies

One recommendation for future work is to further study ionic interactions in IPMCs. A systematic study based on a large variety of ionic liquids and counter-ions, with special attention to the volume and chemical/electrostatic interactions of ions, would help to draw a clear conclusion on precise effects of ions and ionic interactions on the performance of actuators.

To use IEAP actuators in more practical applications, there is need to improve the generated force, response time and strain. A suggestion is to improve electrical conductivity of the CNC layers as more conductive CNC can undergo faster charge/discharge cycles. As a result the response time can be improved. Another suggestion is to fabricate CNCs of larger thicknesses to

first improve the mechanical properties of the actuator, and to increase electrolyte uptake capacity which leads to generation of larger force and strain.

Having already shown functionality of IEAP actuators, another goal should be to use IEAP actuators in micro devices. Although the strain of IEAP actuators is yet not enough for larger scale applications, they generate enough strain for micro devices and applications. Microrobotics is one of the areas of interest for possible use of IEAP actuators, especially since it is proven that IEAP actuators can be made in very small dimensions, **Figure 10.1**. Given the soft and flexible structure of IEAP actuators, they have the closest properties to biological systems and are the best candidate to be used in biomimetic applications.

Figure 10.1. Top: an IEAP actuator place on a bee for size comparison. (Bottom): Overlay images of actuation of a similar size actuator attached to a wing of an insect.

Another recommendation is to study the sensing capabilities of IEAP systems. In this dissertation, the focus was on actuation mechanism and performance; however, the very same structures can be utilized as sensors. Application of a mechanical force causes deformation which redistributes ions in the IPMC; as a result of the motion of ions a minimal electric field is generated. This weak electric field can be easily detected by any ordinary voltmeter. IEAP systems can also be used in engines with high vibration rate, like helicopters or automobiles, to monitor frequency of vibration. Frequency of vibration can be used to monitor performance of the engine or even to detect possible malfunctions before they become more obvious.

Given that hydrogen fuel cells have a similar structure as IEAP actuators, it is also a good approach to study hybrid systems consisting of fuel cell and actuator in one structure. This structure may lead to actuators for autonomous microrobotics where the power source is embedded within the actuator.

Index

D

E

F

G

H

I

L

M

N

O

P

Q

R

S

T

U

V

W

Y

Z